Development and Characterization of Chitosan Crosslinked with Tripolyphosphate as a Sustained Release Agent in Tablets

A

DISSERTATION
in Pharmaceutical Sciences

Presented to the Graduate Faculty
of the University of the Sciences
in Partial Fulfillment of the Requirements for the Degree of

DOCTOR OF PHILOSOPHY

by

Colin Andrew Pinto

June 2017

Development and Characterization of Chitosan Crosslinked with Tripolyphosphate as a Sustained Release Agent in Tablets

Colin Andrew Pinto, Doctor of Philosophy
University of the Sciences, 2017

Abstract

The ability of chitosan and tripolyphosphate to form an ionic crosslinked material and its effectiveness in sustained release formulations has been reported. However, key issues commonly observed with these formulations include inefficiencies and inaccuracies in the drug loading as well as an inability to achieve complete release of drug. Acetaminophen, as a model drug, was added to various chitosan-tripolyphosphate crosslinked powders to assess the sustained release characteristics when drug is added extragranularly as opposed to during the crosslinking process, which is the most common procedure for drug addition in prior literature. The influence of various process and formulation variables including chitosan concentration, chitosan:tripolyphosphate ratio, temperature, ionic strength, and pH was assessed. Design of experiments allowed the identification of factors and two factor interactions that have significant effects on particle size and size distribution, yield, zeta potential, true density, and drug release. Statistical model equations were successfully used to manufacture optimized chitosan-tripolyphosphate crosslinked powders with various properties for further evaluation. Analysis of the compressibility of the optimized powders revealed that the crosslinked powders had enhanced compression properties when compared to chitosan powder. Environmental scanning electron microscopy revealed a correlation between the rigidity and density of the powders and corresponding capabilities for enhanced sustained release. Analysis of the moisture sorption and desorption isotherms from dynamic vapor sorption analysis revealed various types and levels of water present and a correlation between the

quantity of water internally absorbed during sorption and desorption and sustained release capability. Chitosan-tripolyphosphate crosslinked powder can be manufactured with optimized properties that allow desired sustained drug release profiles while simultaneously serving as the primary diluent for solid oral dosage forms.

Keywords Chitosan, tripolyphosphate, design of experiments, ionic crosslinking, dissolution, sustained-release, dynamic vapor sorption analysis, compression, tablets

UNIVERSITY OF THE SCIENCES

This is to certify that the Dissertation prepared by

Colin Andrew Pinto

titled

Development and Characterization of Chitosan Crosslinked with Tripolyphosphate as a Sustained Release Agent in Tablets

Complies with the Policies of the Graduate Faculty
of the University of the Sciences and is Approved
by
the Advisory Committee as Fulfilling the Dissertation
Requirements for the Degree of

DOCTOR OF PHILOSOPHY

_____
Steven H. Neau, Ph.D.
Chairman, Advisory Committee

_____
Matthew A. Howard, Ph.D.
Member, Advisory Committee

_____
Pardeep K. Gupta, Ph.D.
Member, Advisory Committee

_____
Frederick T. Schaefer, Ph.D.
Member, Advisory Committee

_____
Kamal Jonnalagadda, Ph.D.
Reviewer, Advisory Committee

Dedicated to

My Wife, Annie “Vern” Pinto; My Parents, Lori and Carl Pinto Jr.; My Family,

My Mentors, and My Friends

Acknowledgments

Where do I begin, completing my dissertation has been the most mentally trying journey of my life… Starting as a 25 year old part-time student with a full-time job, and living with friends who were still living the "young working adult" party life, as most early-to-mid twenty-year-olds do, there were countless excuses to procrastinate or give up altogether. However, it was the same people who provided the excuses that also provided the motivation to complete my degree and finally get to where I find myself today.

I want to start off by thanking my wife. I can remember just a little over two years ago, she was my fiancé at the time, when I was in a rut with my research and wanted to walk away with a Master's degree. I shared with her my frustrations and told her of my thoughts to walk away. She immediately told me this was not an option; that I had worked so hard, and she knew that wasn't what I really wanted. She was just completing her Doctorate of Physical Therapy program at the time, so it wasn't as if she had no idea what I was going through. She was right, and although there have been several ups and downs since that conversation, there has never been any doubt in my mind that the end goal was always completing my doctoral degree and that eventually the day would come and the hard work would pay off. She's my motivation, my partner, and my best friend.

Next I'd like to thank my parents for being unwavering pillars of support and role models in every aspect of life. I am the person I am today because of what they have taught me along the journey of life. They both worked so hard to enjoy the successes they do today and have always provided anything my siblings and I have ever needed in

life. They have shown me what it means to be a good person and raised us with these values in mind. It's this work ethic and principles that have guided my success in life thus far and continue to provide the basis for who I strive to be. I want to also thank my younger brother and sister, Trevor and Mackenzie, who also live their lives this way, and are always there for support, no matter what.

I want to next thank my advisor, Dr. Neau. Dr. Neau and I are complete opposite personality types and thus it's far more than just his endless knowledge and expertise in his fields that have helped me grow over the past several years. Dr. Neau continues to challenge my thought process and always has a way of engaging in a thought-provoking discussion, regardless the topic.

My influences at Johnson & Johnson have been endless, but there has always been one constant, Dr. Matthew Howard. Matt has been a friend and mentor since day 1 at J&J. He's responsible for influencing me to enroll in the Ph.D. program. While it's been several years since I've reported to Matt, we still chat frequently on all subjects of life. His jovial attitude and constantly working mind make him a pleasure to be around and someone I always look forward to catching up with. An additional thanks is owed to my other peers at J&J, particularly, Kelly, Stevie, and Matty for building my knowledge base in my young career, but more importantly, being friends.

Next is Dr. Kalyan Saripella. I first met Kalyan while he was still a student under Dr. Neau, but then he became a colleague for almost five years before moving on. Kalyan has a brilliant scientific mind and always a smile on his face. He's been and continues to be a wonderful friend in helping with my research along the way. I also

want to thank Nikhil, another student under Dr. Neau, who was there during my time in the program. Nikhil is a wonderful person and was always willing to help.

Lastly, I want to thank my friends and extended family. My core group of friends continues to be the guys I met in high school, and other than us getting old, nothing has changed. They are always there for support and have always been there to grab a beer when I needed a break from the rigors of the Ph.D. program. My family is small and thus we've always been close since my childhood. Whether it's been the constant support from my Grandparents or living with my Uncle after college, they've all contributed to my growth and for that I am both grateful and thankful.

VITA

Colin Pinto was born just outside of Philadelphia, Pennsylvania. He completed his high school education at LaSalle College High School in Wyndmoor, PA. He earned his Bachelor's Degree in Chemistry at the University of Delaware in Newark, DE in 2008. After completion of his undergraduate degree, Colin briefly joined TEVA Pharmaceuticals in their R&D Analytical group before joining Johnson & Johnson Consumer, Inc. in May of 2009 in their Technical Operations group. Colin then began his pursuit of a doctoral degree in Pharmaceutics as a part-time student in 2010 at the University of the Sciences in Philadelphia. In June of 2016, Colin left the Technical Operations organization at Johnson & Johnson Consumer to take one a new role as a Manager in the J&J Global OTC Consumer R&D organization. He is a member of the American Association of Pharmaceutical Scientists and the Rho Chi honor society in Pharmacy. After completion of his graduate degree program, Colin plans to continue his career with Johnson & Johnson.

Table of Contents

List of Figures

List of Tables

CHAPTER 1

Purpose of Study

The trend in the pharmaceutical industry is to generate sustained release formulations for drugs requiring multiple daily dosing in order to improve patient compliance and avoid the peaks and troughs of drug plasma concentration often observed with frequent dosing of immediate release formulations (Fyhr & Downie, 2003). Particularly in the area of over-the-counter (OTC) drugs that represent the majority of pharmaceutical tablets consumed in the U.S., typical dosing is required every 4 – 6 hours, which is easily forgotten over the course of a busy day. Furthermore, terminally ill patients may require drug plasma levels maintained within the therapeutic window to avoid severe pain or side effects that would prohibit them from sleeping through the night in absence of a sustained release form (Aulton & Taylor, 2013).

Chitosan has long been considered appropriate for use in pharmaceutical dosage forms due to its evident safety and low toxicity (Baldrick, 2010) as well as the abundance of the polymer from which it is derived, chitin, the second most common polysaccharide on Earth (Rinaudo, 2006), second only to cellulose. The range of studies of chitosan includes dosage forms suitable for oral, injectable, nasal, ophthalmic, and transdermal delivery (Felt, Buri, & Gurny, 1998). Specific to oral solid dosage forms, claims have been made that, depending on its concentration in the formulation, chitosan can act as a binder, lubricant, or even disintegrant (Picker-Freyer & Brink, 2006).

The overall goal of this research study is to prepare and characterize chitosan crosslinked with tripolyphosphate (TPP) to produce a chitosan-tripolyphosphate (Ch-TPP) complex suitable for use as a sustained release agent in a tablet dosage form. The

effect of pH, chitosan to TPP ratio, chitosan/TPP concentration, temperature, and ionic strength on the particle size and compression properties of the Ch-TPP mixtures will be evaluated. Multiple examples in the literature demonstrate the ability to generate drug-loaded Ch-TPP particles and films with various sustained release profiles (De Campos, Sánchez, & Alonso, 2001; Desai & Park, 2005; Dong, 2013; Dudhani & Kosaraju, 2010; Pati, 2011; Win, Shin-ya, Hong, & Kajiuchi, 2003). Unfortunately, precise and accurate drug entrapment efficiencies are difficult to obtain (Curotto & Aros, 1993), incomplete drug release is typically observed (Desai & Park, 2005; Dudhani & Kosaraju, 2010; Gan & Wang, 2007; Guan et al., 2011; Hu et al., 2008; J. Ko, Park, Hwang, Park, & Lee, 2002; Konecsni, Low, & Nickerson, 2012; Sezer & Akbuğa, 1995; Y. Xu & Du, 2003; L. Zhang & Kosaraju, 2007), and these formulations are not necessarily ideal for patient administration. However, if the integrity of the product and mechanism of sustained release found in these Ch-TPP particles and films can be maintained after its incorporation into a tablet dosage form, the product would represent a means to achieve reproducible production and performance.

Hypotheses

1. Statistically significant models can be generated to predict various chitosan-tripolyphosphate material and tablet properties as a function of inputs (formulation and process variables).
2. Inclusion of drug via direct blending versus inclusion during the crosslinking process will allow complete drug release from chitosan-tripolyphosphate tablets yet still provide sustained drug release.

3. The extent and type of water taken up by different crosslinked chitosan-tripolyphosphate materials will correlate to the rate of drug release.
4. Chitosan-tripolyphosphate crosslinked material can be utilized in tableting at high concentrations and will provide tableting properties similar to other direct compression excipients in addition to the benefits of sustained release.

Specific Aims

1. To use experimental design to statistically determine the effect of formulation and process variables on the properties of chitosan-tripolyphosphate crosslinked materials
2. To generate regression equations that will allow manufacture of chitosan-tripolyphosphate crosslinked material with desired characteristics
3. To assess the release profiles of the various crosslinked structures using a model active pharmaceutical ingredient
4. To investigate the water holding capacity and distribution of water by dynamic vapor sorption analysis of optimized chitosan-tripolyphosphate crosslinked materials
5. To assess the compression properties of optimized Ch-TPP crosslinked materials

Chapter 2

Introduction

Chitosan, said to have been first discovered in 1811 by French botanist, Henri Braconnot, is a polysaccharide derived from the N-deacetylation of the second most abundant natural polysaccharide, chitin (Felt et al., 1998; R. A. A. Muzzarelli et al., 2012). Chitin is primarily found in crustacean shells, but can also be found in insects and fungi at lower percentages (Felt et al., 1998; Ravi Kumar, 2000). The general process for chitosan preparation from chitin includes the following steps: Drying of crustacean shells (or other source) to remove residual moisture; isolation of chitin by boiling the shells in concentrated base to dissolve proteins and sugars; demineralization by a series of acid washes, followed by base, and purified water; deacetylation by an additional step of boiling in concentrated base; and, finally, purification by dissolving, filtering, and removal of metals through the use of surfactants and chelating agents (Puvvada, Vankayalapati, & Sukhavasi, 2012). Chitosan is typically available in flaked or powdered form and is also found in a variety of salt forms including chitosan chloride and chitosan glutamate (Illum, 1998).

Chitosan

Structure and Properties

Chitosan, the *N*-deacetylated version of chitin, is very similar in structure to cellulose with the exception of an acetylated or free amine group instead of an alcohol group at carbon-2. The range of molecular weight for chitosan polymers is generally recognized as approximately 50 – 2000 kDa (Rege, 1999). The weight average molecular weight of chitosan is most frequently and simply determined using viscometry

by applying the Mark-Houwink equation (W. Wang & Xu, 1994). As the deacetylation of chitin to form chitosan is typically incomplete, the demarcation between chitin and chitosan, while not official, is typically when the degree of deacetylation (%DD) is greater than 50%; and although rare, can be maximized to achieve 100% (Illum, 1998). A minimum of 75% DD is almost always achieved when deacetylating chitin as evidenced by the availability of commercial chitosan materials, which typically have a %DD range of 70 – 95% (Moura, Moura, Soares, & Pinto, 2011). As such, the United States Pharmacopeia in its NF Monograph recognizes chitosan as having a %DD of 75.0 – 95.0% (United States Pharmacopeia National Formulary, 2016d).

Four polymorphs for chitosan have been discovered and their formation is directly dependent on the manner in which the chitosan is prepared from the parent chitin structure. These four crystalline polymorphs are referred to as "tendon" (Clark & Smith, 1936), "annealed" (Kozo Ogawa, Hirano, Miyanishi, Yui, & Watanabe, 1984), "L-2" (Sakurai, Takagi, & Takahashi, 1984), and "1-2" (Sakurai, Shibano, Kimura, & Takahashi, 1985). Both the tendon and L-2 crystals are hydrated, while the annealed polymorph is anhydrous (K. Ogawa, Yui, & Miya, 1992). Lastly, the "1-2" polymorph is considered a mixture of the L-2 and annealed forms (K. Ogawa et al., 1992). The crystallinity index (CrI) will be affected by type of polymorph and degree of deacetylation, which are ultimately affected by the preparation process of chitosan; however, some measured CrI values in literature range from approximately 25% (Agrawal, Manek, Kolling, & Neau, 2004) up to approximately 60% (Harish Prashanth, Kittur, & Tharanathan, 2002).

The deacetylation process of chitin results in the presence of free, primary amino groups. These groups, with an average pKa of ~6.5, can facilitate chitosan solubilization by protonation under acidic conditions. It is these properties that lend the characterization of chitosan as the only "pseudonaturally" occurring cationic polymer (Felt et al., 1998). This protonated amine group can then be crosslinked with anionic species to create complex networks. Furthermore, the presence of both amines and hydroxyl groups in the polymer chain lend chitosan to a vast array of modifications and derivations, far too many to be described here.

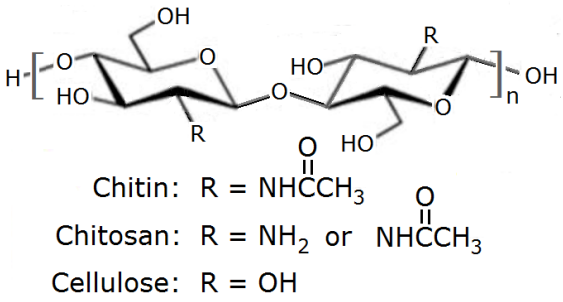

Figure 2.1. Structure of Cellulose, Chitin, and Chitosan

Stability and Interactions

The chemical and physical stability of chitosan and the different dosage forms in which its most commonly used have been reported by several authors (Bharate, Bharate, & Bajaj, 2010; H. Jonassen, Kjøniksen, & Hiorth, 2012; T. Kean & Thanou, 2010; Morris, 2011; Szymańska & Winnicka, 2015; Tsai, Chen, Bai, & Chen, 2011; Viljoen, Steenekamp, Marais, & Kotzé, 2014). Interactions between chitosan and active moieties are largely limited to an ionic interaction as opposed to any chemical reaction. Given the presence of the amine groups on the chitosan polymer chains, there exists the potential in acidic media for there to be an ionic interaction with drugs containing a partial or whole negative charge. It was shown that diclofenac sodium showed greater sustained release when delivered in a tablet using chitosan as the primary excipient due to the ionic interaction between the two components (Jackson, Young, & Pant, 2000; Sabnis, Rege, & Block, 1997). On the other hand, piroxicam showed a marked increase in solubility and thus bioavailability as a result of interaction with chitosan fibers, enabling it to be pulled into solution (Drebushchak et al., 2006).

The breakdown of chitosan *in vivo* is primarily by lysozyme enzymes and bacterial enzymes in the colon (Thomas Kean & Thanou, 2011; Kurita, Kaji, Mori, & Nishiyama, 2000). These enzymes catalyze the cleavage of β-1,4-glycosidic bonds, causing the depolymerization of the chitosan chains, and subsequent deacetylation of amines can alter the original form of the polymer (Szymańska & Winnicka, 2015). The breakdown of chitosan into oligomers was shown to be dependent on both molecular weight and degree of deacetylation (typically expressed as %DD) of the polymer where increased molecular weight and %DD were shown to slow the rate of degradation

(Vårum, Ottøy, & Smidsrød, 2001; J. Xu, McCarthy, Gross, & Kaplan, 1996; Yang, Hu, Wang, & Gu, 2007; H. Zhang & Neau, 2002). This was attributed to the fact that chitosan with higher %DD has a less porous structure, likely due to hydrogen bonding, that limits the uptake of water and subsequent hydrolysis in acidic media (Vårum et al., 2001). Meanwhile, the increased molecular weight should result in a greater extent of entanglement of the 3-D conformational structure that offers protection from depolymerization (Mucha & Pawlak, 2002; Wanjun, Cunxin, & Donghua, 2005), especially since individual chains are less available to enter the active sites of degrading enzymes.

As is the case with many tablet dosage forms, the stability of chitosan tablets has proved to be impacted by temperature and humidity storage conditions. It was demonstrated that the equilibrium moisture content of various chitosan powders in standard temperature and humidity conditions was approximately 7-11% w/w and generally independent of %DD or molecular weight (Rege, 1999). When tablets were compressed at temperatures ranging from 30 – 60 °C, it was shown that, at the higher temperatures, there was negative impact on crushing strength and thus friability of the tablet (Viljoen et al., 2014), while there was no impact at 30 or 40 °C for up to 8 hours after compression. Over a six month period, this effect on crushing strength was also observed when tablets were stored at 25 °C / 60% RH and proved more influential at 40 °C / 75% RH conditions (Viljoen et al., 2014). These results suggest that storage conditions for chitosan dosage forms are critical to maintain an equilibrium moisture content that preserves the physical strength and integrity of the tablets.

The primary means to assess the stability of chitosan-tripolyphosphate particles is an examination of the ability to maintain the particle size over the desired duration (H. Jonassen et al., 2012; Morris, 2011; Tsai et al., 2011). Jonassen et al. showed that particles stored in saline conditions showed greater stability than those stored in pure water. This was attributed to the smaller and more compact initial particle formation in the presence of low salt concentrations as compared to pure water, creating an initial state of greater colloidal stability. Regardless of the solvent, it was shown that at lower chitosan:tripolyphosphate (Ch:TPP) ratios or higher chitosan concentrations, changes in size and compactness were observed over time. This could be attributed to lower zeta potentials and greater initial particle size, both of which led to aggregation of particles. In evaluating the impact of temperature, Morris et al. showed that, upon storage at 40 °C over 6 months, the nanoparticles had essentially disappeared, which was attributed to the hydrolysis of the chitosan polymer and eventual disintegration of the nanoparticles. At 4 and 25 °C, however, very little change to particle size was observed over 12 months, indicating that the nanoparticle physical integrity, and likely release characteristics, could be maintained under these storage conditions.

Uses and Therapeutic Benefits

Chitosan, due to its abundance and safety profile, has been evaluated for use in many industries. One of the primary applications, and most studied, is its use as a flocculant or chelating agent for water treatment at which it is highly effective (Ravi Kumar, 2000), particularly in the textile industry where removal of dyes is critical (Hassan, Li, & Noor, 2009). Chitosan has been shown to effectively remove mercury

(Peniche-Covas, Alvarez, & Argüelles-Monal, 1992), cadmium (Jha, Iyengar, & Rao, 1988), and other metal ions from wastewater (Mckay, Blair, & Gardner, 1982).

These same coagulation properties have resulted in chitosan bandages marketed by HemCon® that rely on the positively charged chitosan to attract red blood cells ("HemCon Bandage PRO Hemorrhage Control Bandages," 2015). This process quickly and effectively results in the clotting of open wounds. Claims of antibacterial properties are supported, as described in the next paragraph. Other chitosan derived products have also been explored and patented for use in the wound care industry, including, but not limited to, chitosan-gelatin complex (Sparkes & Murray, 1986), *N*-carboxy-butyl chitosan (Biagini et al., 1991), and 5-methylpyrrolidinone chitosan (R. A. Muzzarelli, Ilari, & Tomasetti, 1993).

Antimicrobial properties (antiviral, antifungal, and antibacterial) have led to chitosan use in the agriculture industry to promote plant growth. Chitosan is now classified as a biopesticide by the Environmental Protection Agency (*Chitin and Chitosan Final Registration Review Decision*, 2008; El Hadrami, Adam, El Hadrami, & Daayf, 2010) (*Chitin and Chitosan Final Registration Review Decision*, 2008). While the exact mechanism for its antimicrobial properties are still not fully understood, the proposed mechanism is related to the interaction between the positive charges on chitosan and the negatively charged microbial cell membrane (Goy, Britto, & Assis, 2009).

Nutritional companies have announced chitosan's ability to act as a dietary supplement for weight loss, claiming that its cationic properties enable it to bind negatively charged lipids, which subsequently reduces their absorption from the gastrointestinal tract (Deuchi, Kanauchi, Imasato, & Kobayashi, 1995; Zacour, Silva,

Cecon, Bambirra, & Vieira, 1992). There have been several studies and literature reviews, however, that have refuted such claims. Warning letters issued by the U.S. Food and Drug Administration (FDA) to several of these companies are based on a lack of scientific evidence to support such claims (*List of Distributors Receiving Warning Letters for Weight Loss Products*, 2015; Mhurchu, Dunshea-Mooij, Bennett, & Rodgers, 2005).

Perhaps most important to its use in pharmaceutical dosage forms is the mucoadhesive properties of chitosan as well as its ability to increase permeability and bioavailability (Bowman & Leong, 2006). Due to its positive charges, chitosan is able to bind to negatively charged cell membrane proteins, which has been demonstrated to increase paracellular permeability and decrease the trans-epithelial electrical resistance of cell monolayers (Artursson, Lindmark, Davis, & Illum, 1994; Dodane, Amin Khan, & Merwin, 1999). Interaction with the tight junction proteins, occludin and zona occludens 1 (Smith, Wood, & Dornish, 2004), leads to a destabilization of the plasma membrane (Dodane et al., 1999; Fang, Chan, Mao, & Leong, 2001; Thanou, Verhoef, & Junginger, 2001). These properties have been shown to be dependent on the molecular weight and degree of deacetylation of the chitosan (Schipper, Varum, & Artursson, 1996) and also dependent on the pH in the intestinal microenvironment (Bowman & Leong, 2006). The positive charges on the chitosan enable it to bind to the negatively charged glycoproteins that are present in mucus (Deacon et al., 2000).

There have been several submissions to the FDA to determine whether or not chitosan should be considered for "Generally Regarded as Safe (GRAS)" status. Based on the recent acceptance (2011) of *Aspergillus niger*-derived chitosan as GRAS per its intended use as filed by KitoZyme S.A., there are hopes that the FDA will soon consider

chitosan in general to have GRAS status (*Agency Response Letter GRAS Notice No. GRN 000397*, 2011).

Modified Release Formulations

> Modified release dosage forms as defined by Perrie and Rades (2012) are: Dosage forms whose drug release characteristics of time course and/or location are chosen to accomplish therapeutic or convenience objectives not offered by conventional dosage forms such as a solution or an immediate-release dosage form. Modified-release solid oral dosage forms include both delayed- and extended-release drug products.

Delayed release is most often used when side effects of a drug are to be avoided or when drug delivery is targeted for a specific area (Ummadi, Shravani, Rao, Reddy, & Sanjeev, 2013). This is most frequently achieved by applying an enteric coating to the dosage form, which allows for pH modulated release of drug. This can inhibit drug release in the gastric fluid to avoid irritation to the stomach or to protect a drug that will degrade at the acidic pH or due to a pepsin-catalyzed enzymatic reaction. Enteric coatings have even been used to target drug delivery to the colon for indications such as Crohn's disease or ulcerative colitis (Beattie & Walker-Smith, 1994; Guthy, 1996; Norlander, Gotthard, & Strom, 1990).

Conversely, controlled release dosage forms are a specialized form of sustained release aimed to deliver drug at a constant rate, typically with zero order release, to predictably maintain drug plasma levels within the therapeutic window (Perrie & Rades, 2012; Ummadi et al., 2013). As a result, controlled release is more difficult to obtain than sustained release using solid oral dosage forms and thus may require alternate means

of administration such as transdermal, subcutaneous, vaginal, or rectal (Chien & Swarbrick, 1992). The goal of controlled release dosage forms is to produce well defined and reproducible means of maintaining therapeutic drug plasma levels for longer periods of time than traditional immediate release dosage forms (X. Chen, Wen, & Park, 2010; Levina & Rajabi-Siahboomi, 2004).

The primary advantages of these dosage forms are a reduced frequency of dosing (Kojima, Yoshihara, Sawada, Kondo, & Sako, 2008) that inevitably leads to increased patient compliance (Maderuelo, Zarzuelo, & Lanao, 2011); an absence or reduction in side effects associated with "dose dumping" or elevated plasma drug concentrations (Maderuelo et al., 2011); and cost effective manufacturing as a reduced number of doses are needed when compared to immediate release products (Maderuelo et al., 2011; Ali Nokhodchi, Raja, Patel, & Asare-Addo, 2012). The disadvantages of these dosage forms can be that specialized equipment or modes of manufacturing may be required to produce the desired effects; release rates, depending on the polymers used, may be highly dependent on intestinal conditions (e.g., fasted versus fed, pH, or ionic strength); and any damage to the integrity of the dosage form (e.g., capping, erosion, or fracture), could significantly impact the release pattern of the drug (DiMatteo & DiNicola, 1982; Jayanthi, Manna, Madhusudhan, Mohanta, & Manavalan, 2011; Sansom, 1999).

Sustained release drug delivery is often broken down into five categories based on the unique mechanism of release: diffusion-controlled, dissolution-controlled, erosion, ion exchange resins, and transport control or osmotic pump systems (Aulton & Taylor, 2013; Chien & Swarbrick, 1992). In practice, many of these systems overlap in the mechanism observed in the final dosage form.

Diffusion-controlled systems utilize an insoluble polymer that controls the penetration of solvent into the system, which eventually leads to dissolution of drug and diffusion out of the polymer system (Ummadi et al., 2013). Diffusion-controlled systems can be further divided into reservoir and matrix release systems. In a reservoir system (see Figure 2.2), drug is encased in a permeable polymer barrier controlling the release of drug typically through pores in the membrane (Stevenson, Santini, & Langer, 2012). The critical components of such a system include the pore former concentration, plasticizer, and the membrane thickness (Siew, 2013). Ethylcellulose is a material commonly used in reservoir systems as the insoluble polymer (Heng, Chan, & Ong, 2003; Iyer, Hong, Das, & Ghebre-Sellassie, 1990; Parikh, Porter, & Rohera, 1993; Porter, 1989; Wakerly, Fell, Attwood, & Parkins, 1997). Chitosan performed as a pore former in a membrane controlled drug delivery system (Liu et al., 2007). Different levels of enteric coating were able to prevent the formation of these pores in the cellulose acetate membrane until the device arrived at the colon where bacterial enzymes degraded the chitosan in the cellulose acetate membrane.

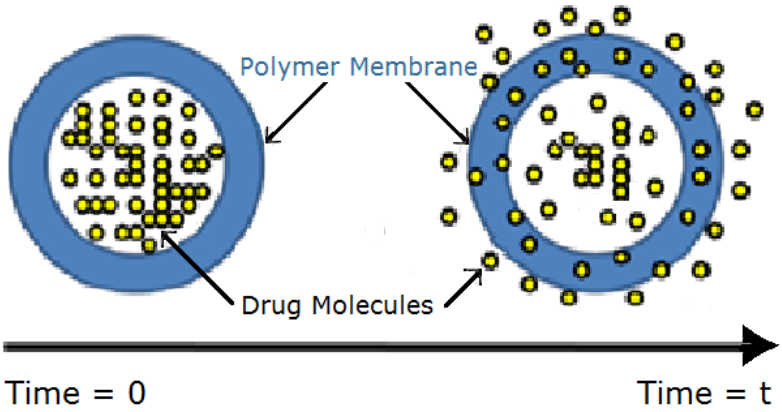

Figure 2.2. Diagram of a Reservoir System (Reproduced with permission from author with minor modifications; licensed under Creative Commons Attribution-NonCommercial 4.0 International Public License - https://creativecommons.org/licenses/by-nc/4.0/legalcode)
(Ali Nokhodchi et al., 2012)

In a diffusion-controlled matrix system, drug is uniformly dispersed throughout a hydrophilic or hydrophobic polymer. This use of hydrophilic matrix systems is the most common method used to provide sustained release in solid oral dosage forms due to their cost effective and reliable means of providing sustained release (Prajapati & Patel, 2010). Drug release from these systems occurs when the polymer, upon contact with the dissolving aqueous medium, swells and forms a gel layer on the polymer surface. The presence of the hydrogel on the surface of the dosage form hinders further diffusion of aqueous medium into the dosage form due to an essentially lost concentration gradient since these hydrogels have a high water content (Hoare & Kohane, 2008). Subsequent drug release from the tablet occurs via drug dissolution and diffusion through the hydrogel matrix, and/or erosion of the hydrogel (Colombo, Bettini, Santi, & Peppas, 2000; Tiwari & Rajabi-Siahboomi, 2008). Various grades of hydroxypropyl methylcellulose (HPMC) are most commonly used polymer in these types of system largely because choosing the appropriate molecular weight of the polymer is a means to obtain the desired degree of sustained release.

In dissolution-controlled systems, release of drug is controlled by slowly dissolving polymers which allows the exposure, dissolution, and release of the drug over time (Ummadi et al., 2013). Similar to diffusion-controlled systems, this can be sub-divided into reservoir or encapsulated dissolution systems as well as matrix dissolution systems (Figure 2.3). In an encapsulated or reservoir system, a drug core is coated with a slowly dissolving polymer. Thus, the rate of dissolution of the polymer and thickness of the polymer layer are critical to the extent of sustained release observed. In these systems, there are typically pellets with varying levels of coating thickness to allow sustained release over a broader time. In the matrix dissolution system, drug is uniformly dispersed, and release of drug is directly dependent on the rate of dissolution of the polymer.

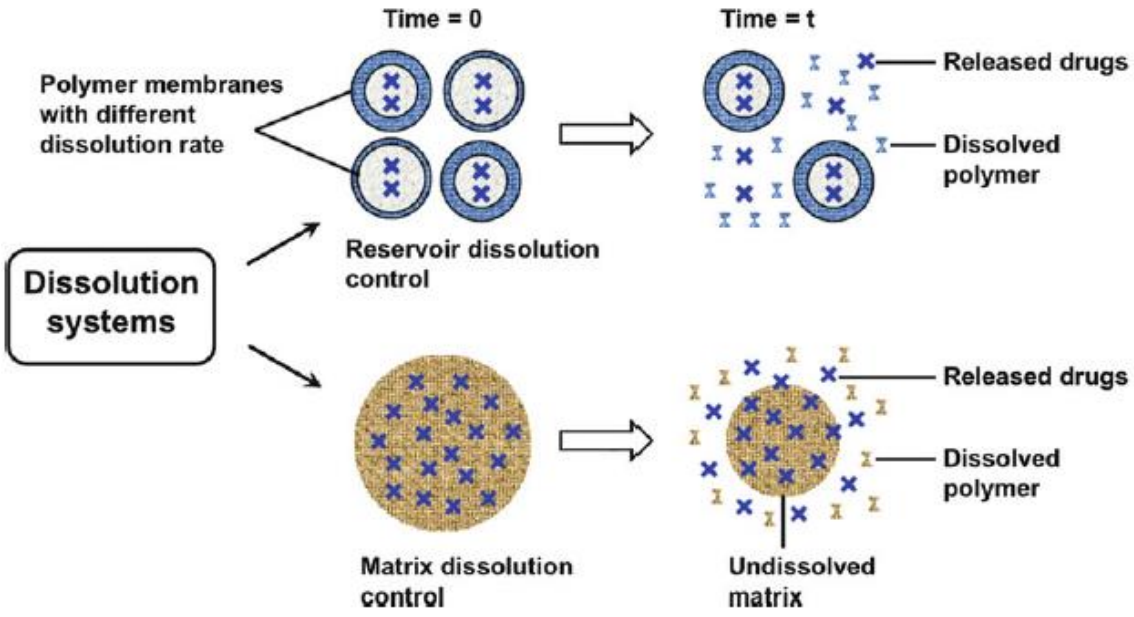

Figure 2.3. Examples of Dissolution Controlled Systems (Reproduced with permission by Springer and Copyright Clearance Center under License #410500597164) (Huynh & Lee, 2014)

In erosion systems, drug is dispersed within a biodegradable, non-toxic polymer upon which drug release depends on erosion or degradation of the polymer (Figure 2.4)

(Ummadi et al., 2013). As a result, these systems are popular for implantable and injectable applications and among the most commonly used bases for these systems are polylactic acid (PLA) and polylactic acid-co-glycolic acid (PLGA) (Siegel & Rathbone, 2012). Erosion of the system can occur throughout the bulk of the system or only at the surface of the dosage form and can occur as a result of several mechanisms (e.g. hydrolysis or enzyme-catalyzed degradation of the polymer). Chitosan matrix systems are reported to undergo swelling and enzymatic degradation (Ren, Yi, Wang, & Ma, 2005) leading to a delivery system like that described in Figure 2.4.

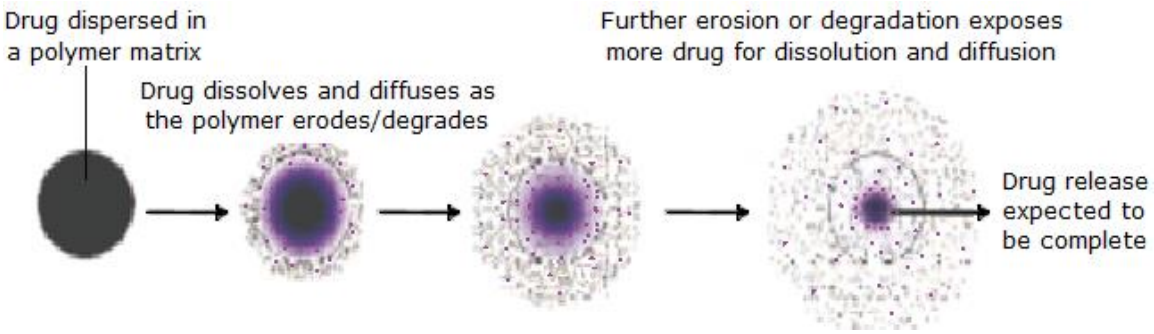

Figure 2.4 Example of an Erosion Sustained Release System (Reproduced with permission of author with minor modifications and permission by Springer and Copyright Clearance Center under License #4106451456312)
(Varma, Kaushal, Garg, & Garg, 2004)

One of the unique and still evolving sustained release delivery systems is known as an osmotic pump drug delivery system, which operate on the principles of osmotic pressure (Mathur & Mishra, 2016). While there are many variations to these systems, the basic components include a semipermeable membrane typically with a laser-drilled orifice for drug release, as well as an active drug layer, and an osmotic agent (Figure 2.5) (Allen & Ansel, 2013). Solvent is taken into the system via the semipermeable membrane where drug is dissolved, while the osmotic agent builds a pressure gradient that pumps drug out of the delivery orifice at a zero order rate (Mathur & Mishra, 2016).

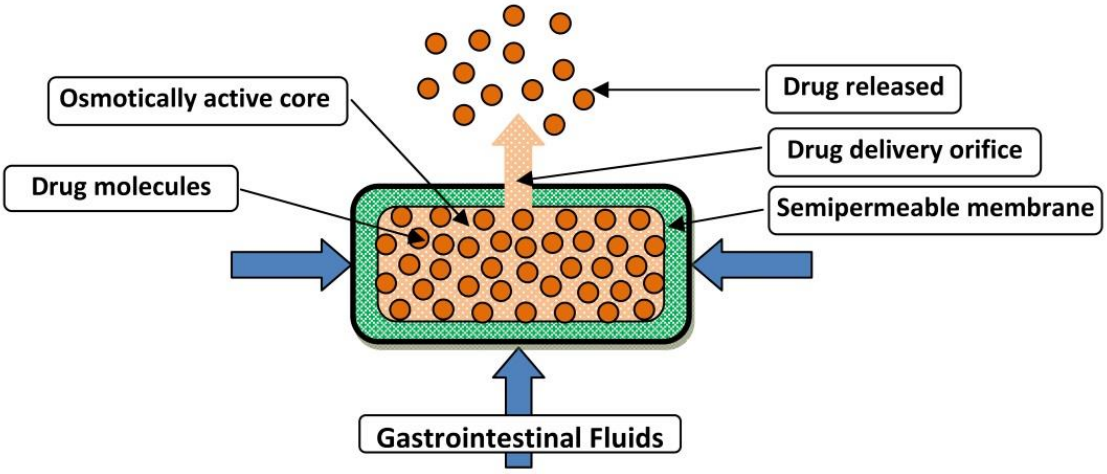

Figure 2.5 Example of an Osmotic Pump Delivery System (Reproduced with permission from author with minor modifications; licensed under Creative Commons Attribution-3.0 Unported - https://creativecommons.org/licenses/by/3.0/legalcode) (Shokri & Adibkia, 2013)

Lastly, in an ion exchange delivery system, drug loaded polymers, referred to as resonates, contain acidic or basic functional groups allowing them to exchange counter-ions with the surrounding solvent (Figure 2.6) (Srikanth, Sunil, Rao, Uhumwangho, & Murthy, 2010). Although chitosan and its derivatives can act as an anion-exchange resin, their applications are largely found in wastewater treatment (S.-T. Lee, Mi, Shen, & Shyu, 2001; Ngah & Isa, 1998) or in biorefinery applications (Sayed & Jardine, 2015; Zeng & Ruckenstein, 1998).

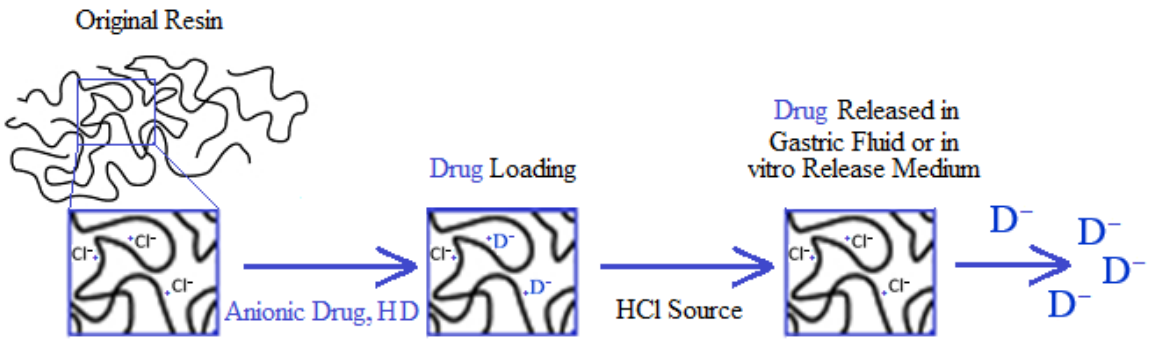

Figure 2.6. Example of an Ion-exchange Drug Delivery System

CHAPTER 3

Ionic Crosslinking of Chitosan-Tripolyphosphate and Statistical Design of Experiments

Introduction

Based on the unique aspect of chitosan as the only naturally occurring cationic polyelectrolyte, chitosan has been used frequently in the formation of nanoparticles and microparticles via crosslinking techniques. Different nanoparticle and microparticle formation mechanisms include, but are not limited to; ionic gelation (Agnihotri, Mallikarjuna, & Aminabhavi, 2004; Pati, 2011; L. Zhang & Kosaraju, 2007), reverse micellular method (Mitra, 2001), emulsion-droplet coalescence (Tokumitsu, 1999), spray drying (He, 1999), and coacervation/precipitation (Nishimura, 1986). The ionic gelation process is simple and takes place under mild conditions, leading to this as the most common and preferred process for chitosan-tripolyphosphate complexation.

Ionic Gelation

Ionic gelation, also referred to as ionotropic gelation or ion-induced gelation, is a technique based on the ability of polyelectrolytes to crosslink (i.e. form a complex) in the presence of counter ions, resulting in the formation of a hydrogel (Patil, 2012). If prepared in the form of hydrogel beads they are sometimes referred to as gelispheres. Hydrogel beads are typically spherical in shape and in the nanoparticle or microparticle size range depending, at least in part, on the extent of crosslinking. The ionic gelation process can be performed completely in aqueous media without the use of organic solvents, an important consideration for the pharmaceutical industry, further lending to its convenience (Y. L. Wang, Puwang; Truong-Dinh Tran, Thao; Zhang, Juan; Kong, Lingxue, 2016).

A diagram of the simple ionic gelation process and an example of the chitosan-tripolyphosphate crosslinked structure can be seen in found in Figures 3.1 and 3.2, respectively.

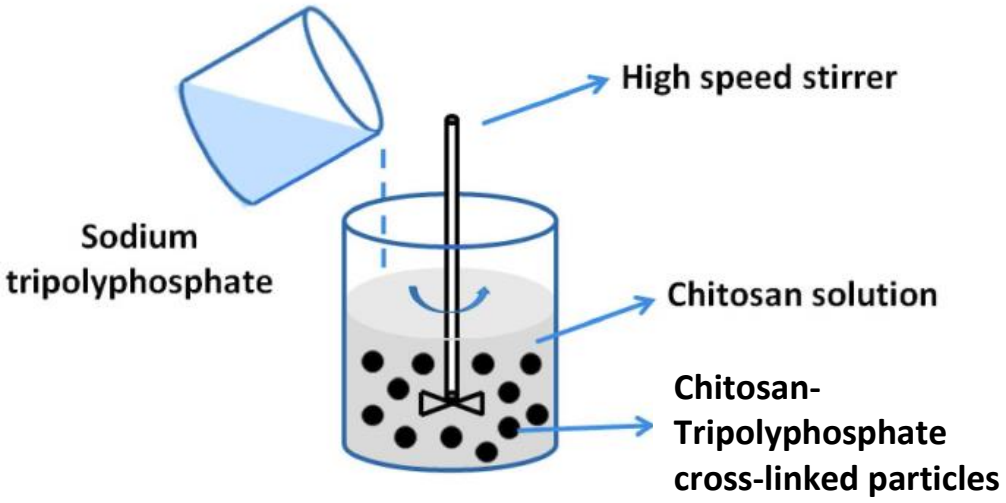

Figure 3.1. Sodium Tripolyphosphate Solution and Chitosan-Tripolyphosphate Crosslinked Particles (Reproduced with permission from author with minor modifications; licensed under Creative Commons Attribution 4.0 International Public License - https://creativecommons.org/licenses/by/4.0/legalcode)
(Y. L. Wang, Puwang; Truong-Dinh Tran, Thao; Zhang, Juan; Kong, Lingxue, 2016)

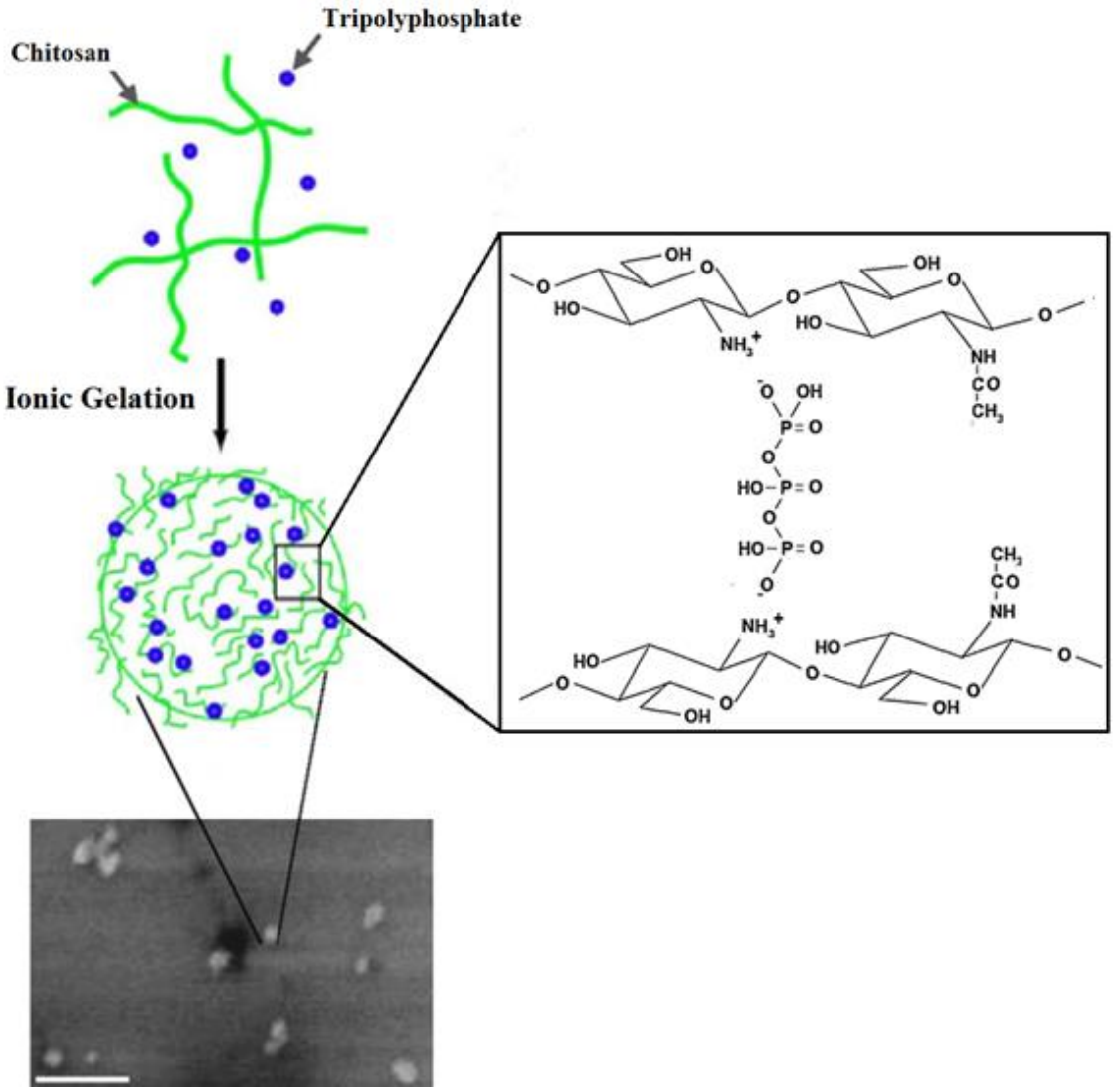

Figure 3.2. Formation of Chitosan-Tripolyphosphate Complex by Ionic Gelation (Reproduced with permission by American Society for Microbiology Journal for the sole purposes of doctoral dissertation as defined by the RightLink® Copyright Clearance Center) (Chávez de Paz, 2011)

As it relates to chitosan and tripolyphosphate, ionic gelation is quite simple. Chitosan is first solubilized in acidic solution (i.e. dilute acetic acid), producing a cationic structure due to the protonation of the amine group. Secondly, an anionic solution of tripolyphosphate is added slowly to the chitosan solution under gentle agitation resulting in instantaneous ionic crosslinking and formation of the chitosan-tripolyphosphate particles. While it's a simple process, there are multiple formulation and process variables than can be manipulated during this process that will have a significant impact on the resulting chitosan-tripolyphosphate particles produced. Systematic evaluation of these factors and a full understanding of their interaction are required to generate a product with desired properties for further pharmaceutical use.

While not specifically speaking to the crosslinking of chitosan and tripolyphosphate, the kinetics of gelation are well described in the following steps:

> In a first step (induction period), doublets of macromolecules are formed leading to a slow rise in viscosity. In the second step (pregel) period the relative viscosity increases very significantly as the system tends to percolate. The third step (size-limitation) begins as soon as microgels reach a size large enough to be broken by the viscous forces exerted by the surrounding medium. The fourth step ending the process is the consolidation/maturation of aggregates by formation of new intermolecular and intra-aggregates crosslinks. These new crosslinks shrink more and more microgels so that the system viscosity decreases even in the absence of rupture of the bonds already formed (Omari, Chauveteau, & Tabary, 2003).

They continue to explain that the four steps are activated by a very short “polymer activation period” in which the crosslinking agent (i.e. tripolyphosphate) affixes itself to at least one end of the polymer side group; the protonated amine in the case of chitosan.

Analysis of particular responses during this gelation process will help elucidate how each of these particular steps may be influenced by changes to both process and formulation.

Effect of Ionic Gelation Process and Formulation Variables on Chitosan-Tripolyphosphate (Ch-TPP) Crosslinking

Chitosan Molecular Weight Influence

The effect of chitosan molecular weight on the final characteristics of Ch-TPP nanoparticles or microparticles is among the most studied factors due to the extensive breadth of molecular weight in commercially available chitosan products, which can range from 50-2000 kDa (Rege, 1999). Generally speaking, an increase in chitosan molecular weight typically leads to an increase in size of the resulting particles (Gan & Wang, 2007; Gan, Wang, Cochrane, & McCarron, 2005; Hu et al., 2008; Nguyen, 2016; Rampino, 2013; Wu, Yang, Wang, Hu, & Fu, 2005). This is expected due to the longer polymer chain lengths associated with higher molecular weight samples, which subsequently results in greater opportunities for intra-molecule crosslinking and an overall increased number of intermolecular crosslinking sites within a single polymer chain. Hu et al. also observed that the particle size range, as measured by the polydispersity index (PDI), also increased with increased molecular weight, which was attributed to shearing degradation of the larger polymer strands resulting in the presence of chains of varying lengths.

In the literature, there are mixed reports on the effect of chitosan molecular weight on the particle zeta potential (Gan & Wang, 2007; Gan et al., 2005; Hu et al., 2008; Nguyen, 2016; Rampino, 2013; Wu et al., 2005). This variation is likely due to differences in the degree of deacetylation associated with the different isolated molecular weight chitosan samples used in these experiments, which is often unknown or not reported. Since exposure to a high concentration of sodium hydroxide is typically used to deacetylate the chitosan amines (Paul, Jayan, Sasikumar, & Cherian, 2014), but also

results in a reduction in molecular weight, the lower the molecular weight of the chitosan sample, the more likely the chitosan also possesses a higher degree of deacetylation (%DD) (Paul et al., 2014). A higher %DD in turn would result in an increase in the number of primary amine groups that are subsequently protonated when chitosan is in solution. Thus, increased %DD should increase the zeta potential for a given molecular weight.

Another common observation is that encapsulation efficiency of an active ingredient increased with an increase in chitosan molecular weight (Gan & Wang, 2007; Hu et al., 2008; J. Ko et al., 2002; Wu et al., 2005; Y. Xu & Du, 2003). This is generally attributed to the ability of longer chains to entangle and thus more efficiently entrap an active ingredient. Xu, et al., observed an increase in encapsulation efficiency of bovine serum albumin from 7% to 19% as chitosan molecular weight increased from 30 kDa to 210 kDa. The ability to more effectively entrap active ingredient at higher chitosan molecular weights also typically leads to an observation of slower release as the active is unable to escape readily from an entangled and crosslinked matrix. Gan and Wang observed 20% and 60% release of BSA at 6 hours when entrapped using low molecular weight and comparatively high molecular weight chitosan, respectively.

Effect of Chitosan Concentration

As one might expect, the impact of chitosan concentration on the characteristics of chitosan-tripolyphosphate particles are similar to those observed for chitosan molecular weight. An increase in chitosan concentration leads to linear increase in particle size and less uniform particle size when crosslinked with tripolyphosphate (Calvo, 1997; Dong, 2013; Dudhani & Kosaraju, 2010; Fan, 2012; Gan & Wang, 2007;

Gan et al., 2005; Hu et al., 2008; Vaezifar, 2013; Wu et al., 2005; Y. Xu & Du, 2003). In dilute solutions, chitosan chains remain sufficiently separate from one another to allow uniform crosslinking with tripolyphosphate, resulting in denser and smaller particles. Conversely, as chitosan concentration increases, the proximity of the molecules results in entanglement and aggregation of polymer chains in a non-uniform fashion, creating larger and less uniform particles upon crosslinking with tripolyphosphate (Dong, 2013).

With respect to drug loading and subsequent drug release from chitosan-tripolyphosphate particle, chitosan concentration also has a significant effect although that effect can depend on characteristics of the active ingredient (Gan & Wang, 2007; Hu et al., 2008; J. Ko et al., 2002; Wu et al., 2005; Y. Xu & Du, 2003). In separate studies, both Xu et al. and Gan et al. found that increasing the chitosan concentration led to a decrease in the amount of bovine serum albumin encapsulated into chitosan-tripolyphosphate particles. This finding was similar to observations by Wu et al. in the encapsulation of ammonium glycyrrhizinate. Conversely, Hu et al. saw in increase in the encapsulation of tea catechins as chitosan concentration was increased. These findings suggest chemical structure and molecular weight of the active being incorporated could play a critical role in encapsulation. Specifically, larger molecules benefit from lower chitosan concentration where there is ample space to interact with individual chitosan chains, while at higher concentrations, the aggregation of some chitosan molecules inhibits interaction with larger actives, but smaller drugs such as tea catechins are still able to incorporate themselves within the crosslinked matrix (Hu et al., 2008). Irrespective of active ingredient characteristics, increased chitosan concentration tends to result in slower and even incomplete drug release as the interchain crosslinking and

increased packing, stemming from agglomeration of particles, inhibits drug release from the matrix.

Effect of Chitosan:Tripolyphosphate (Ch:TPP) Ratio

The mass ratio of chitosan to tripolyphosphate affects several properties of the resulting crosslinked particles. Based on the ionic charges in solution, it is evident that increasing the Ch:TPP ratio will result in an increase in zeta potential as there will be an excess of protonated amine groups that are not crosslinked with tripolyphosphate ions. Multiple authors (Konecsni et al., 2012; Koukaras, 2012; Rampino, 2013; L. Zhang & Kosaraju, 2007) have shown that a Ch:TPP ratio of approximately 4:1 or 5:1 results in the smallest and most uniform particle size. Slight variations might result from differences in degree of deacetylation amongst the different chitosans used. The increasing particle size at lower ratios can be attributed to greater interchain crosslinking that forms larger particles associated with the presence of more tripolyphosphate ions as well as the reduction in zeta potential which reduces the electrostatic repulsion between particles that can lead to aggregation (Konecsni et al., 2012).

The impact of Ch:TPP ratio on entrapment efficiency and subsequent drug release can vary greatly based on the active ingredient. The ratio of Ch:TPP will affect solution pH and particle charge, which could also influence the charge on the active ingredient depending on the functional groups present (Gan & Wang, 2007). The cationic or anionic nature of the charge will dictate the extent of potential ionic interaction between drug and the chitosan-tripolyphosphate particles. With respect to both tea catechins and bovine serum albumin, it was shown that encapsulation of these active ingredients reduced as Ch:TPP ratios increased from 3:1 to 9:1. The increased drug load at lower

ratios was also shown to produce the fastest drug release and a release pattern revealed that drug release was slowed by an increase in the Ch:TPP ratio (Gan & Wang, 2007; Hu et al., 2008). These relationships suggest that a higher drug loading might inhibit the particle ability to sustain release.

Ionic Strength Influence

The influence of solution media ionic strength has been analyzed with respect to its influence on the resulting size and polydispersity of the nanoparticles with varying results and conclusions. Wu et al. reported an increase in both particle size as well as PDI with increasing salt concentration, which they attributed to a screening of the protonated amines available for crosslinking. This screening leads to aggregation of chitosan molecules and limits the extent of crosslinking that can occur with TPP. Huang and Lapitsky also noted a slight increase in particle diameter in the presence of salt but a decrease in the PDI of the resulting nanoparticles. The particle size increase was attributed to a weakened chitosan-tripolyphosphate interaction; however, the decreased PDI was a result of the screening of additional crosslinking sites on the chitosan chains, which prevented interparticle crosslinking, but was not sufficient screening to undermine the individual particle colloidal stability.

Conversely, Jonassen et al. reported a decrease in particle size in the presence of salt. It was described that in the absence of salt, chitosan will typically exist in a more extended form in solution as there is intra-chain electrostatic repulsion stemming from the protonated amine groups. Upon salt addition and screening of the protonated amines, chitosan chains become more relaxed and tend to fold upon themselves, creating more compact particles. This configuration will result in slower and weaker interactions with

tripolyphosphate, but will also prevent interchain crosslinking due to the number of binding sites shielded by miscellaneous ions. The screening effect and its impact on charges and chain configuration is well represented in Figure 3.3. The observations by all authors with respect to the impact of ionic strength on the formation of chitosan-tripolyphosphate particles strongly suggests that different salt levels will produce varying effects and need to be well understood for a desired product.

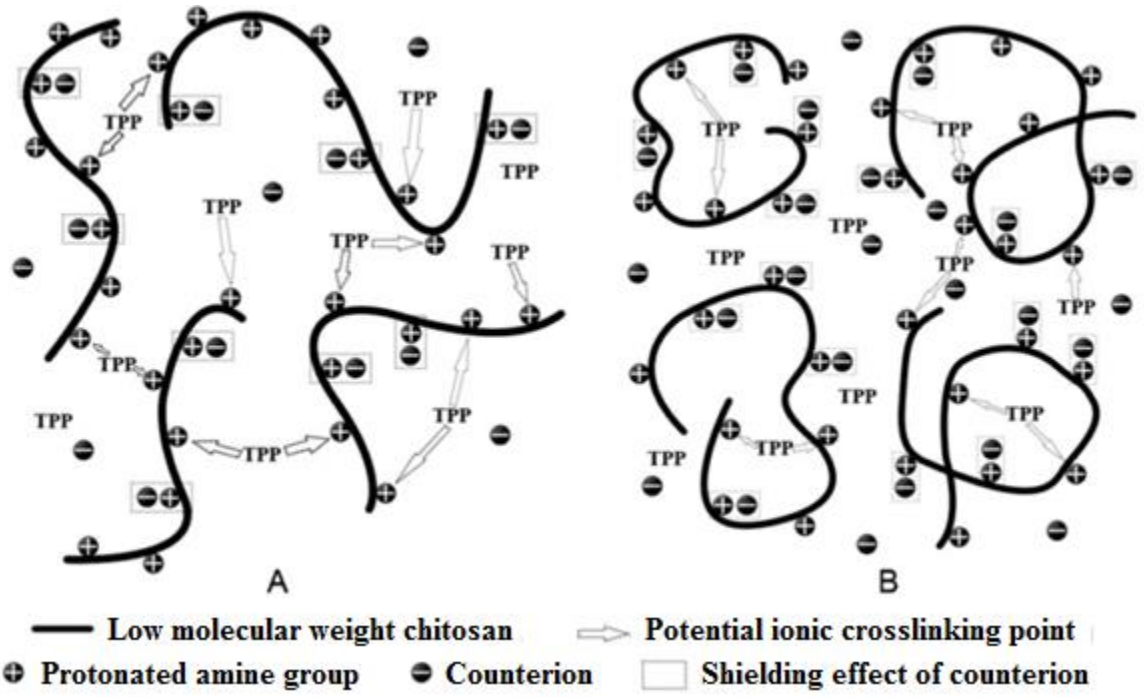

Figure 3.3. Schematic representation of ionic crosslinking reaction between chitosan and TPP in (A) low ionic strength solution and (B) high ionic strength solution (Reproduced with permission by Elsevier and Copyright Clearance Center under License #4105420747437) (Fan, 2012)

Effect of pH

Acknowledging that the opposite charges on chitosan and tripolyphosphate are responsible for the attraction between the two together that results in ionic gelation, one can expect that changes in pH have a significant impact on the extent of crosslinking. With a pKa of approximately 6.5 for the acid form of chitosan (Samal, 2012), a decrease in pH will result in an increase in the number of protonated amine groups on the polymer chain and subsequently more opportunities for crosslinking. Conversely, with five pKa values at approximately 1.0, 2.2, 2.3, 5.7, and 8.5 (Lim, 1993), the extent of tripolyphosphate ionization diminishes with a decrease in pH, as negatively charged oxygen groups become protonated, reducing the number of available sites for crosslinking.

Gan et al. and Hu et al. reported similar patterns in the effect of pH as it relates to both particle size and zeta potential. Above a pH of 5.5, a drastic increase in the zeta potential was observed, which correlates to a point at which the degree of ionization of chitosan begins to precipitously drop (Shu, 2002). The decrease in zeta potential above pH 5.5 also resulted in an increase in particle size, suggesting that the reduction in surface charge decreased the electrostatic repulsion between individual particles, leading to aggregation. Interestingly, a trough has been observed with respect to both particle size and zeta potential in the pH range 4.0-5.5 (Gan et al., 2005; Hu et al., 2008; L. Zhang & Kosaraju, 2007). This suggests that, depending on the molecular weight of chitosan used and the ratio of chitosan:TPP present, there exists an optimal pH where complete ionization of chitosan exists and enhanced ionization of tripolyphosphate occurs leading

to a drop in zeta potential. In this same pH range, the optimal ionization leads to enhanced crosslinking density within individual particles and a reduction in size.

Temperature Influence

The impact of temperature on the formation of chitosan-tripolyphosphate particles has been assessed in only a few studies. Fan et al. observed a decrease in the particle size from 200 nm to approximately 140 nm when the solution media was increased from 10 to 70 °C. The decrease was drastic from 10 to 50 °C, greater than 50 nm, while less than a 10 nm decrease was observed as the media temperature was raised from 50 to 70 °C. As temperature increases, the intrinsic viscosity of the solution decreases and a decrease in the ratio of radius of gyration to average molecular weight of the chitosan is observed (R. H. T. Chen, M. L., 1998). Greater flexibility within the polymer chain and subsequent folding upon itself result in smaller, more dense particles. Additionally, it was reported that the increased temperature results in a reduction in hydrogen bonding between water molecules and chitosan chains, decreasing the specific volume of the chitosan molecule (Noguchi, 1981).

On assessing the impact of temperature as it pertains to the storage and stability of chitosan-tripolyphosphate nanoparticles, Morris et al. observed only a slight decrease in particle size over 12 months when stored at 4 or 25 °C. However, when stored at 40 °C, particle size showed significant reduction after just one month and particles were virtually non-existent after 6 months (Morris, 2011).

Influence of Mixing Time and Mixing Speed

The effect of mixing time upon addition of tripolyphosphate to chitosan solution has been evaluated as it relates to drug release from the resulting particles (J. Ko et al., 2002) and particle size (Vaezifar, 2013). Ko et al. observed slowest release of felodipine from particles that had been prepared via 60 minutes of mixing. The rate of release increased when mixing was decreased to 30 minutes and showed the greatest increase when mixing time was reduced to 15 minutes. The data indicate that an increase in mixing time might allow greater crosslinking of chitosan and tripolyphosphate, creating a denser matrix that provides slower drug release. Vaezifar et al. reported a decrease in particle size as mixing time was increased from 30 to 60 minutes but an increase in particle size when mixing time was increased to 90 minutes, suggesting that beyond 60 minutes, aggregation might begin to occur.

Several studies have demonstrated a decrease in particle size with an increase in mixing speed (Fàbregas, 2013; Fan, 2012; Shirsat, 2015). However, there might be a limit to this effect. Beyond 800 rpm, an increase in mixing speed increased the PDI (Fàbregas et al.) but a decrease in product yield was observed (Shirsat et al.). While optimal speeds are specific to each case, the data suggest that, at some point, a higher mixing speed could generate a shear force sufficient to break the ionic crosslinking or to disrupt the repulsive forces between individual particles leading to aggregation (Fan, 2012).

Statistical Experimental Design

Statistical experimental design, also known as design of experiments (DOE), is a systematic approach to determine the relationship between the parameters of a process or formulation (factors) and their impact on a specific process output or product characteristic (response). Factorial design, a commonly used DOE approach, was first introduced by R.A. Fisher in 1926, and represents a means to simultaneously assess the effect of various factors on multiple responses, the relative importance of each effect, and any interactions between factors that may exist (Armstrong, 2006). Analysis of such interactions is something that cannot be accomplished using the traditional one-factor-at-a-time (OFAT) approach to experimentation. For an experimental design, factors can be quantitative or qualitative. Quantitative factors require established specified levels to allow later data analysis. These levels should be carefully selected based on initial screening experiments or previous knowledge of a factor's range known to affect a response. Responses represent a measurable output or characteristic of the experiment that can be assigned a numerical value for data analysis and the generation of model equations that describe the relationship between factor levels and their influences on responses.

In instances where a large number of factors are being evaluated, a fractional factorial design is often utilized. This is because the number of experiments for a full factorial design grows exponentially, becoming cost-prohibitive and a significant investment in time. A fractional factorial design allows evaluation of both main factor and binary interaction contributions to responses with half (for a half-fraction factorial design) the number of experiments required (Howard, Neau, & Sack, 2006). While

higher order interactions cannot be estimated (i.e. interactions involving three factors or more), such interactions are rare and typically have negligible effect on responses (Armstrong, 2006). A two-factor interaction is one where the level of factor X influences the impact that factor Y has on a particular response, such that in the absence of X, Y may have a reduced or completely different effect on the response. Resolution is the terminology used to classify the extent of aliased effects in a fractional factorial design (Oehlert, 2010). As described by Oehlert, "A resolution *R* design is one in which no interaction of *j* factors is aliased to an interaction with fewer than $R - j$ factors." Thus, for a five factor, two-level, half fractional factorial design (2^{5-1}), its resolution of 5 (V) indicates that no main effect is aliased with another main effect, a two-factor interaction, or a three-factor interaction; but a main effect can be aliased with a four-factor interaction and a two-factor interaction can be aliased with a three-factor interaction.

For a two-level design, inclusion of center point experiments is encouraged as this not only increases the degrees of freedom, but more importantly, allows a measure of pure error (purely random error) that cannot be controlled when modifying the levels of the factors and facilitates an analysis for the presence of curvature in a response when factors levels are increased (Montgomery, 2008). The mistake of not including centerpoint experiments in a design can lead one to falsely believe that a response behaves linearly over the design space since a linear model may adequately describe the factor level extremes correctly but misrepresents the space in between.

Once experiments are completed at the pre-defined factor levels and all responses are measured, analysis of variance (ANOVA) is the statistical tool used to evaluate main factor and two-factor interactions that have a statistically significant impact on the

response and the magnitude of that impact. Run order is randomized to eliminate any potential bias experienced during the execution of a design. Additionally, an experimenter should make the effort to see that all runs are performed in exactly the same way, with only changes to the factor levels themselves so as to allow for analysis as a single block of experiments. When ANOVA identifies that significant curvature is present in a two-level fractional factorial design, this typically indicates that the response cannot be described using a first order model, and that the design must be augmented to consider higher order model equations (e.g., model equations with quadratic terms). Similarly, a measure of "lack of fit" is an ANOVA tool used to determine if a particular model can adequately describe a response. Significant lack of fit may indicate that a higher order model is required or that the data should be transformed prior to ANOVA.

When significant lack of fit or curvature is indicated, a central composite design is commonly used to augment the factorial design. Central composite designs fall under a broader category called response surface designs. In this second block of experiments, additional runs are performed at axial points and center points. Depending on limitations for the factor ranges, the axial points may be at the factor limits in the original design space or could extend beyond the initial design space in an effort to define the curvature in the response to factor level changes by expanding the data or the number of factor levels, respectively. The intent of the response surface method approach is really to understand the landscape of the response over the entire design space (Oehlert, 2010). This enables an experimenter to understand where minimum and maximum values for a response can be found within the design space and to predict a response at any given pre-defined set of factors within that design space. To aid in the visualization of how a

response will change over the design space, 3-D contour plots are most commonly generated.

When performing ANOVA, there are times when transformation of the data is required. Transformations are used when non-transformed data cannot be used to generate a statistically significant model, but a transformation of the data (e.g., a square root or logarithmic transform) allows a model in which assumptions basic to the appropriate use of ANOVA, such as a normal distribution of error, are not violated over the design space evaluated (Oehlert, 2010). A Box-Cox Plot is a tool often used to identify the most appropriate transformation for a given response. A Box-Cox Plot determines the power (λ) transformation by performing ANOVA following use of a range of λ values such that the value that best reduces the sum of squares error (a measure of total variability) is recommended (Oehlert, 2010). The Box-Cox Plot recommended λ value is often very specific, for example -1.126, or it is subsequently rounded to a number with a reduced number of significant figures.

When performing ANOVA on the results from a factorial design of experiments to derive a statistically significant model equation to describe a response, backwards hierarchical regression is the preferred approach. Using this method, one can eliminate terms in the model equation that are not significant as indicated in the ANOVA table by a *p*-value higher than the alpha value chosen for significance. One starts with a model equation that includes all possible terms. Then one systematically eliminates one by one those terms that are not significant based on the highest *p*-values observed in the ANOVA table, starting with the most complex terms (e.g. quadratic terms). During the elimination process, hierarchy is maintained by keeping the term in the model equation

for any factor in a two-factor interaction term or a higher order term for that particular factor (Oehlert, 2010). For example, if the term for an interaction between factor A and factor B is deemed significant, by default, the terms for factor A and factor B cannot be eliminated from the model equation irrespective of the *p*-value for these main factor terms.

Once a model equation is established, certain plots of the relevant data can provide much information on characteristics of the data as a whole or of individual experiments within the experimental design. Residuals are the differences between the predicted response value derived from the model equation using factor levels defined for a particular experiment and the actual response value measured during experimentation. Residuals that are normalized as a function of standard deviation are further referred to as internally studentized residuals. A probability plot that confirms the random distribution of internally studentized residuals is known as a Normal Plot of Residuals. This plot, which presents a cumulative frequency analysis of residuals from lowest to highest, displays a straight line when residuals are characterized as a normal distribution of error. Deviation from linearity may indicate an outlier exists or an improper model equation was chosen to describe the data. A plot of internally studentized residuals versus predicted values provides a further means to assess the appropriate fit of a model equation and to seek out outliers. In this Residuals vs. Predicted Plot, residuals should be randomly scattered (both negative and positive values) around the horizontal line where the residual value is set to zero. Residuals greater than three standard deviations from this line are typically flagged as evidence of potential outliers. Outliers represent an extremely abnormal response value compared to those associated with the remaining

experimental runs and can be expected in designs that include a higher number of experiments or when complex procedures were used. When outliers are observed, the experimental conditions can be repeated to confirm or refute the previously obtained response value, average the response values obtained, or eliminate the data point from consideration. Elimination of the single data point is more common in designs involving a greater number of experiments as ANOVA can still be performed in the absence of a single or even a few data experiments.

Upon completion of an experimental design, one can expect to arrive at a statistically significant model equation for each response in the fashion of:

$$Y_1 = \beta_0 + \beta_1 X_1 + \beta_2 X_2 + \ldots \beta_{12} X_1 X_2 + \beta_{13} X_1 X_3 + \ldots \beta_1 X_1^2 + \beta_2 X_2^2 + \ldots$$

where Y_1 represents a particular response, β_0 is the average of the responses Y_1, β_i represents the different coefficients for each term generated by ANOVA, and X_i represents the different factors established as significant with respect to the particular response. Terms included can be derived from main factor effects, interaction effects, quadratic effects, or even higher order effects depending on the number of experiments and particular design used.

With the established models, optimization of responses can be performed particularly in cases where a response surface method has been used. This optimization is simplified using statistical software such as Minitab from Minitab Inc. (State College, PA) or Design Expert from StatEase (Minneapolis, MN). Optimization using such software can allow you to target a desired response value or identify a minimum or maximum in a response with a weighted importance on conditions established for each factor or response, resulting in combinations of factor levels within the design space

evaluated that most probably produce the desired response. A Desirability is assigned to each suggested combination to indicate how well the combination of factor levels achieved the desired goals.

CHAPTER 4

Evaluation of Chitosan-Tripolyphosphate via Statistical Design of Experiments

Introduction

In this chapter, the formation of Chitosan-Tripolyphosphate crosslinked substance via ionic gelation has been investigated. The effects of formulation and process variables on the characteristics of the crosslinked substance and their impact on dissolution of a model drug was studied using a five factor, two-level, half-fractional factorial design with center points as a screening design (19 total experiments). Based on statistically significant ($p < 0.05$) curvature observed in multiple responses, the design of experiments (DOE) was expanded to a central composite design, which included an additional ten experiments plus two additional center points for a total of 31 total experiments.

Materials

Powdered chitosan, purchased from DCV BioNutritionals (Wilmington, DE), with a 92% degree of deacetylation and an average molecular weight of 470 kD (Omwancha, Kouba, Yelamanchili, & Neau, 2011) was used for all experiments. Sodium tripolyphosphate (NaTPP) was purchased from Sigma-Aldrich (St. Louis, MO). Acetaminophen from Mallinckrodt Pharmaceuticals (St. Louis, MO) was used as a model active pharmaceutical ingredient (API) for dissolution testing. Hydrochloric acid, 37%; glacial acetic acid, ≥ 99.7%; and sodium hydroxide were all purchased from Fisher Scientific (Fair Lawn, NJ).

Methods

Statistical Design

A five factor, two-level, half-fractional factorial design with three center points was generated using Design Expert® software version 10.0 (StatEase, Minneapolis, MN). The design was subsequently expanded to a face-centered cube, central composite design with an additional two center points using the Design Expert® software. The five factors included the chitosan concentration in solution, the mass ratio of chitosan to tripolyphosphate (Ch:TPP) in the final solution, the pH of the solution just prior to initiation of crosslinking, the temperature of the solution, and the concentration of NaCl added to the solution. The levels used for each factor in the experimental design are presented in Table 4.1. The factor levels and response values for each of the experimental runs for the initial two-level, half-fractional factorial design and for the expanded central composite design are presented in Table 4.2 and Table 4.3, respectively. Factor levels in Table 4.2 and Table 4.3 are coded using -1, +1, and 0 representing high, low, and center point settings, respectively. Analysis of variance (ANOVA) was performed as previously defined in chapter 3 and strictly following the Design Expert® software guidance and recommendations.

Table 4.1. Experimental design factor levels for Ch-TPP crosslinking

Factors		Levels		
		Low (-1)	Center Point (0)	High (1)
A	Chitosan Conc. (mg/ml)	1	3	5
B	Ch:TPP Ratio	1	3	5
C	Temperature (°C)	25	45	65
D	pH	3	4	5
E	NaCl Conc. (mM)	0.00	0.01	0.02

Table 4.2. A five factor, two-level, half-fractional factorial design (2^{5-1}) with three center points and responses for each experimental run

Run Number	A	B	C	D	E	d50 (μm)	Span	True Density (g/ml)	Zeta Potential (mV)	Yield (%)	t_{50} (min)	t_{90} (min)
11	-1	-1	-1	-1	1	0.235	13.540	1.568	6.4	63.41	32	168
13	1	-1	-1	-1	-1	2.591	46.959	1.613	4.1	67.09	87	331
12	-1	1	-1	-1	-1	0.187	3.212	1.655	51.8	20.72	168	614
1	1	1	-1	-1	1	0.794	99.981	1.800	51.5	65.40	32	606
19	-1	-1	1	-1	-1	0.239	7.932	1.656	7.7	66.57	80	295
2	1	-1	1	-1	1	1.226	70.690	1.898	5.5	79.50	216	595
14	-1	1	1	-1	1	0.170	2.424	1.694	40.5	49.50	206	669
15	1	1	1	-1	-1	0.313	4.024	1.599	50.7	59.04	148	532
7	-1	-1	-1	1	-1	0.233	9.656	1.636	7.6	73.23	137	390
4	1	-1	-1	1	1	0.872	73.867	1.689	0.3	75.53	169	492
9	-1	1	-1	1	1	0.221	4.327	1.575	20.3	79.38	134	435
16	1	1	-1	1	-1	0.763	92.870	1.550	36.6	85.85	94	304
18	-1	-1	1	1	1	0.159	5.778	1.665	5.6	88.17	181	545
17	1	-1	1	1	-1	0.199	6.221	1.618	4.6	94.30	214	692
3	-1	1	1	1	-1	0.615	77.951	1.899	25.6	66.82	343	1052
5	1	1	1	1	1	0.726	148.096	1.727	30.2	79.87	84	273
8	0	0	0	0	0	0.217	8.918	1.634	23.2	95.11	214	694
6	0	0	0	0	0	0.236	10.573	1.612	21.0	93.89	151	488
10	0	0	0	0	0	0.240	10.645	1.644	24.4	94.43	322	1042

Table 4.3. Additional experiments to expand initial five factor, two-level, half-fractional factorial design to a central composite design with an additional two center points and responses for each experimental run

Run Number	A	B	C	D	E	d50 (μm)	Span	True Density (g/ml)	Zeta Potential (mV)	Yield (%)	t_{50} (min)	t_{90} (min)
20	-1	0	0	0	0	0.202	5.102	1.845	22.6	84.27	270	874
21	1	0	0	0	0	0.287	9.136	1.653	22.6	91.71	205	664
22	0	-1	0	0	0	0.225	10.183	1.666	2.8	64.56	292	851
23	0	1	0	0	0	0.205	3.650	1.617	37.8	60.99	180	585
24	0	0	-1	0	0	0.217	14.345	1.614	27.6	92.98	245	895
25	0	0	1	0	0	0.810	96.702	1.623	29.1	93.73	242	784
26	0	0	0	-1	0	0.198	5.969	1.610	32.7	91.36	118	382
27	0	0	0	1	0	0.929	130.504	1.588	23.0	96.50	455	1361
28	0	0	0	0	-1	0.235	8.126	1.607	27.7	95.96	293	951
29	0	0	0	0	1	0.230	8.400	1.605	23.9	96.47	261	846
30	0	0	0	0	0	0.228	9.321	1.608	26.6	97.05	281	912
31	0	0	0	0	0	0.227	9.569	1.600	26.6	95.58	252	818

Ionic Gelation Process for the Formation of Ch-TPP

The ionic gelation crosslinking process was performed as described by several authors in the literature (Calvo, 1997; De Campos et al., 2001; Y. Xu & Du, 2003; L. Zhang & Kosaraju, 2007) with slight modifications based on the factors being analyzed and factor levels.

Chitosan stock solutions were prepared by dissolving chitosan in 2% acetic acid solution at concentrations such that 850 ml of the stock solution would provide 1, 3, or 5 mg/ml chitosan concentration when diluted to 1 liter. Sodium tripolyphosphate (NaTPP) stock solutions were prepared by dissolving the appropriate amount of NaTPP such that 100 ml of the stock solution would provide the appropriate Ch:TPP ratio when diluted to 1 liter.

An 850 ml portion of appropriate chitosan stock solution was dispensed into a 1500 ml beaker. If applicable, the required amount of NaCl was added to the chitosan solution and dissolved by mixing for 10 minutes at 300 rpm using a Fisher stirring hotplate (Fair Lawn, NJ). The solution was then heated to the desired temperature using the hotplate and monitored via thermometer. The solution was covered with tight fitting aluminum foil to prevent evaporation. The sample pH was then modified to the desired pH using stock solutions of 5 N NaOH or 5 N HCl based on the initial pH. The volume required for pH modification was then q.s. to 50 ml with purified water.

Finally, 100 ml of the appropriate NaTPP solution was added dropwise to the chitosan solution and the solution was mixed for 1 hour at 300 rpm. Small aliquots were extracted for response testing as needed. The remainder of the sample was centrifuged at 10,000 rpm for 20 minutes using a Sorvall LYNX 6000 centrifuge by Thermo Scientific

(Darmstadt, Germany). The sample was lightly rinsed using purified water and centrifuged again for another 20 minutes at 10,000 rpm.

Solid sample was then isolated from the centrifuge tubes and lyophilized for 36 hours using a VirTis AdVantage 2.0 bench top lyophilizer by SP Scientific (Gardiner, NY).

Particle Size

Particle size analysis was performed using a Mastersizer 2000 by Malvern Instruments (Westborough, MA). d50 represents the median particle size while span is a value calculated to represent the width of particle size distribution and is determined using the following equation:

$$Span = \frac{d_{90} - d_{10}}{d_{50}}$$

where d_{90} represents the particle size diameter that 90% of the particles fall under; d_{10} represents the particle size diameter that 10% of the particles fall under; and d_{50} represents the particle size diameter that 50% of the particles fall under, also known as the median (d50) ("Understanding and Interpreting Particle Size Distribution Calculations," n.d.).

Liquid samples from the 1 liter Ch-TPP mixture were withdrawn in triplicate using a plastic pipette and analyzed within 24 hours of manufacture. The samples were sonicated in the Mastersizer for 90 seconds prior to data analysis. Based on previous experimentation (data not shown here), 90 seconds was shown to be adequate to break up aggregates that may have formed with no significant reduction in particle size shown at 120 or 180 seconds of sonication.

True Density

True density of lyophilized Ch-TPP powders were analyzed in triplicate using a Stereopycnometer™ helium pycnometer by Quantachrome Instruments (Boynton Beach, FL). Samples were tested in triplicate.

Zeta Potential

Zeta Potential was measured using a Nano S ZetaSizer by Malvern Instruments (Westborough, MA). Liquid samples from the 1 liter Ch-TPP mixture were withdrawn in triplicate using a plastic pipette and analyzed immediately.

Yield

Percent yield was calculated based on theoretical weight of Ch-TPP samples. Specifically, 100 ml sample from the 1 liter Ch-TPP mixture was withdrawn and centrifuged separately from the remainder of the bulk sample. The solid sample was removed from the centrifuge tubes and lyophilized in pre-weighed vials where final percent yield was calculated as:

$$\%Yield = \frac{final\ mass}{theoretical\ mass\ of\ Chitosan + TPP\ per\ 100\ mL} \cdot 100$$

Analysis was performed in triplicate.

Tablet Manufacture and Dissolution Analysis

Tablets for dissolution testing were made using Ch-TPP crosslinked material from each of the 31 experiments. Samples were blended with acetaminophen as a model drug at 10% w/w and compressed into tablets (300 mg target weight) using 3/8" standard

concave tooling using 38,500 psi (2 tons) of pressure on a bench top press (Natoli NP-RD10A, St. Charles, MO). Three tablets were made for each Ch-TPP material.

Dissolution testing of tablets was performed in triplicate using a USP <711> Apparatus II (United States Pharmacopeia National Formulary, 2016b) model 2100C dissolution apparatus (Distek, North Brunswick, NJ) using equipped with at a paddle speed of 50 rpm. Simulated intestinal fluid (SIF) without pancreatin was used as the dissolution media with samples pulled at intervals over 12 hours (15, 30, 34, 60, and 90 min; 2, 4, 6, 8, 10, 12 h) using a model 2230A autosampler (Distek, North Brunswick, NJ). Drug concentration in these samples was determined at 245 nm using a SpectraMax Plus UV/Vis photospectrometer (Molecular Devices, Sunnyvale, CA).

Dissolution results were fit with SigmaPlot® (Systat Software, Inc.,version 12.5) software using several established kinetic models for drug release from controlled release systems, including the Korsmeyer-Peppas equation (Korsmeyer, Gurny, Doelker, Buri, & Peppas, 1983), Higuchi equation (Higuchi, 1963), and the Baker-Lonsdale equation (Baker, 1974). The Higuchi equation was shown to be the most appropriate fit for the mechanism of release and is described by the following equation:

$$\frac{M_t}{M_\infty} = k \cdot \sqrt{t} + c$$

where M_t is defined as the amount of drug released at time t; M_∞ is defined as the amount of drug released as time approaches infinity, which is assumed to equal the theoretical drug mass in a tablet; k is the Higuchi constant dependent on the initial drug concentration, solubility, diffusion coefficient, as well as the surface area available for drug release; and c is a constant that accounts for burst release ($c > 0$) or lag time ($c < 0$)

for initial drug release (Siepmann & Peppas, 2011). Only time points with less than 80% drug release was considered for equation fitting (Costa & Sousa Lobo, 2001). The time for 50% drug release (t_{50}) was then calculated using the derived Higuchi equation for each experimental run.

Results and Discussion

Particle Size

Particle size and size distribution as measured by both d50 and Span, showed a range of 0.159 – 2.59 μm and 2.4 – 148.1, respectively, across the entire 31 experiments. Analysis of each of these responses following completion of the initial half-fractional factorial design revealed significant curvature and/or lack of fit ($p < 0.05$; Appendix 1, Table 7.1) warranting the additional experiments to complete a central composite design. Generally, the d50 results above about 0.300 μm and Span values above approximately 15 indicated the presence of a substantial bimodal distribution, suggesting the existence of aggregated particles. Experiments with results below these values generally showed a single peak in Mastersizer particle size distribution graphs slightly skewed to the right of the curve, indicating a limited extent of aggregation.

Analysis of variance reports for d50 and Span suggest significant quadratic models ($p < 0.05$) for each response. For d50, an inverse transformation (lambda = -1) was used as recommended by a Box-Cox plot. Standard runs #25 and #27 were sequentially removed from the data analysis as these were identified as outliers using the Residuals versus Predicted plot for d50 (i.e. Internally Studentized Residual > 3 or < -3). For Span, an inverse transformation (lambda = -1) was used as recommended by a Box-Cox plot and standard run #4 was removed from the data analysis as it was identified as

an outlier in the Residuals versus Predicted plot. Final ANOVA reports yielded excellent R^2 values (>0.9) and showed no significant lack of fit (see Table 4.4).

For d50, all five factors, viz. chitosan concentration (A), Ch:TPP ratio (B), temperature (C), pH (D), and NaCl concentration (E), proved to be statistically significant. Five significant two factor interactions exist: chitosan concentration-temperature (AC), chitosan concentration-pH (AD), chitosan concentration-NaCl concentration (AE), Ch:TPP ratio-temperature (BC), and Ch:TPP ratio-pH (BD). Two quadratic terms, chitosan concentration (A^2) and NaCl concentration (E^2) were shown to be significant. The model equation for the coded factor levels:

$$1/d50 = 4.51 – 1.30A – 0.080B + 0.35C – 2.838E\text{-}003D + 0.15E + 0.42AC + 0.38AD – 0.68AE – 0.41BC – 0.87BD – 0.59A^2 – 0.51E^2$$

is significant ($p < 0.0001$) and has a good fit to the data ($R^2 = 0.9638$). Lack of fit is not statistically significant ($p = 0.1044$) indicating that the d50 results for the 31 experiments are described well by the equation.

The Normal Plot (Figure 4.1) indicates that the residuals for d50 are randomly distributed. The Residuals vs. Predicted plot (Figure 4.2) does not reveal a trend in the residual data.

For Span, all five factors, chitosan concentration (A), Ch:TPP ratio (B), temperature (C), pH (D), and NaCl concentration (E) are statistically significant. Five significant two factor interactions exist, viz. chitosan concentration-NaCl concentration (AE), Ch:TPP ratio-temperature (BC), Ch:TPP ratio-pH (BD), Ch:TPP ratio-NaCl concentration (BE), and temperature-NaCl concentration (CE). Three quadratic factors,

chitosan concentration (A^2), Ch:TPP ratio (B^2), and temperature (C^2), were shown to be significant. The model equation for the coded factor levels:

$$1/\text{Span} = 0.10 - 0.037A + 0.062B - 3.563E\text{-}003C - 0.058D + 0.018E - 0.022AE - 0.033BC - 0.083BD + 0.037BE - 0.013CE + 0.042A^2 + 0.075B^2 - 0.071C^2$$

is significant ($p < 0.0001$) and has a good fit to the data ($R^2 = 0.9748$). Lack of fit is not significant ($p = 0.0557$), indicating that the Span results for the factorial experiments are described well by the equations.

The Normal Plot (Figure 4.3) indicates that the residuals for Span are randomly distributed. The Residuals vs. Predicted plot (Figure 4.4) does not reveal a trend in the residual data.

Table 4.4. Analysis of Variance: d50 and Span

	d50	Span
Source	p-value	
Model	< 0.0001	< 0.0001
A	< 0.0001	< 0.0001
B	0.4092	< 0.0001
C	0.0024	0.5332
D	0.9971	< 0.0001
E	0.8720	0.0061
AC	0.0007	---
AD	0.0016	---
AE	< 0.0001	0.0023
BC	0.0009	< 0.0001
BD	< 0.0001	< 0.0001
BE	---	< 0.0001
CE	---	0.0463
A^2	0.0210	0.0068
B^2	---	< 0.0001
C^2	---	< 0.0001
E^2	0.0430	---
Lack of Fit	0.1044	0.0557
R^2	0.9638	0.9748
Adj R^2	0.9348	0.9530

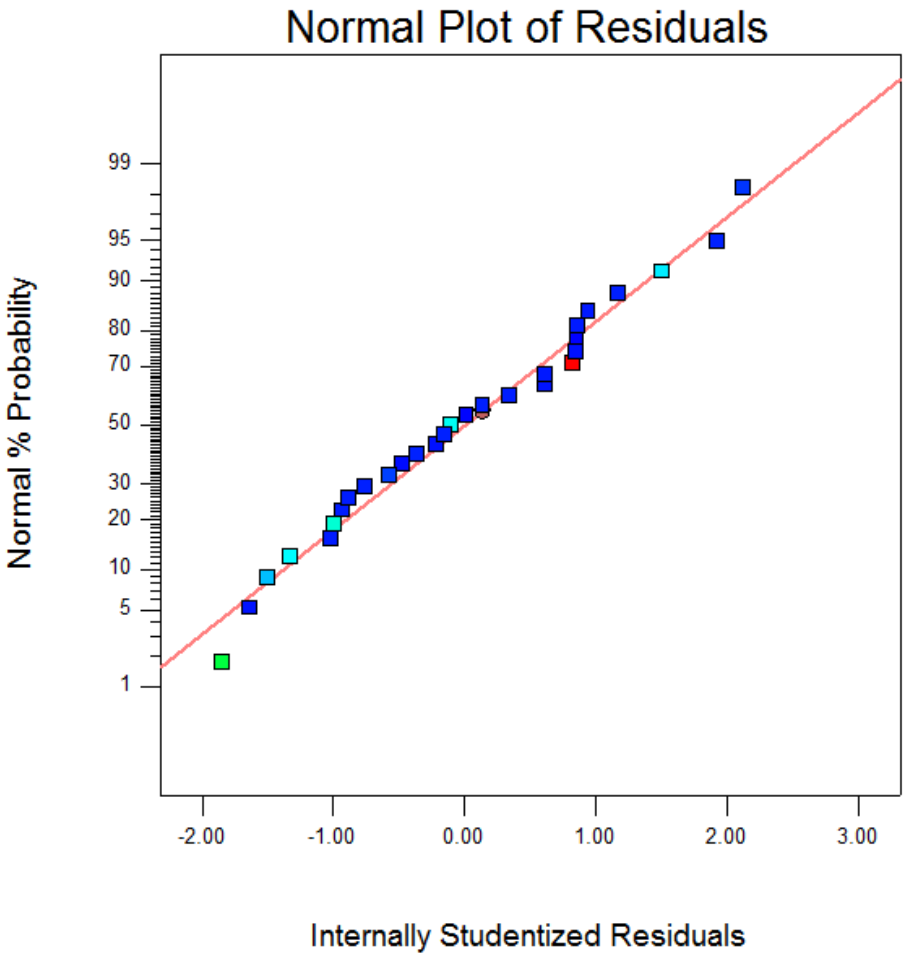

Figure 4.1. Normal Plot of Residuals: d50

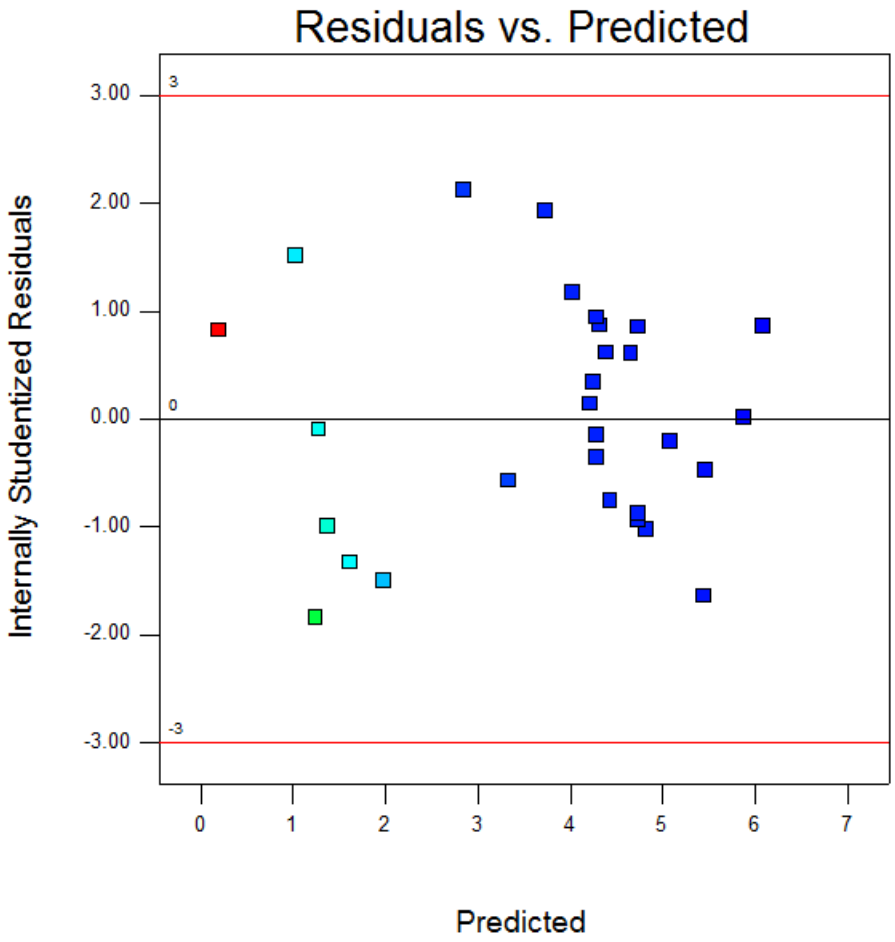

Figure 4.2. Residuals Plot: d50

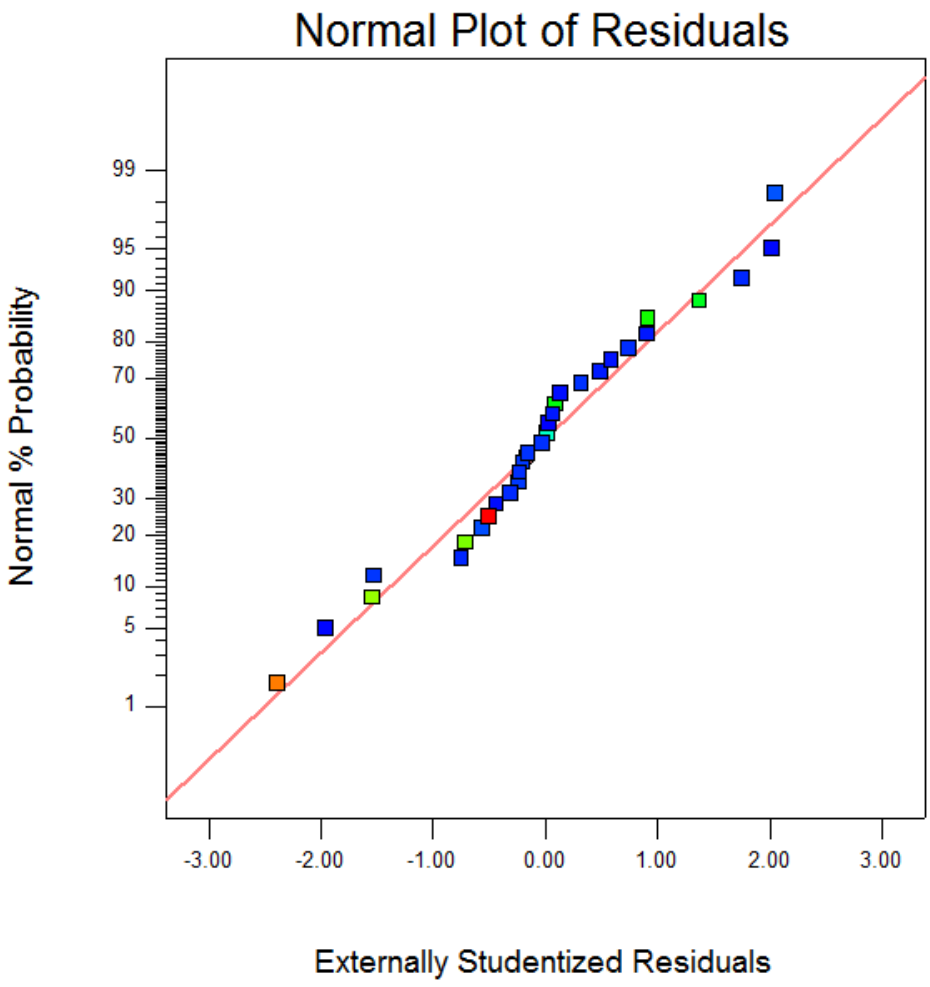

Figure 4.3. Normal Plot of Residuals: Span

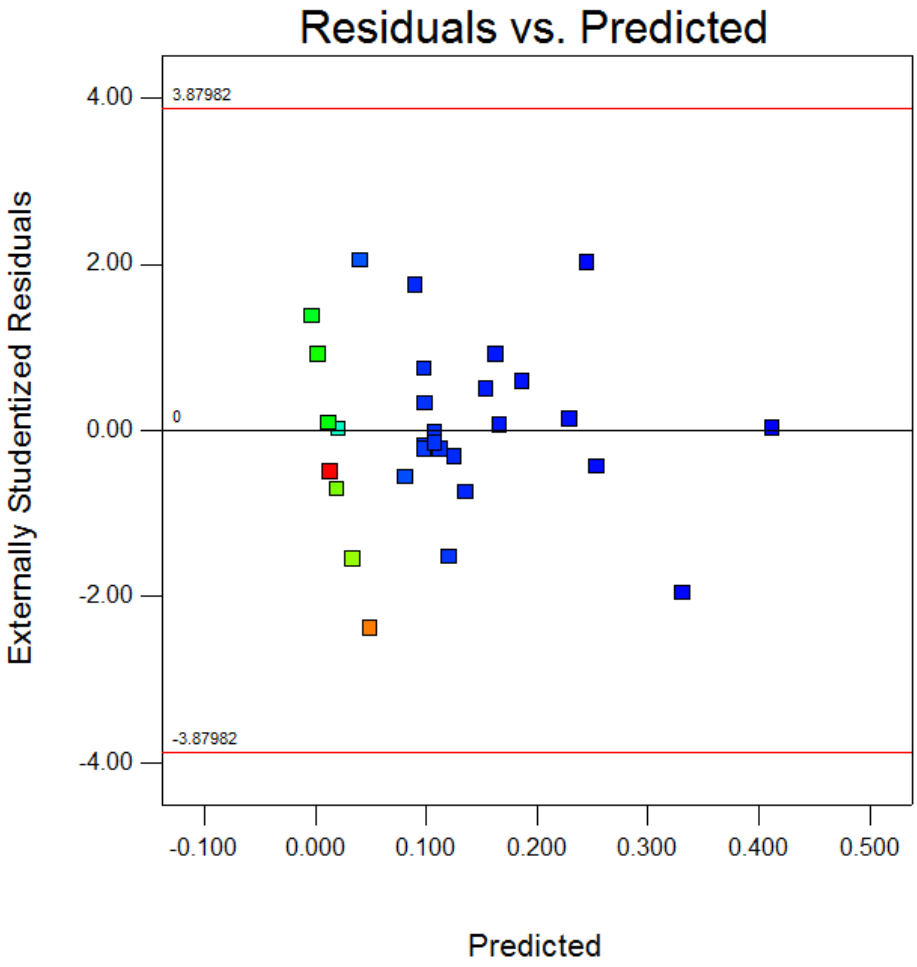

Figure 4.4. Residuals Plot: Span

The interaction of chitosan concentration and temperature (Figure 4.5) shows that particle size, as measured by d50, does not change significantly across the temperature range studied when using a low chitosan concentration (1 mg/ml). However, when its concentration is increased to 3 mg/ml, and more drastically at 5 mg/ml, d50 tends to increase significantly at lower temperatures. This can be attributed to the increase in viscosity at lower temperatures, which subsequently leads to slower particle movement and insufficient energy to prevent aggregation.

In Figure 4.6, the interaction between chitosan concentration and NaCl concentration suggests that in the absence of NaCl, particle size only increases slightly as chitosan concentration increases, while in the presence of 0.02 M NaCl concentration, a significant increase in particle size is observed at high chitosan concentrations. This suggested that the crosslinking density could be weakened by the presence of higher salt concentrations, leading to larger particle size (Huang & Lapitsky, 2011).

Particle size distribution, as measured by Span, shows a drastic spike at low temperatures in the absence of salt, while showing very little impact from NaCl levels at higher temperatures (Figure 4.7). Consistent with the findings from Huang & Lapitsky, this data suggests that the presence of low concentration of salt may actually stabilize the colloidal system preventing further crosslinking and subsequent agglomeration leading to a wide range of particle sizes. At elevated temperatures, the lower viscosity and increased particle energy is sufficient to prevent this agglomeration and a subsequent spike in Span, which was also exhibited by a measure of d50 in Figure 4.5.

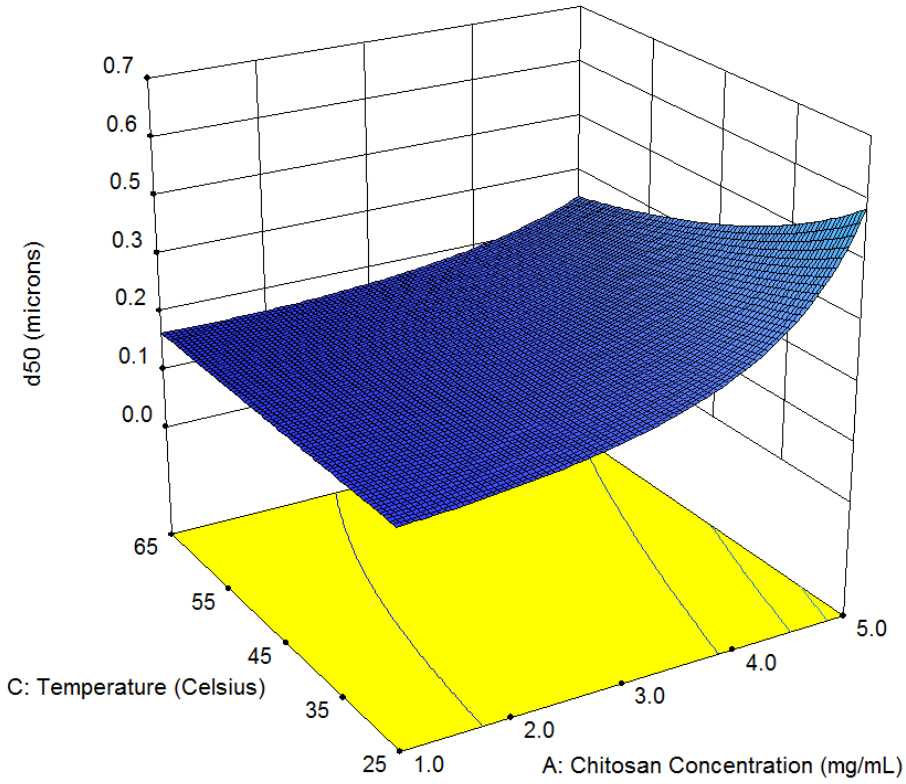

Figure 4.5. Response Surface Plot for Particle Size (d50) as a Function of Chitosan Concentration and Temperature

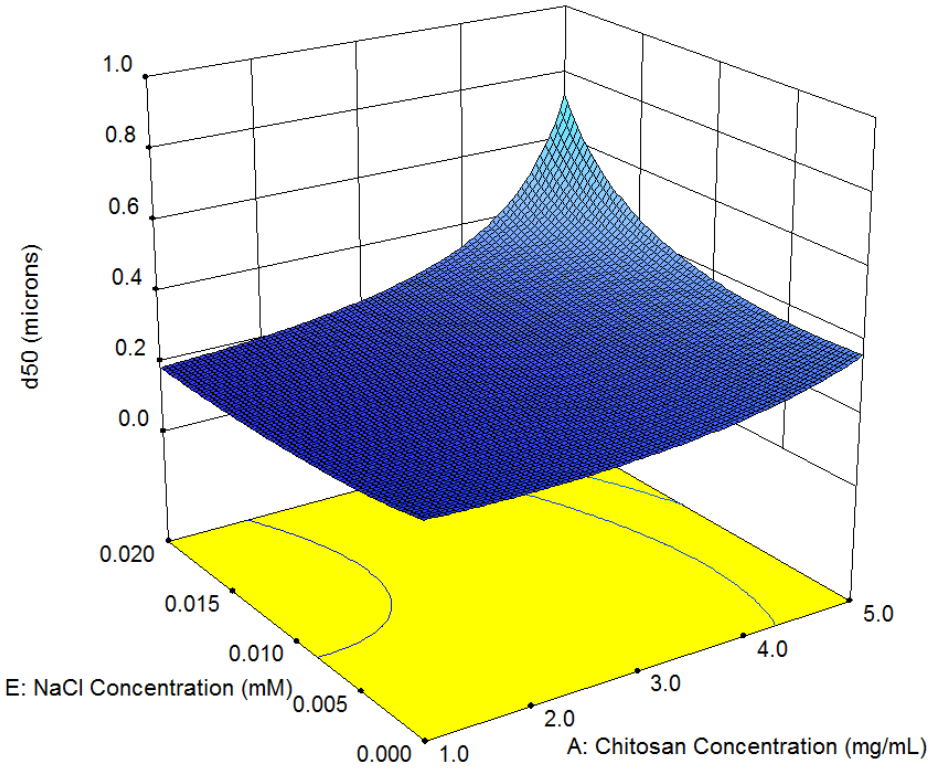

Figure 4.6. Response Surface Plot for Particle Size (d50) as a Function of Chitosan Concentration and NaCl Concentration

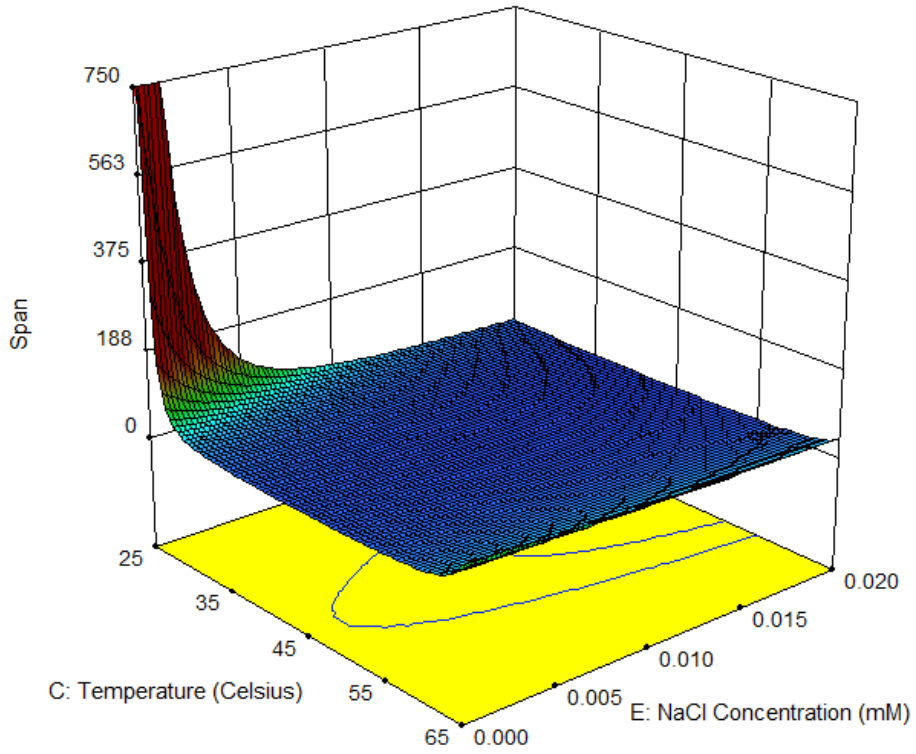

Figure 4.7. Response Surface Plot for Particle Size Distribution (Span) as a Function of NaCl Concentration and Temperature

True Density

True density showed a range of 1.550 – 1.899 g/ml across the entire 31 experiments. Analysis of this response following completion of the initial half-fractional factorial design yielded a statistically significant model with no significant curvature or lack of fit ($p > 0.05$; Appendix 1, Table 7.2). As additional experiments were completed to satisfy a central composite design for the responses d50 and span, true density was also measured for these samples in an effort to create a more robust model based on the additional experimental runs.

The analysis of variance report for the central composite design shows that a quadratic model is significant ($p < 0.05$) for true density. No transformation (lambda = 1) was recommended by the Box-Cox plot and standard run #20 was removed from the data analysis as this was identified as an outliers using the Residuals versus Predicted plot. Final ANOVA reports yielded an excellent R^2 value (>0.9) and showed no significant lack of fit (reference Table 4.5).

For true density, all five variables; chitosan concentration (A), Ch:TPP ratio (B), temperature (C), pH (D), and NaCl concentration (E) are statistically significant. Six significant two factor interactions exist; chitosan concentration-Ch:TPP ratio (AB), chitosan concentration-temperature (AC), chitosan concentration-pH (AD), chitosan concentration-NaCl concentration (AE), temperature-pH (CD), and pH-NaCl concentration (DE). One quadratic factor, Ch:TPP ratio (B^2), was shown to be significant. The model equation for the coded factor levels:

True Density = 1.62 + 0.011A + 5.944E-003B + 0.038C – 8.111E-003D + 0.022E – 0.027AB – 0.018AC – 0.033AD + 0.067AE + 0.016CD – 0.030DE + 0.041B^2 is

significant ($p < 0.0001$) and has a good fit to the data ($R^2 = 0.9349$). Lack of fit is not statistically significant ($p = 0.1175$) indicating that the results for the factorial experiments are described well by the equations.

The Normal Plot (Figure 4.8) indicates that the residuals for true density are randomly distributed. The Residuals vs. Predicted Plot (Figure 4.9) does not reveal a trend in the residual data.

While the overall variation in true density was relatively small, it can be seen in Figure 4.10 that minimum true density values were observed at lower chitosan concentrations and lower Ch:TPP ratios suggesting that weaker crosslinking occurs at these conditions, resulting in a more porous structure. Conversely, at high chitosan concentrations, Ch:TPP ratios of both 1:1 and 5:1 showed higher true density values with a dip observed at the centerpoint. This trend suggests that a Ch:TPP ratio of 3:1 may produce a crosslinked structure that is more loosely bound.

In Figure 4.11, the response surface plot shows that when the NaCl concentration is zero, there is only a slight increase in true density as pH increases from 3.0 to 5.0. Conversely, in the presence of the high level of NaCl, true density increases as pH decreases from 5.0 to 3.0, suggesting that perhaps sodium and chloride ions are embedding themselves within the crosslinked structure and contributing to the overall density.

Table 4.5. Analysis of Variance: True Density

Source	**p-value**
Model	< 0.0001
A	0.1110
B	0.3685
C	< 0.0001
D	0.2248
E	0.0040
AB	0.0010
AC	0.0171
AD	0.0002
AE	< 0.0001
CD	0.0370
DE	0.0004
B^2	0.0074
Lack of Fit	0.1175
R^2	0.9349
Adj R^2	0.8861

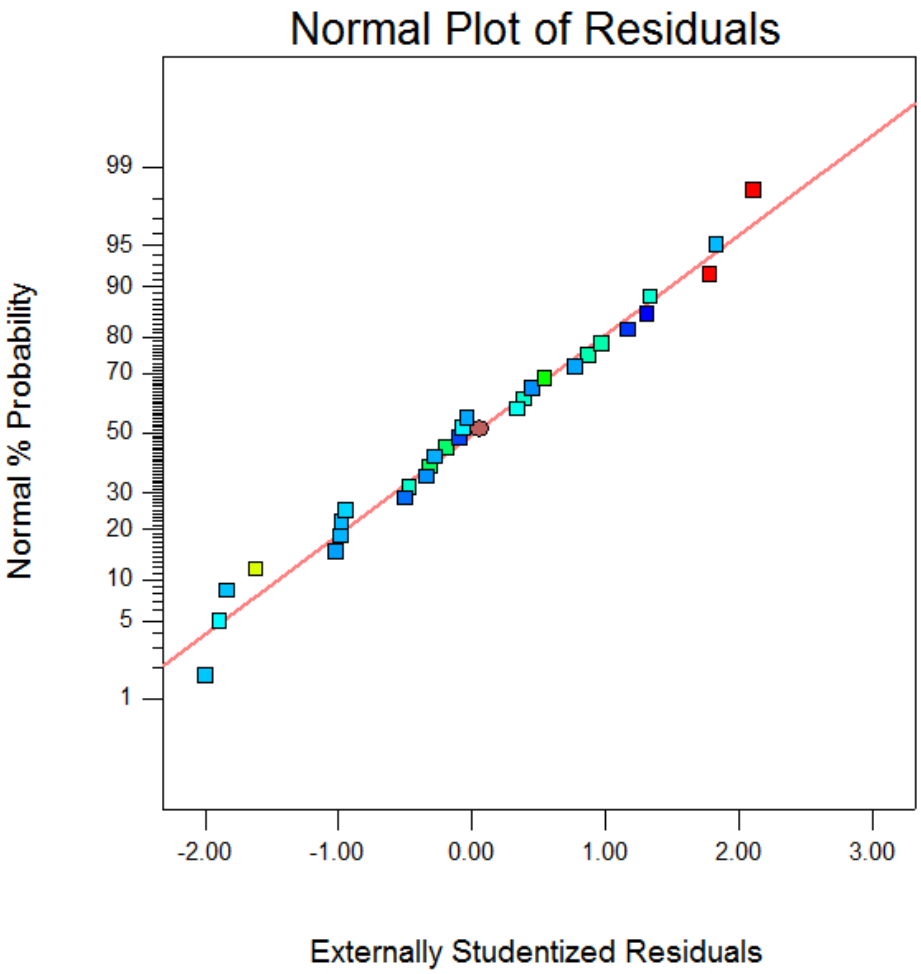

Figure 4.8. Normal Plot of Residuals: True Density

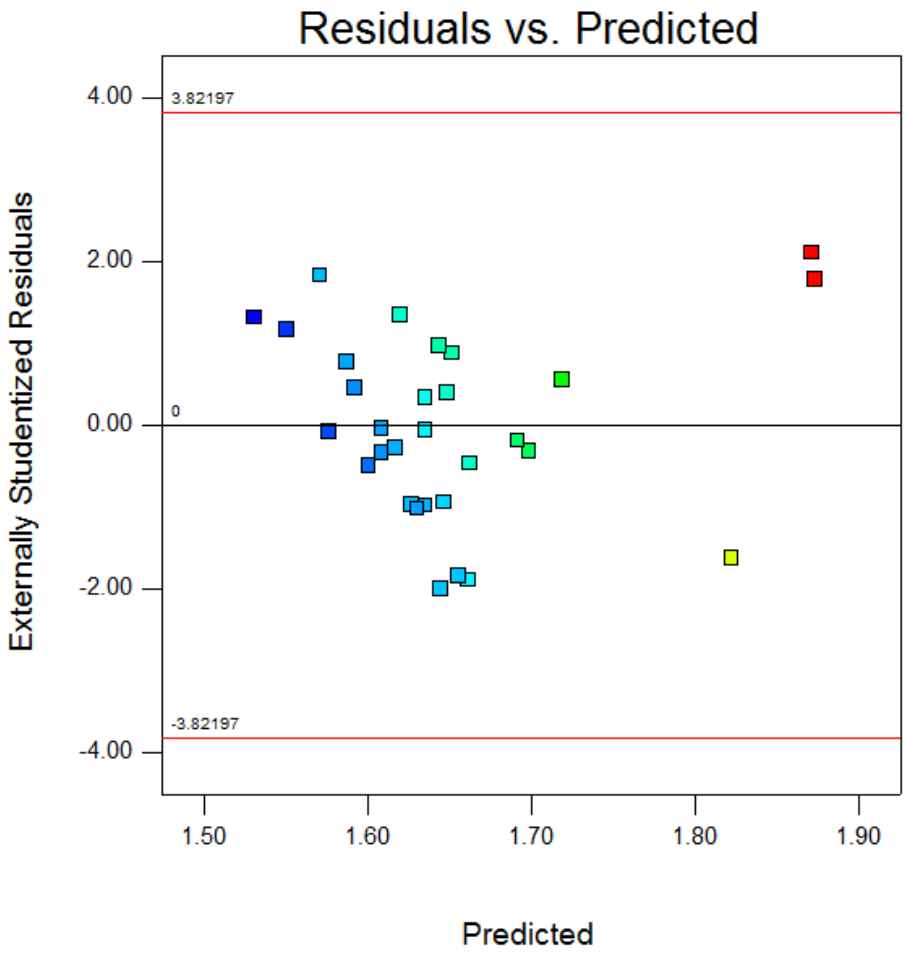

Figure 4.9. Residuals Plot: True Density

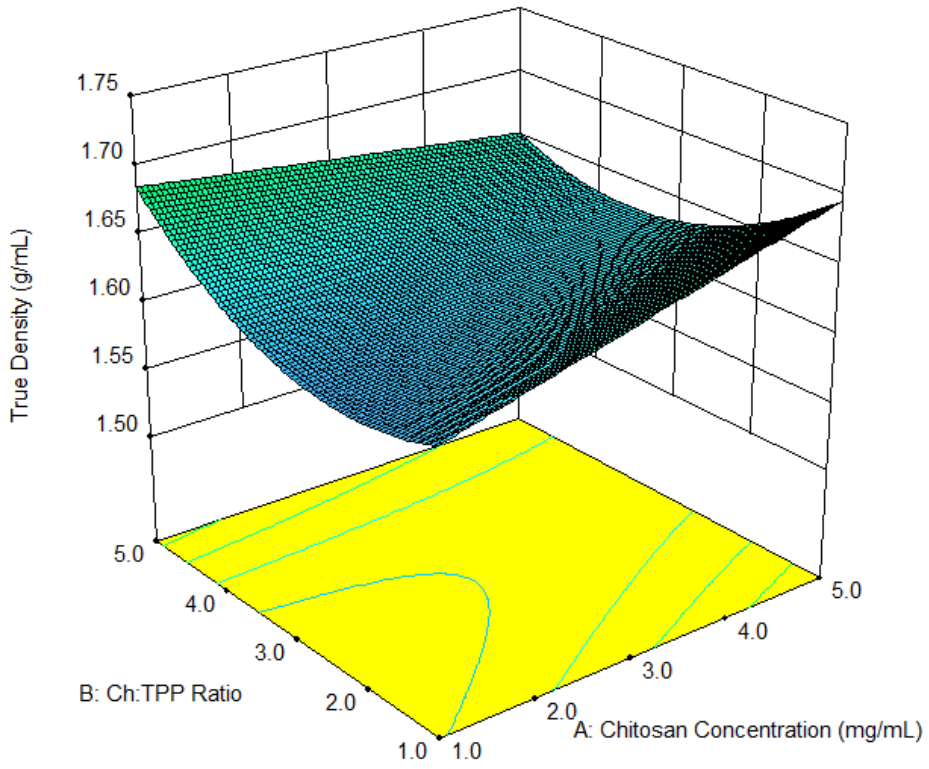

Figure 4.10. Response Surface Plot for True Density as a Function of Chitosan Concentration and Ch:TPP Ratio

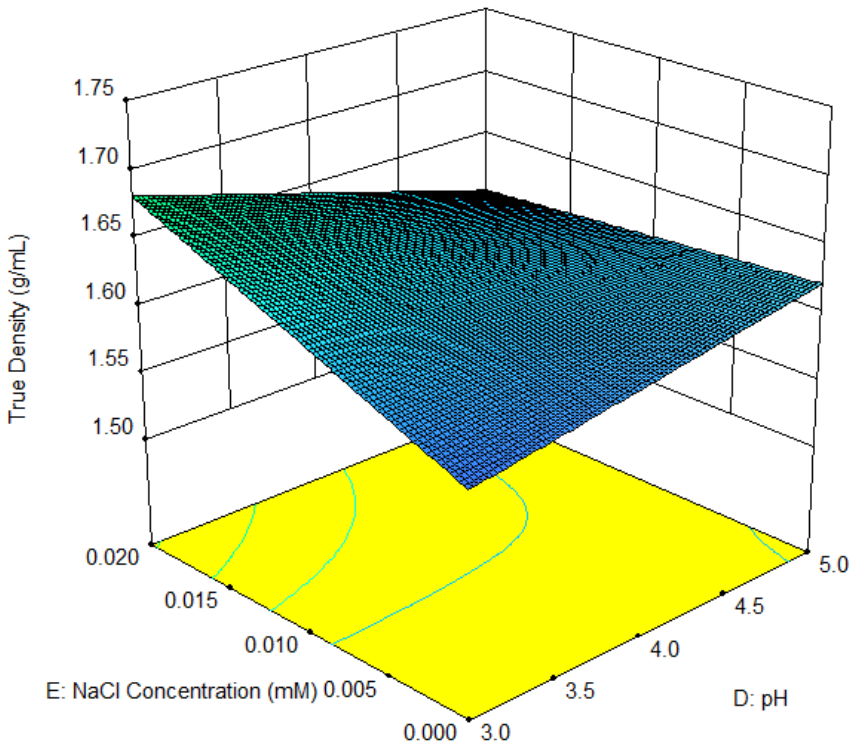

Figure 4.11. Response Surface Plot for True Density as a Function of NaCl Concentration and pH

Zeta Potential

Zeta potential showed a range of 0.30 – 51.8 mV across the entire 31 experiments. Analysis of this response following completion of the initial half-fractional factorial design yielded a statistically significant model with no significant curvature or lack of fit ($p > 0.05$; Appendix 1, Table 7.3). As additional experiments were completed to satisfy a central composite design for the responses d50 and span, zeta potential was also measured for these samples in an effort to create a more robust model based on the additional experimental runs.

Analysis of variance report revealed that a quadratic model is significant ($p < 0.05$) for zeta potential. No transformation (lambda = 1) was used as recommended by the Box-Cox plot and no experimental runs were removed from the analysis. The final ANOVA reported an excellent R^2 value (>0.9) and showed no significant lack of fit (reference Table 4.6).

For zeta potential, all five factors; chitosan concentration (A), Ch:TPP ratio (B), temperature (C), pH (D), and NaCl concentration (E) are statistically significant. Five significant two factor interactions exist; chitosan concentration-Ch:TPP ratio (AB), Ch:TPP ratio-temperature (BC), Ch:TPP ratio-pH (BD), Ch:TPP ratio-NaCl concentration (BE), and temperature-NaCl concentration (CE). Four quadratic factors; chitosan concentration (A^2), Ch:TPP ratio (B^2), temperature (C^2), and pH (D^2) were shown to be significant. The model equation for the coded factor levels:

Zeta Potential = $24.29 + 1.00A + 16.69B – 0.37C – 5.39D – 1.79E + 2.73AB – 1.14BC – 4.76BD – 1.00BE + 0.92CE – 2.51A^2 – 4.81B^2 + 3.24C^2 + 2.74D^2$

is significant ($p < 0.0001$) and has a good fit to the data ($R^2 = 0.9935$). Lack of fit is not statistically significant ($p = 0.4193$) indicating that the results for the central composite design are described well by the equations.

The Normal Plot (Figure 4.12) indicates that the residuals for zeta potential have a normal distribution. The Residuals vs. Predicted plot (Figure 4.13) does not reveal a trend in the residual data.

Figure 4.14 shows a general trend across all chitosan concentrations that as the Ch:TPP ratio decreases from 5 to 1, there is a corresponding decrease in zeta potential from approximately +35 mV to 0 mV. This trend shows that at higher ratios, there is an excess of protonated amine groups ($-NH_3^+$) present on the chitosan chains that do not experience crosslinking and are dictating the positive zeta potential. As the ratio decreases, the anionic oxygen species on tripolyphosphate are crosslinking with the protonated amine groups on chitosan and creating a more neutral zeta potential.

The response surface plot in Figure 4.15 shows the zeta potential as a function of the relationship between pH and Ch:TPP ratio. The figure demonstrates that at low chitosan concentration (1.0 mg/ml), the zeta potential remains generally stagnant with changing pH. This is due to the fact that the low concentration of chitosan is not sufficient to drive changes to zeta potential, which is evidenced by the fact that the zeta potential values at these concentrations are less than +10 mV. Conversely, as the chitosan concentrations increase, the zeta potential also increases. This increase is intensified at lower pH due to the presence of additional free H+ ions, which further protonate the amine groups present on chitosan side chains as the pH is reduced.

Table 4.6. Analysis of Variance: Zeta Potential

Source	**p-value**
Model	< 0.0001
A	0.0214
B	< 0.0001
C	0.3541
D	< 0.0001
E	0.0003
AB	< 0.0001
BC	0.0147
BD	< 0.0001
BE	0.0286
CE	0.0406
A^2	0.0293
B^2	0.0003
C^2	0.0072
D^2	0.0190
Lack of Fit	0.4193
R^2	0.9935
Adj R^2	0.9874

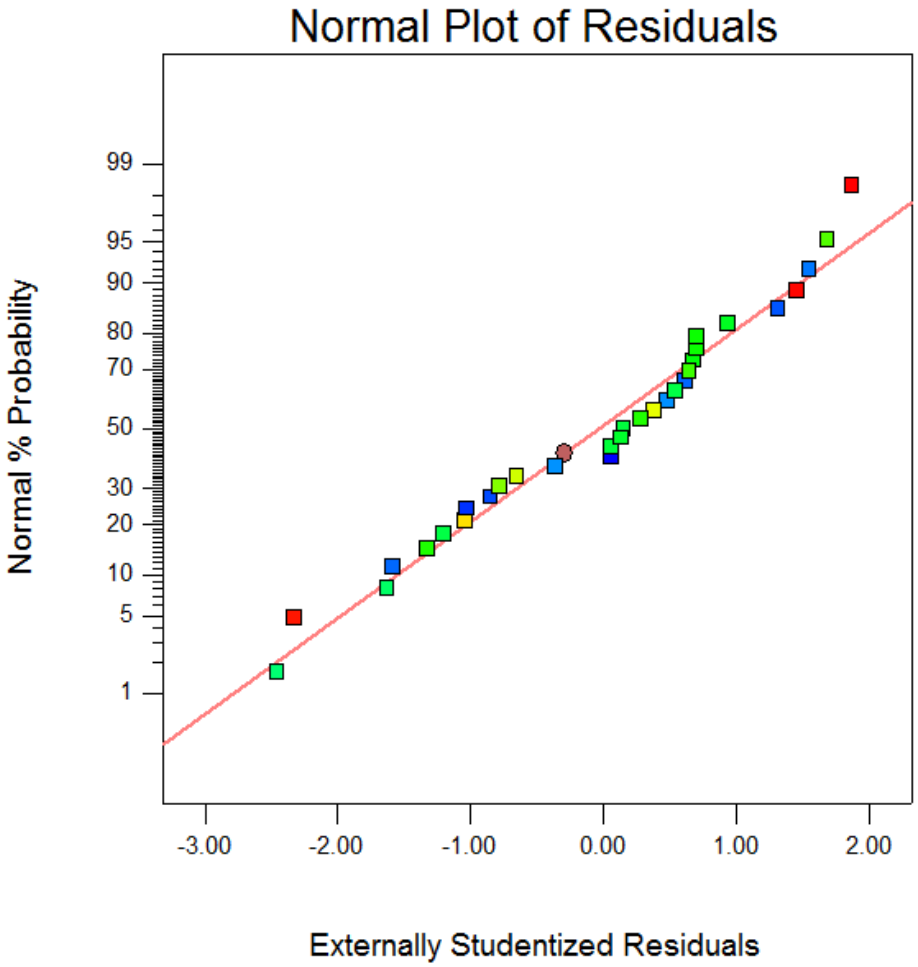

Figure 4.12. Normal Plot of Residuals: Zeta Potential

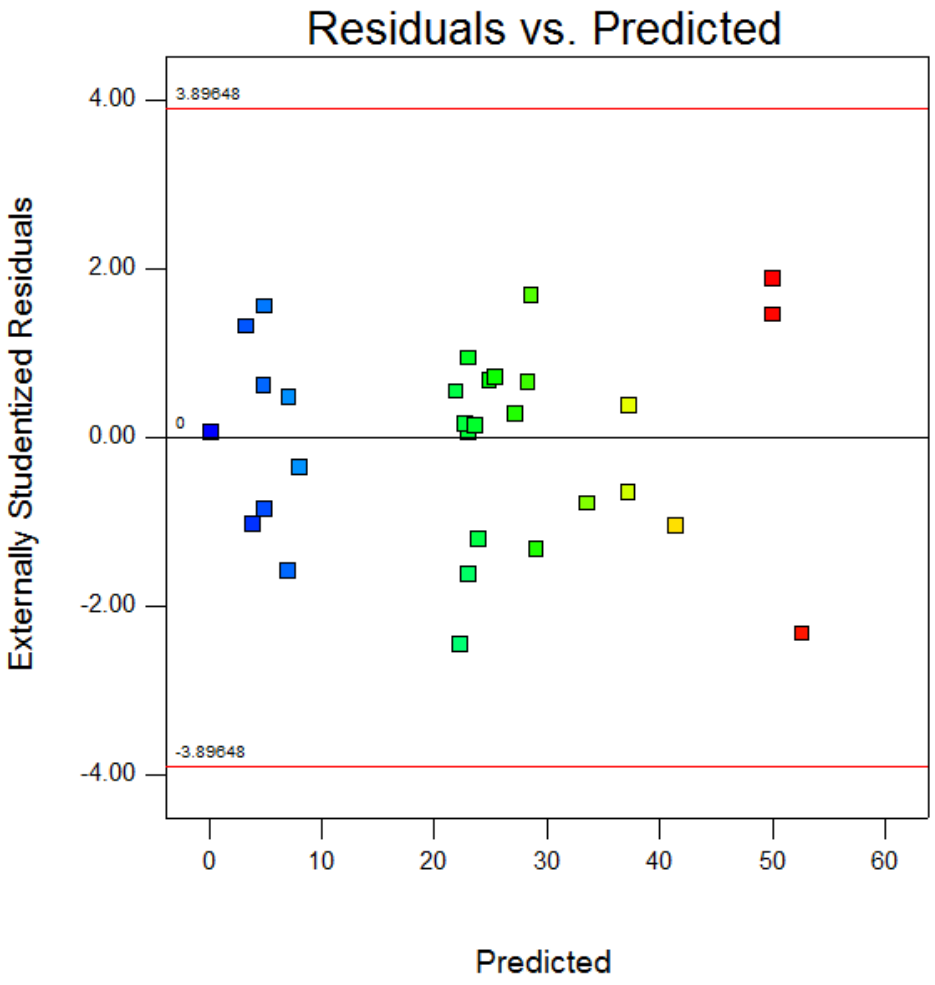

Figure 4.13. Residuals Plot: Zeta Potential

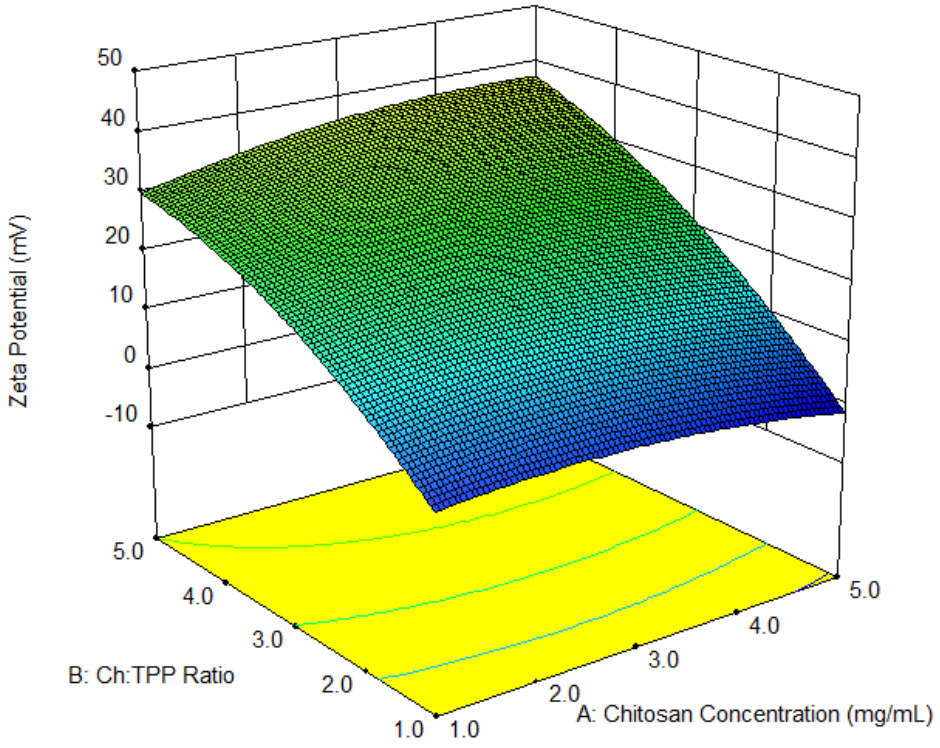

Figure 4.14. Response Surface Plot for Zeta Potential as a Function of Chitosan Concentration and Ch:TPP Ratio

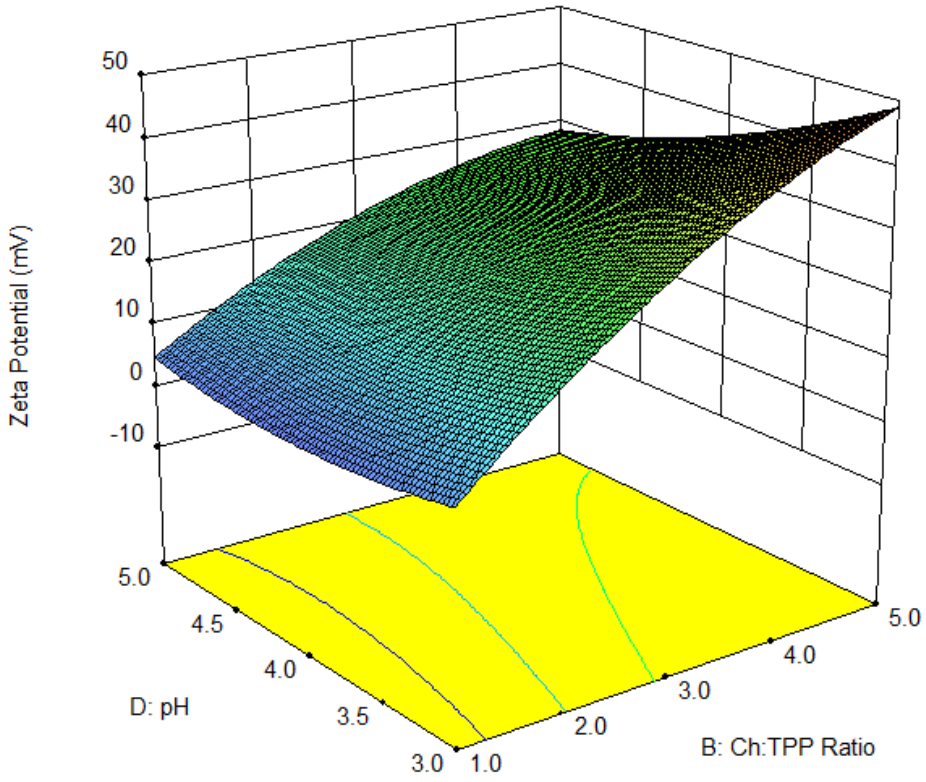

Figure 4.15. Response Surface Plot for Zeta Potential as a Function of Ch:TPP Ratio and pH

Yield

Yield showed a range of 20.7 – 97.1% across the entire 31 experiments. Analysis of this response following completion of the initial half-fractional factorial design could not produce a statistically significant model using backwards hierarchical regression methodology and both curvature and lack of fit were significant ($p < 0.05$, Appendix 1, Table 7.4) warranting additional experiments to complete the central composite design.

Analysis of variance indicates that a quadratic model is significant ($p < 0.05$) for yield. No transformation (lambda = 1) was recommended by Box-Cox plot and standard runs #3, 10, 26, 30 and 31 were removed from the data analysis as these were identified as outliers using the residuals versus predicted plot. The final ANOVA reported an excellent R^2 value (>0.9) and showed no significant lack of fit (reference Table 4.7).

For yield, all five variables; chitosan concentration (A), Ch:TPP ratio (B), temperature (C), pH (D), and NaCl concentration (E) are statistically significant. Six significant two factor interactions exist; the chitosan concentration-temperature (AC), the chitosan concentration-NaCl concentration (AE), Ch:TPP ratio-temperature (BC), Ch:TPP ratio-pH (BD), temperature-pH (CD), and temperature-NaCl concentration (CE). Four quadratic factors; chitosan concentration (A^2), Ch:TPP ratio (B^2), temperature (C^2), and NaCl concentration (E^2), were shown to be significant. The model equation for the coded factor levels:

$$\text{Yield} = 92.41 + 2.84A - 2.76B + 0.63C + 7.22D - 0.42E + 2.48AC - 1.03AE - 6.29BC + 1.25BD + 2.02CD + 1.79CE - 2.61A^2 - 27.82B^2 + 2.76C^2 + 5.62E^2$$

is significant ($p < 0.0001$) and has a good fit to the data ($R^2 = 0.9974$). Lack of fit is not statistically significant ($p = 0.1966$) indicating that the results for the central composite design are described well by the equations.

The Normal Plot (Figure 4.16) indicates that the residuals for true density are randomly distributed. The Residuals vs. Predicted Plot (Figure 4.17) does not reveal a trend in the residual data.

The surface plot presented in Figure 4.18 shows that yield is maximized when the Ch:TPP ratio is 3:1, essentially independent of temperature, suggesting that this ratio maximizes the extent of crosslinking between chitosan and tripolyphosphate. Further, the plot shows that at a Ch:TPP ratio of 1:1, yield slightly increases with an increase in temperature, while at a ratio of 5:1 the relationship is inverted and a slight decrease in yield is observed with increasing temperature. This trend suggests that a decreased viscosity promotes crosslinking when the ratio is 1:1, perhaps providing greater translational motion so that oppositely charged species can come into contact. However, when the ratio is 5:1, the increased yield at lower temperature may be a result of excess chitosan aggregation due to an increased viscosity, while the lower yield at higher temperatures is likely a more accurate representation of yield of crosslinked species.

Figure 4.19 also demonstrates that a Ch:TPP ratio of 3:1 results in maximum yield, but yield also increases as pH increases from 3.0 to 5.0. This increase is associated with increasing the negative charges present on the tripolyphosphate, which enables a greater extent of crosslinking.

Table 4.7. Analysis of Variance: Yield

Source	**p-value**
Model	< 0.0001
A	0.0003
B	0.0004
C	0.0685
D	< 0.0001
E	0.4262
AC	0.0016
AE	0.0155
BC	< 0.0001
BD	0.0040
CD	0.0054
CE	0.0104
A^2	0.0065
B^2	< 0.0001
C^2	0.0047
E^2	< 0.0001
Lack of Fit	0.1966
R^2	0.9974
Adj R^2	0.9930

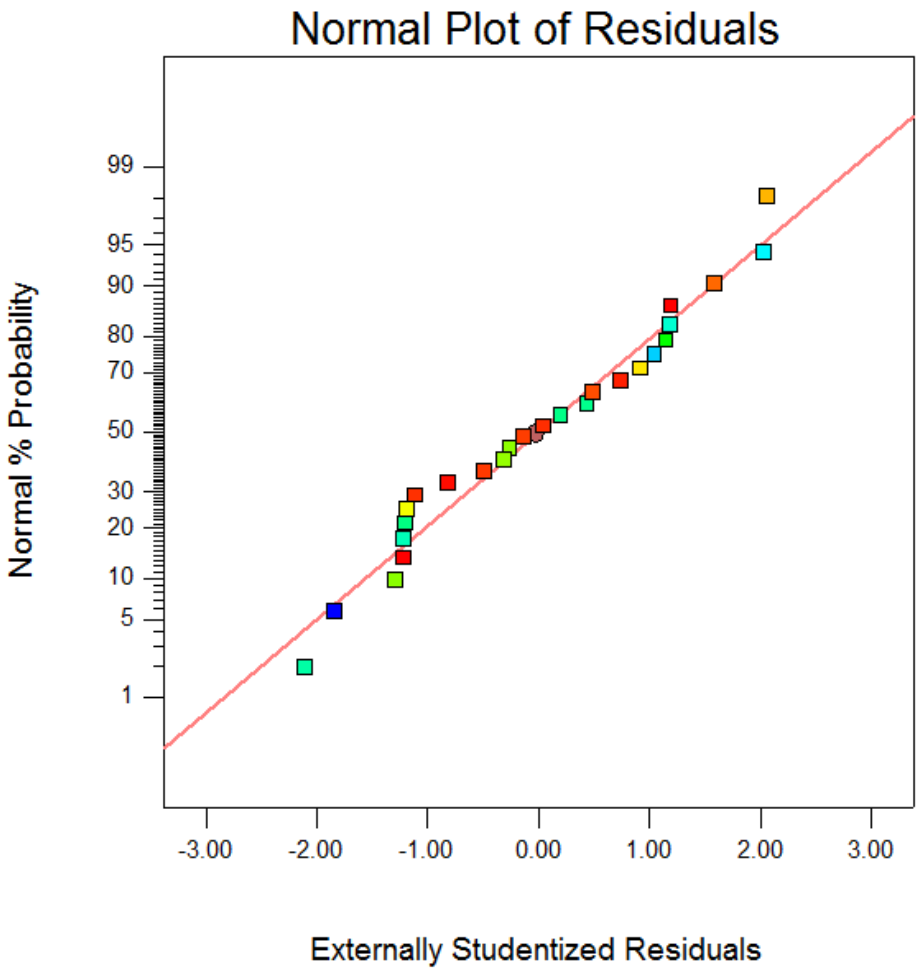

Figure 4.16. Normal Plot of Residuals: Yield

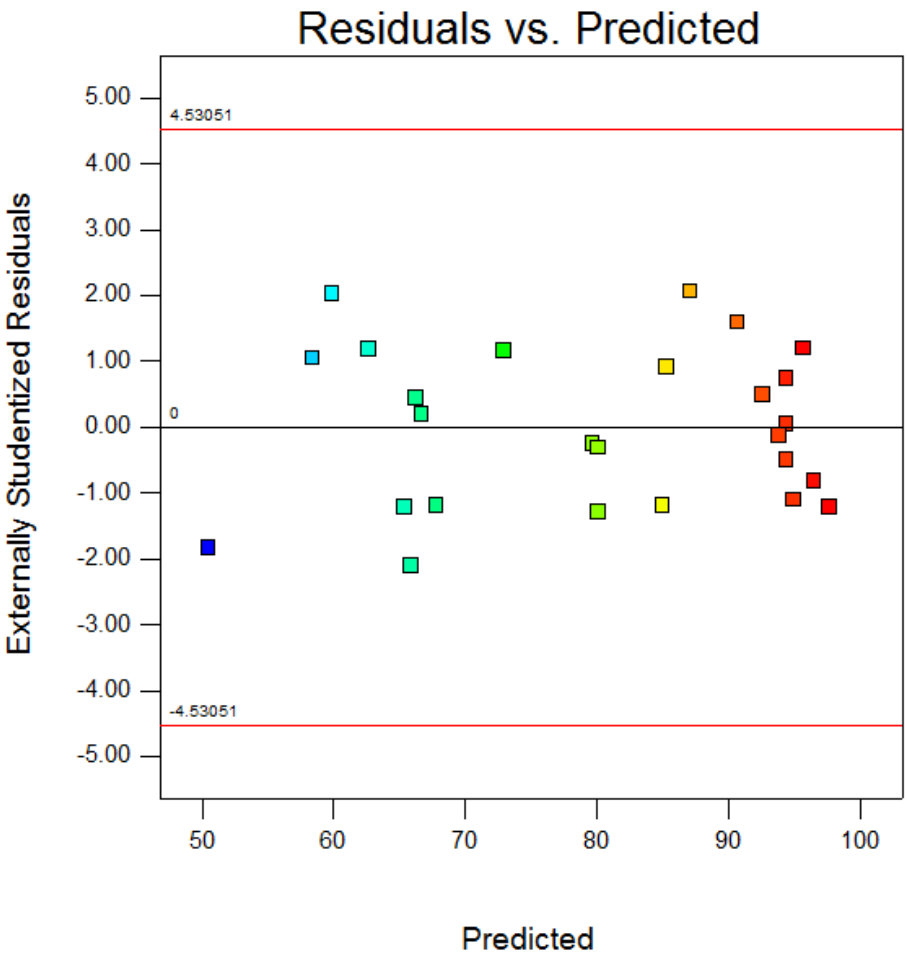

Figure 4.17. Residuals Plot: Yield

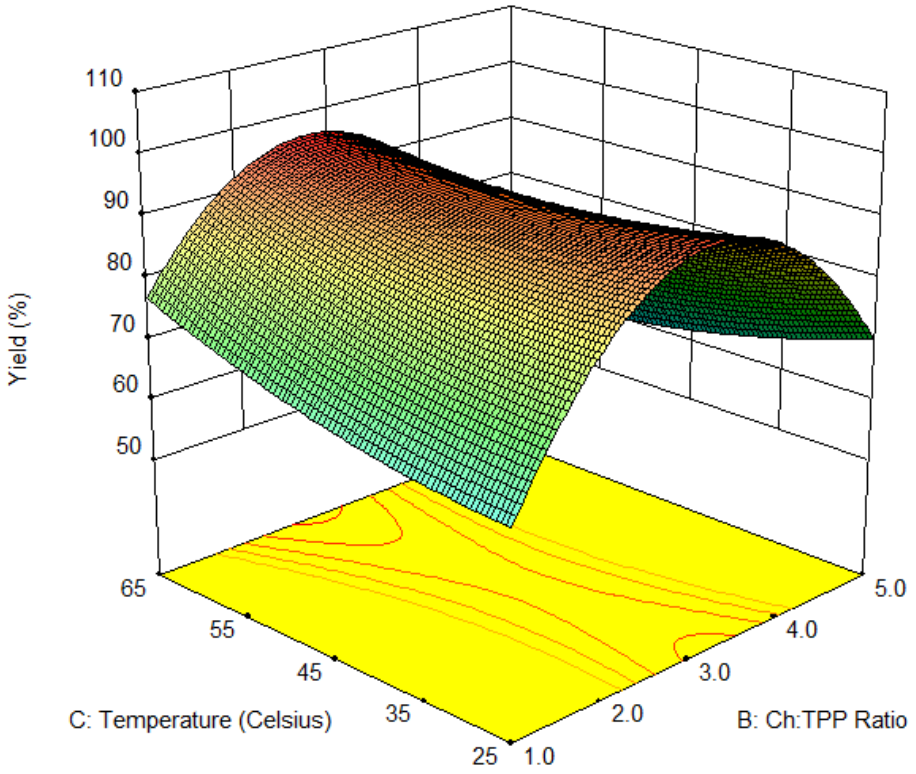

Figure 4.18. Response Surface Plot for Yield as a Function of Ch:TPP Ratio and Temperature

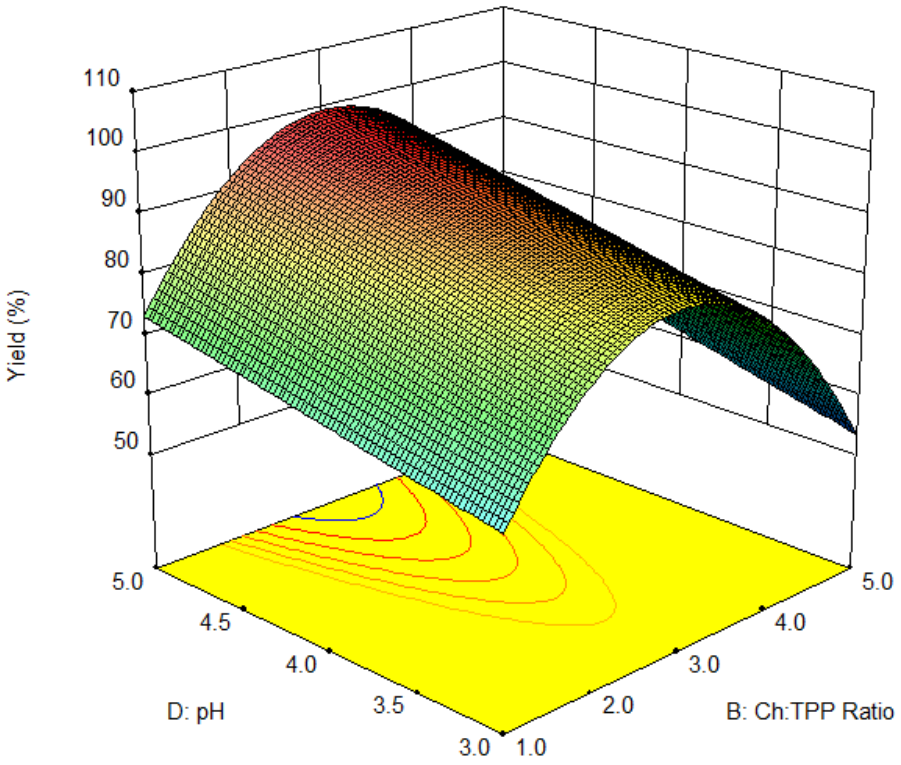

Figure 4.19. Response Surface Plot for Yield as a Function of Ch:TPP Ratio and pH

Dissolution (t_{50})

Fitting of dissolution data using Sigma Plot® yielded a range of t_{50} of 32 – 455 minutes across the entire 31 experiments. Higuchi parameters for each experimental run are found in Table 4.8 and Table 4.9. As the Higuchi equation describes release kinetics as a function of the square root of time (Siepmann & Peppas, 2011), example of this correlation is provided in Figure 4.20 using three different experimental runs with varying sustained release durations.

Table 4.8. Higuchi equation parameters for each experimental condition (Std. Runs #1 – 16)

Std #	Time* (min) / (% release)	k / (s.e.) / p-value	c / (s.e.) / p-value	R^2	Model p-value	t_{50}
1	120 / (77)	5.4731 / (0.3882) / < 0.0001	19.0591 / (3.0071) / 0.0032	0.9803	0.0001	32
2	240 / (75)	4.5139 / (0.2259) / < 0.0001	7.8232 / (2.2304) / 0.0127	0.9852	< 0.0001	87
3	480 / (76)	3.3835 / (0.1746) / < 0.0001	6.1774 / (2.2226) / 0.0239	0.9791	< 0.0001	168
4	120 / (78)	5.7794 / (0.3453) / < 0.0001	17.2550 / (2.6748) / 0.0030	0.9859	< 0.0001	32
5	240 / (79)	4.8736 / (0.2395) / < 0.0001	6.3499 / (2.3644) / 0.0363	0.9857	< 0.0001	80
6	480 / (77)	4.1209 / (0.1150) / < 0.0001	- 10.5144 / (1.4635) / < 0.0001	0.9938	< 0.0001	216
7	480 / (72)	3.4801 / (0.0537) / < 0.0001	N/A	0.9889	< 0.0001	206
8	360 / (71)	3.6716 / (0.1921) / < 0.0001	5.3519 / (2.1618) / 0.0425	0.9812	< 0.0001	148
9	240 / (66)	4.9665 / (0.2544) / < 0.0001	-8.1070 / (2.5117) / 0.0180	0.9845	< 0.0001	137
10	360 / (73)	4.3550 / (0.1723) / < 0.0001	-6.6399 / (1.9389) / 0.0111	0.9892	<0.0001	169
11	360 / (75)	4.3172 / (0.1083) / < 0.0001	N/A	0.9691	< 0.0001	134
12	180 / (69)	5.1654 / (0.0415) / < 0.0001	N/A	0.9969	< 0.0001	94
13	360 / (70)	4.0387 / (0.0832) / < 0.0001	-4.2862 / (0.9367) / 0.0026	0.9970	< 0.0001	181
14	600 / (78)	3.4206 / (0.0791) /< 0.0001	N/A	0.9771	< 0.0001	214
15	720 / (71)	2.8765 / (0.0756) / <0.0001	-3.2789 / (1.1829) / 0.0197	0.9931	< 0.0001	343
16	180 / (73)	5.4455 / (0.0762) / < 0.0001	N/A	0.9914	<0.0001	84

*Time refers to the last dissolution sampling time point used for the Higuchi equation fitting.
k = Higuchi constant; s.e. = standard error; c = constant accounting for burst release (positive value) or lag time (negative value)

Table 4.9. Higuchi equation parameters for each experimental condition (Continued, Std. Runs #16 – 31)

Std #	Time* (min) / (% release)	k / (s.e.) / p-value	c / (s.e.) / p-value	R^2	Model p-value	t_{50}
17	480 / (72)	3.4160 / (0.0655) / < 0.0001	N/A	0.9841	< 0.0001	214
18	360 / (74)	4.0743 / (0.0640) / < 0.0001	N/A	0.9881	< 0.0001	151
19	720 / (72)	2.7884 / (0.0425) / < 0.0001	N/A	0.9890	< 0.0001	322
20	600 / (70)	3.0442 / (0.0543) / < 0.0001	N/A	0.9854	< 0.0001	270
21	480 / (74)	3.4932 / (0.0777) / < 0.0001	N/A	0.9802	< 0.0001	205
22	600 / (71)	3.3115 / (0.1117) / < 0.0001	-6.6117 / (1.5875) / 0.0024	0.9899	< 0.0001	292
23	360 / (70)	3.7224 / (0.0833) / < 0.0001	N/A	0.9802	< 0.0001	180
24	600 / (71)	2.8026 / (0.1157) / < 0.0001	6.1754 / (1.6432) / 0.0045	0.9849	< 0.0001	245
25	600 / (76)	3.2141 / (0.0804) / < 0.0001	N/A	0.9752	< 0.0001	242
26	240 / (68)	4.6027 / (0.0685) / < 0.0001	N/A	0.9886	< 0.0001	118
27	720 / (62)	2.5686 / (0.0665) / < 0.0001	-4.7634 / (1.0407) / 0.0010	0.9933	< 0.0001	455
28	720 / (74)	2.9186 / (0.0681) / < 0.0001	N/A	0.9752	< 0.0001	293
29	600 / (71)	3.0939 / (0.0616) / < 0.0001	N/A	0.9818	< 0.0001	261
30	600 / (70)	2.9804 / (0.0634) / < 0.0001	N/A	0.9805	< 0.0001	281
31	600 / (73)	3.1474 / (0.0713) / < 0.0001	N/A	0.9772	< 0.0001	252

*Time refers to the last dissolution sampling time point used for the Higuchi equation fitting.
k = Higuchi constant; s.e. = standard error; c = constant accounting for burst release (positive value) or lag time (negative value)

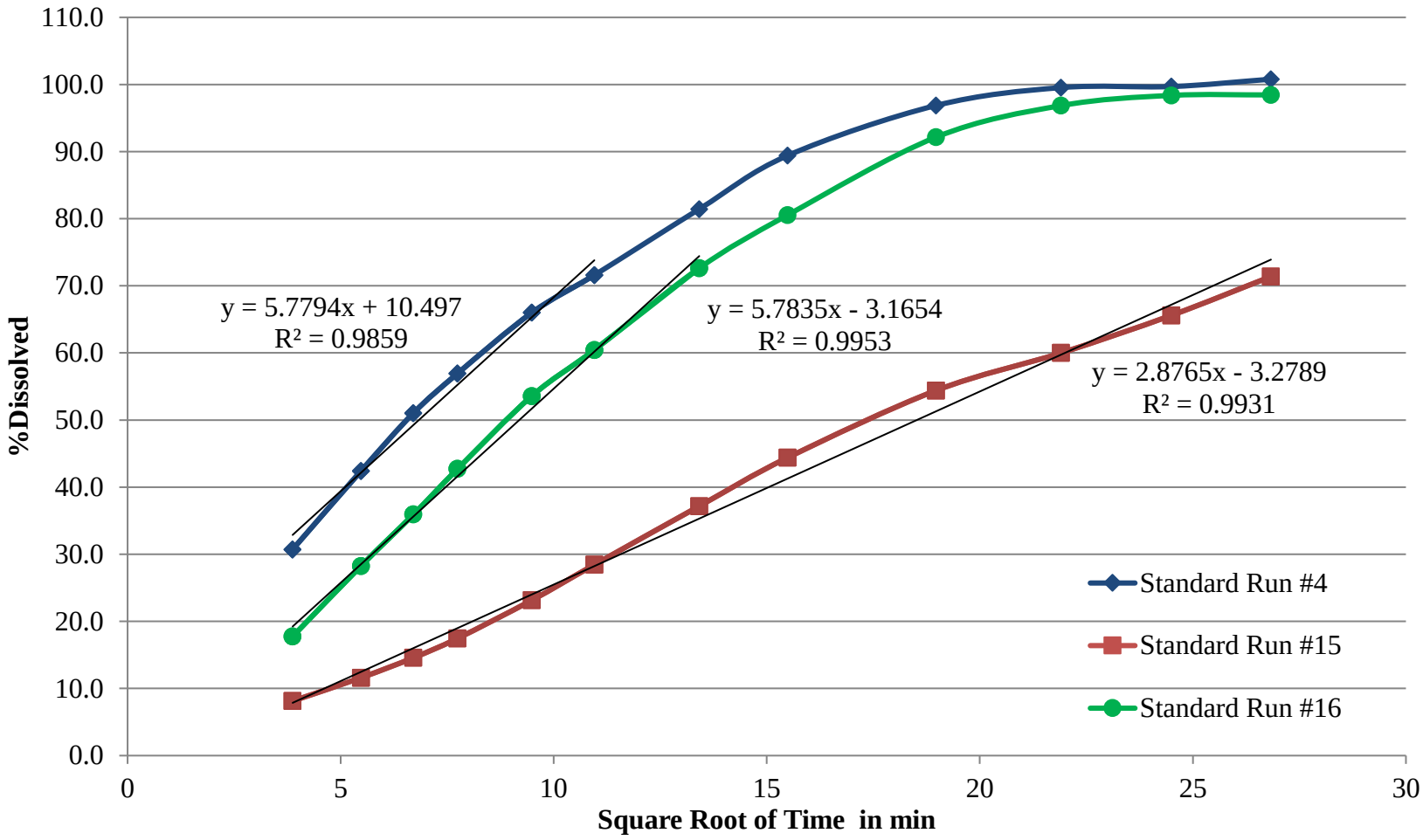

Figure 4.20. Drug release as a function of the square root of time with an overlay of the relationship described by the Higuchi equation

Analysis of this response following completion of the initial half-fractional yielded significant curvature ($p < 0.05$; Appendix 1, Table 7.5), warranting the additional experiments to complete a central composite design.

Analysis of variance showed that a quadratic model is significant ($p < 0.05$) for t_{50}. An inverse square root transformation (lambda = 0.5) was used as recommended by Box-Cox plot and no experimental runs were removed from the data analysis. Final ANOVA reports yielded a good R^2 value (>0.8) and showed no significant lack of fit (reference Table 4.10).

For t_{50}, all five variables; chitosan concentration (A), Ch:TPP ratio (B), temperature (C), pH (D), and NaCl concentration (E) are statistically significant. Five significant two factor interactions exist; the chitosan concentration-Ch:TPP ratio (AB), Ch:TPP ratio-pH (BD), Ch:TPP ratio- NaCl concentration (BE), temperature-pH (CD), and temperature-NaCl concentration (CE). One quadratic factor, pH (D^2), was shown to be significant. The model equation for the coded factor levels:

$$1/\text{sqrt}(t_{50}) = 0.068 + 3.622E\text{-}003A + 3.094E\text{-}004B - 0.014C - 0.014D + 8.455E\text{-}003E + 0.019AB + 6.601E\text{-}003BD + 6.387E\text{-}003BE + 0.010CD - 8.695E\text{-}003CE + 0.019D^2$$

is significant ($p < 0.0001$) and has a good fit to the data ($R^2 = 0.8989$). Lack of fit is not statistically significant ($p = 0.5131$) indicating that the results for the central composite design are described well by the equations.

The Normal Plot (Figure 4.21) indicates that the residuals for t_{50} are randomly distributed. The Residuals vs. Predicted Plot (Figure 4.22) does not reveal a trend in the residual data.

Table 4.10. Analysis of Variance: t_{50}

Source	**p-value**
Model	< 0.0001
A	0.1906
B	0.9088
C	< 0.0001
D	< 0.0001
E	0.0052
AB	< 0.0001
BD	0.0312
BE	0.0363
CD	0.0023
CE	0.0065
D^2	0.0034
Lack of Fit	0.5131
R^2	0.8989
Adj R^2	0.8370

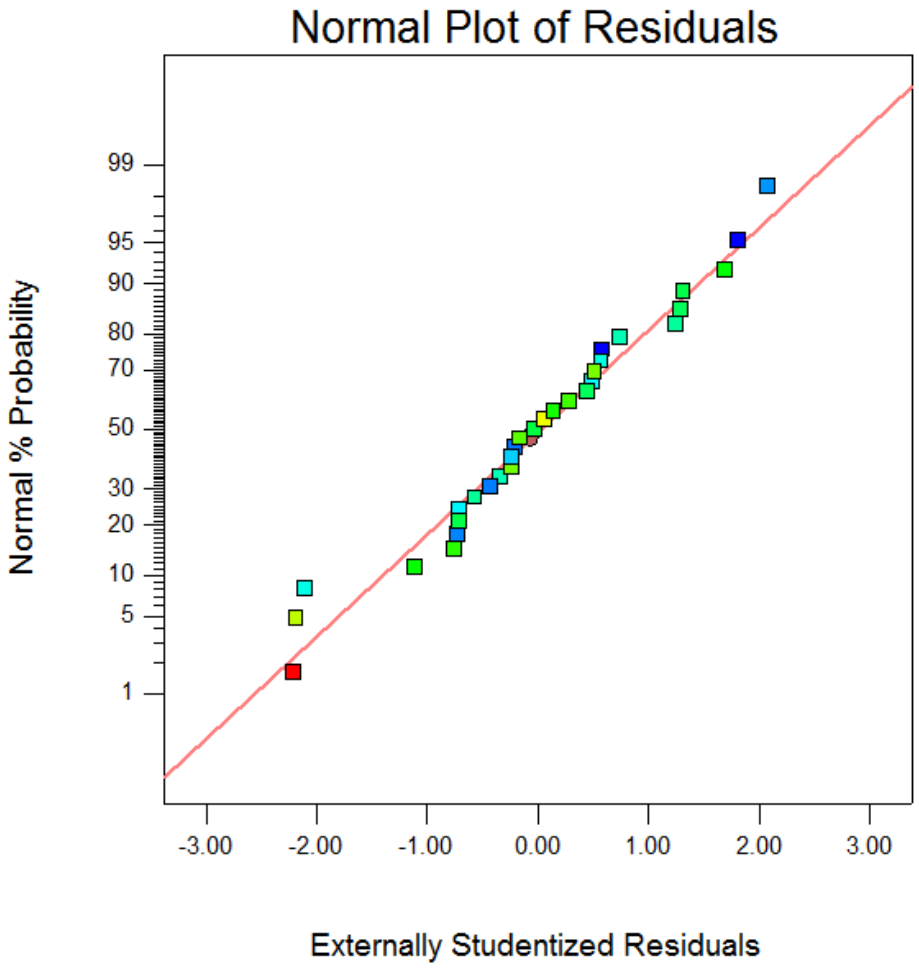

Figure 4.21. Normal Plot of Residuals: t_{50}

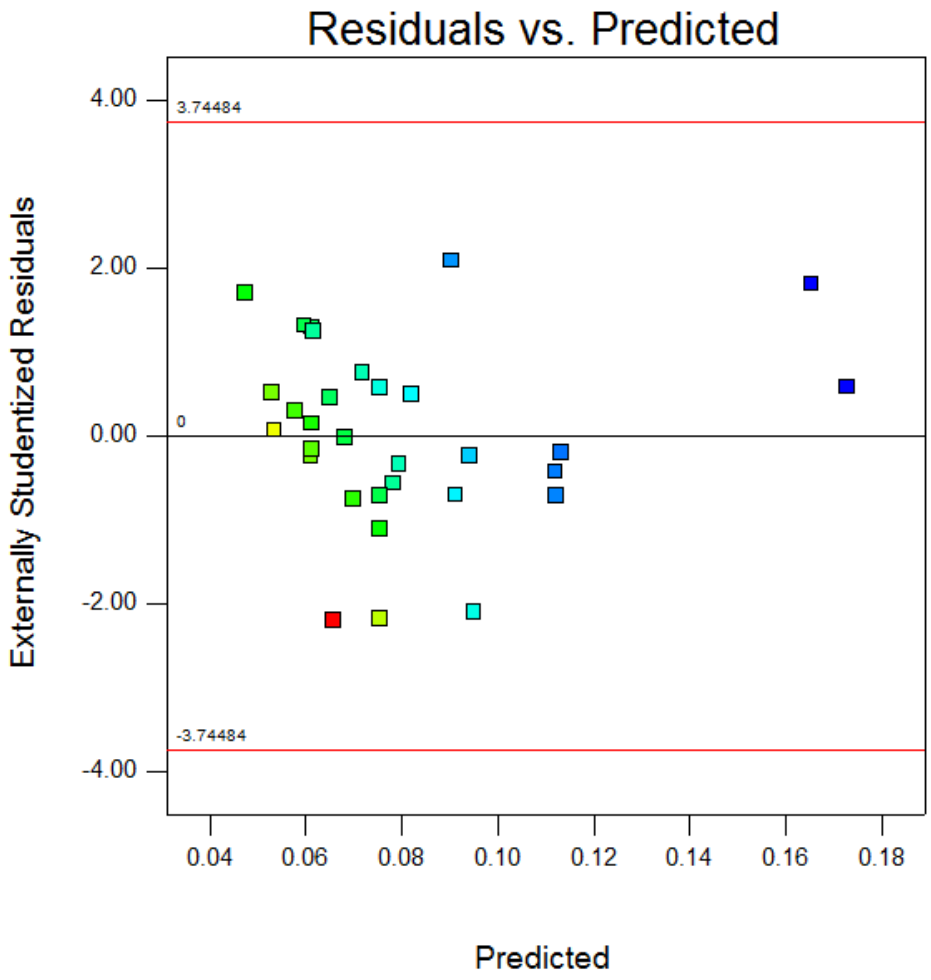

Figure 4.22. Residuals Plot: t_{50}

The response surface plot presented in Figure 4.23 depicts very different durations of release with varying chitosan concentration and Ch:TPP ratio. At maximum chitosan concentration, maximum release times were observed when Ch:TPP ratios were 1:1 and release began to speed up as the ratio increased to 5:1. This trend suggests that at the high chitosan concentrations and 1:1 Ch:TPP ratio, maximum crosslinking exists and drug can become embedded in this matrix. Conversely, at low chitosan concentration, drug release slowed as the ratio of Ch:TPP increased from 1:1 to 5:1. Data in Table 4.2 also show that these conditions (chitosan concentration = 1 mg/ml, Ch:TPP ratio = 5:1) produced some of the smallest nanoparticles. Thus, the slower release could suggest that at these conditions, the chitosan chains tended to fold over themselves, created a tighter complex, making it more difficult for drug to escape.

In Figure 4.24, a general trend is observed that regardless of Ch:TPP ratio, drug release slows as the NaCl concentration decreases from 0.02 mM to 0.0 mM. This trend further supports previous hypothesis that the presence of salt may result in a "looser" crosslinked structure, which subsequently allows drug to more easily release from the chitosan-tripolyphosphate ionically crosslinked matrix.

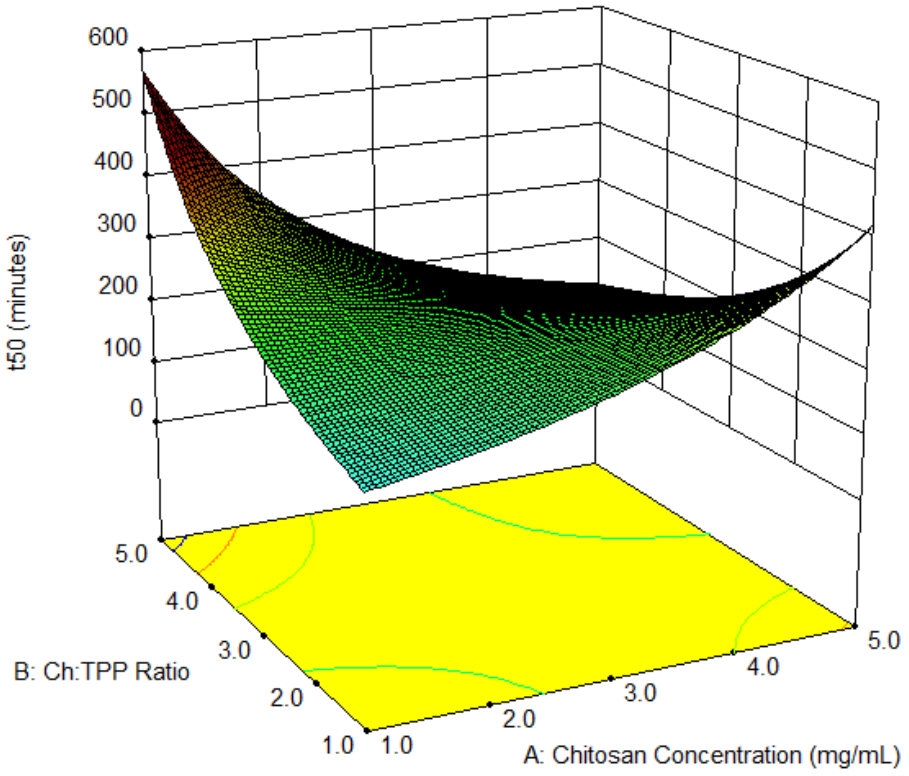

Figure 4.23. Response Surface Plot for t_{50} as a Function of Ch:TPP Ratio and Chitosan Concentration

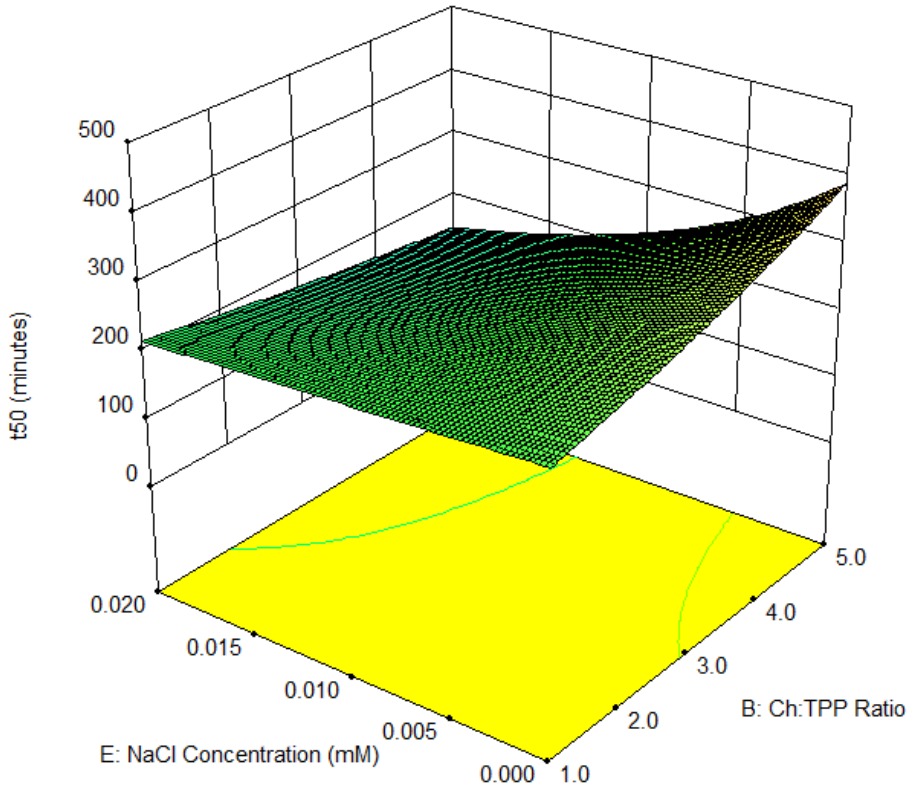

Figure 4.24. Response Surface Plot for t_{50} as a Function of Ch:TPP Ratio and NaCl Concentration

Conclusions

While there are previous studies evaluating various formulation and process factors in the preparation of chitosan-tripolyphosphate ionically crosslinked particles, this study represents the most comprehensive and systematic investigation of the variables and responses analyzed. Further, the focus of previous studies included incorporation of drug prior to crosslinking and did not evaluate the use of a solid dose tablet as the final dosage form. This study used acetaminophen as a model drug in a dry blend with the chitosan-tripolyphosphate crosslinked material with no additional tableting excipients required.

The influence of the various factors and associated two-factor interactions was effectively assessed and characterized by using statistical experimental design. The generation of model equations, by means of ANOVA, for each response can be used to estimate response values for future experimentation within the design space studied.

CHAPTER 5

Optimization and Characterization of Chitosan-Tripolyphosphate Using Model Equations for Solid State Evaluation

Introduction

In this chapter, previously established model equations generated via statistical experimental design were used to generate sufficient quantities of three unique chitosan-tripolyphosphate crosslinked materials with optimized properties for further characterization. Results for each response were compared to the 95% confidence and tolerance intervals generated using Design Expert® point prediction statistical tools. Further analysis of the materials, including environmental scanning electron microscopy (eSEM) and dynamic vapor sorption (DVS) analysis, was performed to better understand properties of the materials.

Water Sorption Analysis

Adsorption and absorption of water by the chitosan-tripolyphosphate crosslinked material, in essence, controls the release of drug from the matrix. The crosslinking density of the chitosan-tripolyphosphate matrix will control the extent and rate of water adsorption and absorption, which subsequently leads to swelling and breakdown of the matrix, resulting in drug release (J. A. Ko, Park, Park, Hwang, & Park, 2003; Remuñán-López, 1997). Given the manufacturing processes used to develop the chitosan-tripolyphosphate particles in the present study, which includes crosslinking in solution, followed by centrifugation and lyophilization, the high contribution of water and removal of water in these processes ultimately affects the final water content of the product and consequently its ability to take up moisture in the final dosage form (Ahlneck & Zografi, 1990). Further understanding of how a material takes up water and the types of water

associated with that material at equilibrium can reveal much about the properties of the material and ultimately lead to a better understanding of the manufacturability and critical quality attributes of the final dosage form (A. Nokhodchi, Ford, & Rubinstein, 1997).

Sorption of water to polymer surfaces generally begins due to hydrogen bonding of water molecules with polar functional groups present in the polymer (Bell & Labuza, 2000; Brittain, 1995). In the literature, this process has been evaluated via both differential scanning calorimetry (DSC) and dynamic vapor sorption (DVS) analysis for various natural polymers, including chitosan (Agrawal et al., 2004; Aguirre-Loredo, Rodriguez-Hernandez, & Velazquez, 2017; Kachrimanis, Noisternig, Griesser, & Malamataris, 2006; Vílchez et al., 2016). Three different types of water are generally addressed when discussing the hydration of polymers (Agrawal et al., 2004; Basu, Shivhare, & Mujumdar, 2006; Hamaura & Newton, 1999; Joshi & Wilson, 1993; Kunio Nakamura, Hatakeyama, & Hatakeyama, 1981; K. Nakamura, Hatakeyama, & Hatakeyama, 1983):

1. Free Water (Type I) – this water is classified as unbound water and generally exhibits properties similar to those of pure water. It can commonly be found in void spaces and capillaries of polymer materials.
2. Freezing Bound Water (Type II) – this water is classified as associating loosely with the water already bound to hydrophilic functional groups of a polymer. As a result of these interactions, it is known to have a higher enthalpy of vaporization and a lower melting temperature than pure water has.
3. Nonfreezing Bound Water (Type III) – this water is strongly associated with the polymer by strong polar intermolecular forces. By superimposing itself in

a bond between polar functional groups found in a polymer molecule or between two polymer molecules, water can function as a plasticizer by breaking intrapolymer and interpolymer bonds, respectively, that make a polymer material rigid. This type of water will not be available for chemical reactions. The melting point and enthalpy of vaporization are not generally detected or measurable with only DSC analysis.

The method most commonly used to identify these types of water is known as dynamic vapor sorption (DVS) analysis, a process that involves accessing data for both a sorption and a desorption isotherm for the particular polymer. This is performed by exposing a polymer material to stepwise increases in relative humidity at constant temperature and assessing equilibrium at each relative humidity by monitoring for a new constant mass (sorption), followed by the same assessment of a constant mass under stepwise decreasing relative humidity conditions (desorption). When no further weight fluctuation is observed at each step of the analysis, equilibrium is presumed to exist between the hydrated polymer sample and the moisture in the vapor phase (Bell & Labuza, 2000).

A plot of the sorption or desorption data for a specific polymer at a particular temperature is known as an isotherm. Five types of isotherms have been identified and are categorized as Types 1 – 5 based on their general shape (Brunauer, Deming, Deming, & Teller, 1940). The type most commonly attributed to water insoluble hydrophilic polymers is Type II, which has a sigmoidal or S-shaped curve (Agrawal et al., 2004). The desorption isotherm generally exhibits a higher amount of water associated with the sample at equilibrium than observed in the sorption isotherm at a given relative humidity;

the difference between the two curves is referred to as a hysteresis (Young & Nelson, 1967a). Differences in the curves are attributed to an array of circumstances including conformational changes to the polymer chains, such as swelling or relaxation, and both entropy and enthalpy effects resulting from polymer-water bonds and molecular ordering, respectively (Agrawal et al., 2004; J. H. de Boer, 1968; Hollenbeck, Peck, & Kildsig, 1978; Zografi & Kontny, 1986).

Various mechanisms have been proposed for water behavior and mathematical equations have been published over the past century to account for the data based on those mechanisms (Basu et al., 2006). Upon generating sorption and desorption isotherms, these model equations have been fit to the data to describe the locations of water and the strength of the bonds between water and the polymer. The GAB equation and the Young and Nelson equations are the models most commonly used in analysis of sorption and desorption curves for water association with polymer samples. The GAB equation, developed by Edward Guggenheim (Guggenheim, 1966), Robert Anderson (Anderson, 1946; Anderson & Hall, 1948), and Jan de Boer (J. De Boer, 1953), is an elaboration of a model first published by Stephen Brunauer, Paul Emmett, and Edward Teller (Brunauer, Emmett, & Teller, 1938), commonly referred to as the BET model. The BET equation only accounts for monolayer water, but the GAB equation includes a constant, *K*, to account for sorption of multiple layers of water (Basu et al., 2006). The BET model is thus considered inaccurate when the water activity (a_w) is above approximately 0.4 (Boquet, Chirife, & Iglesias, 1978) which suggests the likelihood of formation of multiple layers of water on the sample. On the other hand, some claim that water content with water activity as high as 0.93 has been described using the GAB

equation (Basu et al., 2006). The Young and Nelson equations (Young & Nelson, 1967a, 1967b) boast the additional ability to describe the desorption isotherm. The Young and Nelson model describes three types of water including a tightly bound monolayer, externally adsorbed moisture, and internally absorbed water, but requires a combination of multiple nonlinear regression analysis in an iterative fashion to adequately fit the model to the sorption and desorption data (Agrawal et al., 2004; Kachrimanis et al., 2006; A. Nokhodchi et al., 1997).

The DVS analysis presented in this study is intended to elucidate how the crosslinking of the optimized samples impacts its ability to take up and distribute water. Sorption and desorption isotherms for each sample are analyzed using GAB and Young and Nelson model equations.

Materials

Powdered chitosan, purchased from DCV BioNutritionals (Wilmington, DE), with a 92% degree of deacetylation and an average molecular weight of 470 kD (Omwancha et al., 2011) was used for all experiments. Sodium tripolyphosphate (NaTPP) was purchased from Sigma-Aldrich (St. Louis, MO). Acetaminophen from Mallinckrodt Pharmaceuticals (St. Louis, MO) was used as a model active pharmaceutical ingredient (API) for dissolution testing. Hydrochloric acid, 37%; glacial acetic acid, ≥ 99.7%; and sodium hydroxide were all purchased from Fisher Scientific (Fair Lawn, NJ).

Methods

Statistical Design

Using the previously established statistically significant models generated by completion of the design of experiments presented in Chapter 4, the optimization node in Design Expert® software was used to suggest factor levels to produce material with a pre-defined set of desired outputs or responses. First, criteria are defined for each applicable factor and/or response and an importance factor, weighted 1-5, is assigned to each defined criterion. When no criterion is defined for a specific factor or response, that specific attribute is allowed to "float" to best achieve the defined criteria; this is designated as "in range" for factors and "none" for responses. For factors, "in range" indicates that the value must be within the design space already explored.

Once the criteria are defined, Design Expert® software generates a list of probable solutions that best achieve the desired criteria. Each solution is assigned a Desirability factor from 0 – 1.0, such that as values increase from 0 to 1.0, it is expected that the suggested factor settings will better achieve the desired response criteria. From the list of solutions, factor settings can be selected and/or modified to simplify the experimentation (e.g. rounding fractional numbers to whole numbers) and ultimately predict a new set of responses. The criteria used for the optimization are presented in Table 5.1. The goal for each set of experimental conditions and the resulting optimized crosslinked product were the following:

- Optimized Sample A: Generate material that produces a release profile similar to that observed when the model API is combined with chitosan alone (i.e. no

crosslinking with TPP) as a control in later studies and subsequently assess any impact on compressibility and other physical properties

- Optimized Sample B: Generate material with a normal particle size distribution that provides sustained release of model API
- Optimized Sample C: Generate material with a broad particle size distribution relative to that of Sample B that provides sustained release of model API to assess differences in compressibility and other physical properties

Solutions for each optimization were reviewed (data not presented here) and factor settings were selected based on desirability but also taking into account the feasibility to execute manufacture of the material under the specified conditions, such that certain factor levels were rounded up or down accordingly. The final set of factors for production of optimized samples and the resulting desirability are presented in Table 5.2.

Once the experimenter defines the factors to be used for experimentation, the Design Expert® optimization node can be used to identify the desirability using the pre-defined factor settings. The Design Expert® point prediction node is then able to generate predicted statistics for the response values to be measured including mean, median, error, and the confidence and tolerance intervals. Actual results gained through experimentation can then be compared to predicted results to assess the accuracy, predictability, and practical significance of the established models.

Table 5.1. Optimization criteria used for each factor and response and associated rationale, where applicable. Importance values are presented in parenthesis and can range from 1 to 5.

		Optimized Sample A	Optimized Sample B	Optimized Sample C
Factors	Chitosan Concentration	Maximize (3) – generate maximum quantities of usable crosslinked material	Maximize (3) – generate maximum quantities of usable crosslinked material	Maximize (3) – generate maximum quantities of usable crosslinked material
	Ch:TPP Ratio	In Range (3)	In Range (3)	In Range (3)
	Temperature	In Range (3)	In Range (3)	In Range (3)
	pH	In Range (3)	In Range (3)	In Range (3)
	NaCl Concentration	In Range (3)	In Range (3)	In Range (3)
Responses	d50	None (3)	None (3)	None (3)
	Span	Minimize (3) – generate a normal particle size distribution	Minimize (3) – generate a normal particle size distribution	Maximize (3) – generate a broad particle size distribution
	True Density	None (3)	None (3)	None (3)
	Zeta Potential	None (3)	None (3)	None (3)
	Yield	Maximize (3) – generate maximum quantities of usable crosslinked material	Maximize (3) – generate maximum quantities of usable crosslinked material	Maximize (3) – generate maximum quantities of usable crosslinked material
	t_{50}	Target: 90 minutes (5) – match t_{50} observed for tablets made of only chitosan and model API (see Chapter 4)	In Range: 240 – 300 minutes (5) – exhibit sustained release when compared to Sample A (release across small intestine)	Target: 240 – 300 minutes (5) – exhibit sustained release similar to that of Sample B

Table 5.2. Factor set points used for optimization experiments and the associated Desirability values

Sample	Chit. Conc. (g/ml)	Ch:TPP Ratio	Temp (°C)	pH	NaCl Conc. (mM)	Desirability
Optimized Sample A	5.0	4.5	35	4.0	0.01	0.899
Optimized Sample B	5.0	3.0	60	4.5	0.02	0.944
Optimized Sample C	5.0	2.0	65	3.4	0.02	0.709[1]

Note: To generate a desirability value for sample C, a target of 248 minutes was used for t_{50}. This represents the t_{50} generated when using the numerical optimization node in Design Expert® for Optimized Sample B using the factor set points defined in Table 5.2.

Ionic Gelation for the Formation of Ch-TPP Crosslinked Material

The ionic gelation crosslinking process was performed as described by several authors in the literature (Calvo, 1997; De Campos et al., 2001; Y. Xu & Du, 2003; L. Zhang & Kosaraju, 2007). Slight modifications were made to production parameters to achieve target factor conditions as described in Table 5.2.

Chitosan stock solutions were prepared by dissolving the desired mass of chitosan in 2% acetic acid solution to yield concentrations such that 850 ml of the stock solution would provide 1, 3, or 5 mg/ml chitosan concentration when diluted to 1 liter. Sodium tripolyphosphate (NaTPP) stock solutions were prepared by dissolving the appropriate amount of NaTPP such that 100 ml of the stock solution would provide the appropriate Ch:TPP ratio when diluted to 1 liter.

An 850 ml portion of appropriate chitosan stock solution was dispensed into a 1500 ml beaker. If applicable, the required amount of NaCl was added to the chitosan solution and was dissolved by mixing for 10 minutes at 300 rpm using a Fisher stirring hotplate (Fair Lawn, NJ) and magnetic stir bar. The solution was then heated to the desired temperature using the hotplate and temperature was monitored with a thermometer. The solution was covered with tight fitting aluminum foil to minimize evaporation. The sample pH was then modified to the desired pH using stock solutions of 5 N NaOH or 5 N HCl based on the initial pH (taken when final temperature was reached). The volume required for pH modification was then supplemented to 50 m1 with purified water.

Finally, 100 ml of the appropriate NaTPP solution was added dropwise to the chitosan solution and the solution was mixed for 1 h at 300 rpm. Small aliquots were extracted for response testing as needed. The remainder of the sample was centrifuged at

10,000 rpm for 20 min using a Sorvall LYNX 6000 centrifuge (Thermo Scientific, Darmstadt, Germany). The sample was lightly rinsed using purified water and centrifuged again for another 20 min at 10,000 rpm.

Solid sample was then isolated from the centrifuge tubes and lyophilized for 36 hours using a VirTis AdVantage 2.0 bench top lyophilizer (SP Scientific, Gardiner, NY). The entire manufacturing process was repeated ten times for each set of optimized conditions presented in Table 5.2 to provide sufficient quantities for further analysis.

Particle Size (d50 and Span)

Particle size analysis was performed using a Mastersizer 2000 (Malvern Instruments, Westborough, MA). d50 represents the median particle size while Span is intended to represent the width of the particle size distribution as a single value and is calculated using the following equation:

$$Span = \frac{d_{90} - d_{10}}{d_{50}}$$

where d_{90} represents the particle size diameter that 90% of the particles by mass fall under; d_{10} represents the particle size diameter that 10% of the particles fall under; and d_{50} represents the particle size diameter that 50% of the particles fall under, also known as the median (d50) ("Understanding and Interpreting Particle Size Distribution Calculations," n.d.).

Liquid samples from the 1 liter Ch-TPP mixtures were drawn using a plastic disposable pipette. Samples were taken from each of the 10 individual 1 liter production batches to generate d50 and Span results representative of the entire population for the specific experimental conditions. For 1 liter mixtures produced on the same day, liquid samples were combined such that a total of n = 3 samples were generated to be

representative of the n = 10 total population. The samples were sonicated in the Mastersizer for 90 sec prior to data analysis, consistent with the method used in the initial design of experiments.

True Density

The True Density of lyophilized Ch-TPP powders was analyzed in triplicate using a Stereopycnometer™ helium pycnometer (Quantachrome Instruments, Boynton Beach, FL). Samples were taken from a homogenous mixture of powder derived from the 10 individual 1 liter production batches to provide true density results representative of the entire population for each of the specified experimental conditions.

Zeta Potential

Zeta Potential was measured using a Nano S ZetaSizer (Malvern Instruments, Westborough, MA). Liquid samples from each of the 10 individual 1 liter Ch-TPP production batches were drawn using a plastic disposable pipette and analyzed immediately to generate Zeta Potential results representative of the entire population for each of the specified experimental conditions.

Yield

Percent yield was calculated based on the theoretical weight of Ch-TPP samples. Yield was calculated using the combined mass of material generated for each of the ten individual 1 liter productions for each of the specified experimental conditions. Any material lost as a result of sampling for other tests while in the liquid phase was considered negligible for the purposes of calculating the bulk yield. Each of the 1 liter Ch-TPP batches was centrifuged in its entirety by dividing the solution equally into four 250 ml centrifuge tubes. The liquid was decanted and the solid sample was removed from the centrifuge tubes and lyophilized in beakers. Lyophilized material from each of

the ten production batches was then combined such that final percent yield was calculated as:

$$Yield\ (\%) = \frac{final\ mass}{theoretical\ mass\ of\ Chitosan + TPP} \cdot 100\%$$

Tablet Manufacture and Dissolution Analysis

Tablets for dissolution testing were compressed using Ch-TPP crosslinked material from the bulk material generated for each of the three optimized conditions. Additionally, given the broad particle size distribution of Sample C, tablets were made using fine, medium, and coarse particles representative of equal 1/3 splits by mass of the larger bulk sample to further assess the impact of particle size on drug release. Samples were blended with acetaminophen as a model drug at 10% w/w and compressed into tablets (300 mg target weight) using 3/8" standard concave tooling under 38,500 psi (2 tons) of pressure on a NP-RD10A bench top press (Natoli, St. Charles, MO). Three tablets were made for each Ch-TPP material.

Dissolution testing of tablets was performed in triplicate using a USP <711> Apparatus II (United States Pharmacopeia National Formulary, 2016b) model 2100C dissolution apparatus (Distek, North Brunswick, NJ) at a paddle speed of 50 rpm. Simulated intestinal fluid (SIF) without pancreatin was used as the dissolution medium with samples pulled at intervals over 12 hours (15, 30, 34, 60, and 90 min; 2, 4, 6, 8, 10, 12 h) using a model 2230A autosampler (Distek, North Brunswick, NJ). Drug concentration in these samples was determined at 245 nm using a SpectraMax Plus UV/Vis photospectrometer (Molecular Devices, Sunnyvale, CA).

Several established kinetic models for drug release from controlled release systems were fit to dissolution data using SigmaPlot® v. 12.5 software (Systat Software, Inc., San Jose, CA). The models included the Korsmeyer-Peppas equation (Korsmeyer et al., 1983), the Higuchi equation (Higuchi, 1963), and the Baker-Lonsdale equation (Baker, 1974). The Higuchi equation was shown to be the most appropriate fit to the release data and is described by the following equation:

$$\frac{M_t}{M_\infty} = k \cdot \sqrt{t} + c$$

where M_t is defined as the amount of drug released at time t; M_∞ is defined as the amount of drug released as time approaches infinity, which is assumed to equal the theoretical drug mass in a tablet; k is the Higuchi constant dependent on the initial drug concentration, solubility, diffusion coefficient, as well as the surface area available for drug release; and c is a constant that accounts for burst release ($c > 0$) or lag time ($c < 0$) for initial drug release (Siepmann & Peppas, 2011). Only time points with less than 80% drug release were considered for equation fitting (Costa & Sousa Lobo, 2001). The time for 50% drug release (t_{50}) was then calculated using the derived Higuchi equation for each experimental run.

Environmental Scanning Electron Microscopy (eSEM)

Images were taken of pure chitosan and chitosan-tripolyphosphate crosslinked powders (optimized samples A, B, and C) using a Quanta 250 environmental electron scanning microscope (FEI, Hillsboro, OR). Small quantities of each sample for analysis were mounted on aluminum mounts using carbon adhesive tabs. Images were captured under low vacuum mode using a large field detector (LFD). Brightness and contrast were

fine-tuned until a clear image appeared. Sample images were taken at various magnifications ranging from 50 to 2500x.

Dynamic Vapor Sorption (DVS) Analysis

Dynamic vapor sorption analysis was performed for pure chitosan and chitosan-tripolyphosphate crosslinked powders (optimized samples A, B, and C) using a DVS Intrinsic (Surface Measure Systems Ltd., Allentown, PA). Each of the samples was dried under a vacuum for 24 h at 60 °C prior to being placed into the sample chamber. The samples were exposed to relative humidity conditions from 0 to 90% at 10% increments. Humidity conditions remained constant until the mass change of the sample was observed to be not more than 0.005% for more than 5 min, at which point equilibrium conditions were assumed to be established.

The GAB equation (Equation 5.1), as developed by Guggenheim, Anderson and de Boer (J. H. de Boer, 1968; Van den Berg, 1981) is:

$$W = \frac{W_m C_G K\left(P/P_0\right)}{\left[1-K\left(P/P_0\right)\right]\left[1-K\left(P/P_0\right)+C_G K\left(P/P_0\right)\right]} \tag{5.1}$$

where W is the grams of water sorbed per gram of solid sample, W_m is the grams of water in the form of a monolayer per gram of solid sample, C_G and K are parameters related to the heats of sorption, and P/P_0 is the water vapor relative pressure (the relative humidity expressed as a fraction). The parameter K accounts for a layer or layers of sorbed molecules, that are taken up with a degree of binding that is intermediate to that of the monolayer at the polymer-water interface and of bulk water (Saripella, 2012). Parameters K and C_G can be defined as:

$$K = B_1 \times \exp\left[\frac{H_L - H_m}{RT}\right] \tag{5.2}$$

and

$$C_G = D \times \exp\left[\frac{H_1 - H_m}{RT}\right] \tag{5.3}$$

where B_1 and D are constants, H_L is the heat of condensation of water, H_m is the heat of sorption of water when sorbed in the intermediate layer, H_1 is the heat of sorption of water in the first sorbed monolayer, R is the ideal gas constant, and T is the absolute temperature.

The Young and Nelson equations (Equations 5.4 – 5.9) were derived to describe the equilibrium water sorption and desorption of natural materials, e.g., starch (Young & Nelson, 1967a, 1967b). They can be used to differentiate three forms of moisture: a "tightly bound" or adsorbed monolayer at the surface of the polymer sample, "normally condensed" or external moisture (the combination of monolayer and multilayer water from the GAB descriptions of types of sorbed water), and "absorbed" or internalized moisture (Agrawal et al., 2004; Saripella, 2012). The six Young and Nelson equations required to calculate the different parameters are as follows:

$$E = exp\left[-\left(q_1 - q_L\right)/kT\right] \tag{5.4}$$

$$\theta = \frac{rh}{rh + (1 - rh)E} \tag{5.5}$$

$$\psi = rh \times \theta \tag{5.6}$$

$$\beta = -\frac{E \times rh}{E-(E-1)rh} + \frac{E^2}{E-1}\ln\left(\frac{E-(E-1)rh}{E}\right) - (E+1)\ln(1-rh) \quad (5.7)$$

$$M_s = A(\theta + \beta) + B \times \psi \quad (5.8)$$

$$M_d = A(\theta + \beta) + B \times \theta \times rh_{\max} \quad (5.9)$$

where θ is the fraction of the surface covered by a monomolecular layer of water, ψ is the fraction of the surface covered by a layer of water two or more molecules thick, β is the total amount of adsorbed moisture found in multilayers, M_s and M_d are the moisture contents of the powder during sorption and desorption conditions, *rh* and rh_{max} are the relative humidity and the maximum relative humidity expressed as fractions. *A*, *B*, and *E* are parameters unique to each test material. *E* is described by equation 5.4, where q_1 is the heat of adsorption of water molecules bound to the surface, q_L is the heat of condensation of pure water molecules, *k* is Boltzmann's constant, and *T* is the absolute temperature. *E* can be estimated as a function of the constants *K* and C_G determined in the application of the GAB equation to the sorption data. This initial estimate assumes that the constants B_1 and *D* in equations 5.2 and 5.3, respectively, are approximately equal to 1. A rearrangement of the equations results in an estimated value of *E* from the relation $\ln E \approx \ln K - \ln C_G$. The value of *A* and *B* parameters in equations 10 and 11 are:

$$A = \frac{V_m \times \rho_w}{W_m'} \quad (5.10)$$

$$B = \frac{V_a \times \rho_w}{W_m'} \quad (5.11)$$

where V_m and V_a are the molecular volumes of the adsorbed and absorbed moisture, respectively, ρ_w is the density of water, and W'_m is the mass of the material being analyzed. As the values for V_m and V_a are difficult to determine experimentally, the values of *A* and *B* are not calculated directly. Instead, these values are estimated by fitting equations 5.8 and 5.9 to the moisture sorption data. This was accomplished by varying the value of *E* until a maximum R^2 was achieved for fitting both the sorption and desorption isotherms with the added stipulation that values for *A* and *B* were each statistically significant ($p < 0.05$) for the fit to sorption and desorption data using non-linear regression analysis. These values are then used to determine $A\theta$, the amount of moisture present as a monolayer; $A(\theta + \beta)$, the externally adsorbed moisture that includes monolayer moisture; and $B\psi$, the amount of the internally absorbed moisture during the sorption cycle, each in units of g/g of sample (Agrawal et al., 2004; Saripella, 2012).

Results and Discussion

Particle Size (d50 and Span)

Particle size and size distribution results as measured by d50 and Span for chitosan-tripolyphosphate crosslinked mixtures (optimized samples A, B, and C) are presented in Table 5.3 along with the statistical predictions generated using Design Expert® point prediction node. Particle size (d50) results were generally in agreement with the predicted values as the average results fell within the 95% confidence intervals, substantiating the predictability of the model equations established from the initial design of experiments (DOE). It should be noted that sample A and sample B had slightly higher standard deviations for d50, suggesting an inconsistent agglomeration in the samples. From the initial DOE performed, samples with a d50 greater than 0.300 μm

generally suggested the presence of agglomeration and revealed a bimodal particle size distribution. d50 values were observed both above and below this 0.300 μm threshold for sample A and sample B, but for sample C, all individual results were above 0.450 μm.

For particle size distribution results, Span results did not match the predicted values. However, as expected, the patterns observed in Span results were consistent with those observed for d50 results. Specifically, for sample A and sample B, high standard deviations were evident. The range in Span values measured for each of these samples at the lower end had individual values of ~10-13 and values at the upper end ranging from 425-638. These individual results show that in the absence of agglomeration, Span results for sample A and sample B would be more in line with the predicted values. For sample C, each of the individual span values was above 275, suggesting a higher extent of agglomeration and hence a broader particle size distribution.

To better understand the true particle size and distribution of the chitosan-tripolyphosphate particles formed, further analysis of these attributes was performed in the powder form using standard powder sieving techniques. This analysis is performed in Chapter 6 and is likely a more appropriate means of evaluating the particle size of these materials given their intended use as powders to be compressed into solid oral dosage forms. This sieve analysis will also further enable evaluation of efficiency in the ability to produce materials with the desired Span characteristics as presented in Table 5.1.

Table 5.3. Particle size (d50 and Span) results for chitosan-tripolyphosphate crosslinked mixtures and prediction statistics. Standard deviation for actual results are presented in parenthesis. All d50 results are in units of microns (μm). Span is a unitless value.

Particle Size – d50

Optimized Sample	Actual Results	Predicted Mean	Predicted Median	Predicted Std. Dev.	95% CI for Mean	95% TI for Individuals
Sample A	0.500 (0.252)	0.441	0.429	0.076	0.354 – 0.588	0.235 – 2.466
Sample B	0.407 (0.233)	0.342	0.336	0.046	0.290 – 0.419	0.205 – 0.938
Sample C	0.517 (0.037)	0.524	0.503	0.105	0.397 – 0.776	0.253 – 45.472

Particle Size Distribution – Span

Optimized Sample	Actual Results	Predicted Mean	Predicted Median	Predicted Std. Dev.	95% CI for Mean	95% TI for Individuals
Sample A	220.986 (242.196)	5.23	5.16	0.592	4.534 – 6.174	3.356 – 11.276
Sample B	350.800 (316.887)	11.1	10.6	2.58	8.334 – 16.948	5.003 – Error*
Sample C	504.325 (189.789)	303	77.6	345	23.940 – Error*	8.026 – Error*

Note: CI = Confidence Interval. TI = Tolerance Interval. Tolerance Intervals represent 95% Confidence Intervals for 99% of population. Error values for transformed responses indicate that the predicted value was invalid when presented in the original scale (e.g. results in a negative value).

True Density

True density for chitosan-tripolyphosphate crosslinked mixtures (optimized samples A, B, and C) are presented in Table 5.4 along with the statistical predictions generated using Design Expert® point prediction node. True density results were generally in agreement with the predicted values and the trend order for predicted true density from least to greatest was aligned with that of the test values. While not all average results fell within the 95% confidence intervals, all individual results fell within the 95% tolerance intervals substantiating the adequacy of the models established from the initial DOE.

Each of the optimized samples exhibited a marked increase in true density compared to chitosan alone, which was measured to have a density of 1.474 g/ml. As hypothesized, the crosslinking process resulted in chitosan chains more tightly bound as a result of crosslinking with tripolyphosphate with intra-chain folding resulting in denser structures than would be evident in the parent pure powdered chitosan form.

Table 5.4. True density results for chitosan-tripolyphosphate crosslinked mixtures and prediction statistics. Standard deviation for actual results are presented in parenthesis. All results are in units of grams per milliliter (g/ml).

Optimized Sample	Actual Results	Predicted Mean	Predicted Median	Predicted Std. Dev.	95% CI for Mean	95% TI for Individuals
Sample A	1.62 (0.002)	1.63	1.63	0.027	1.606 – 1.655	1.510 – 1.751
Sample B	1.70 (0.013)	1.65	1.65	0.027	1.622 – 1.671	1.527 – 1.766
Sample C	1.70 (0.031)	1.80	1.80	0.027	1.757 – 1.836	1.665 – 1.928

Note: CI = Confidence Interval. TI = Tolerance Interval. Tolerance Intervals represent 95% Confidence Intervals for 99% of population.

Zeta Potential

Zeta Potential results for chitosan-tripolyphosphate crosslinked mixtures (optimized samples A, B, and C) are presented in Table 5.5 along with the statistical predictions generated using Design Expert® point prediction node. Zeta potential results were generally in agreement with the predicted values substantiating the adequacy of the model equations established from the initial design of experiments. Sample B and Sample C average results fell within the 95% confidence interval for the mean, while sample A average fell just outside this range, but well within the 95% tolerance interval for individuals.

The trend of zeta potential results is not surprising given the chitosan-tripolyphosphate ratios used for the formulations, as presented in Table 5.2. The ratio of chitosan to tripolyphosphate was highest for sample A (4.5), less for sample B (3.0), and further decreased for sample C (2.0). The results for zeta potential in Table 5.5 also trend from highest to lowest in this order. As was shown in the initial design of experiments, the higher ratio of chitosan results in the presence of uncrosslinked free protonated amine groups that drive the increase in zeta potential. As this ratio decreases, amine groups are crosslinked with tripolyphosphate and the resulting surface charge decreases. These results would also suggest a greater crosslinking density within the particles formed with lower zeta potential. Furthermore, with decreasing zeta potential, the stability of the particles is weakened as there is not a surface charge sufficient to repel other particles to prevent aggregation. This greater tendency toward aggregation is consistent with the increasing Span results for each of the samples as presented in Table 5.3.

Table 5.5. Zeta Potential results for chitosan-tripolyphosphate crosslinked mixtures and prediction statistics. Standard deviation for actual results are presented in parenthesis. All results are in units of millivolts (mV).

Optimized Sample	Actual Results	Predicted Mean	Predicted Median	Predicted Std. Dev.	95% CI for Mean	95% TI for Individuals
Sample A	39.9 (0.1)	36.1	36.1	1.7	33.7 – 38.4	30.0 – 44.1
Sample B	23.1 (0.6)	24.0	24.0	1.7	21.6 – 26.3	15.9 – 32.0
Sample C	18.2 (0.5)	17.7	17.7	1.7	15.0 – 21.5	9.4 – 26.1

Note: CI = Confidence Interval. TI = Tolerance Interval. Tolerance Intervals represent 95% Confidence Intervals for 99% of population.

Yield

Total percent Yield for chitosan-tripolyphosphate crosslinked mixtures (optimized samples A, B, and C) is presented in Table 5.6 along with the statistical predictions generated using Design Expert® point prediction node. Yield results were in agreement with the predicted values substantiating the adequacy of the models established from the initial DOE. Sample A and sample B average results fell within the 95% confidence interval for the mean, while sample C average fell just outside this range, but well within the 95% tolerance interval for individuals.

Sample A provided a significantly lower yield than did sample B or sample C, which was expected as models and response surface plots from the initial design of experiments showed that chitosan:tripolyphosphate ratios of ~2.0 – 3.5 resulted in optimum yield results. At the ratio of 4.5, used to manufacture the product labeled sample A, lower yield can be attributed to uncrosslinked (i.e. free) chitosan chains that remained in solution as there was insufficient tripolyphosphate present to use all of the potential crosslinking sites on the chitosan present. The chitosan that never precipitated from the solution because it participated in crosslinked particles would then be removed as free chitosan during the centrifugation and rinsing process.

Table 5.6. Yield for chitosan-tripolyphosphate crosslinked mixtures and prediction statistics. Yield was calculated based on mass generated from entire population of samples made for each manufacturing condition, thus a calculation of standard deviation is not applicable. All results are expressed as percentages (%).

Optimized Sample	Actual Results	Predicted Mean	Predicted Median	Predicted Std. Dev.	95% CI for Mean	95% TI for Individuals
Sample A	74.9	76.4	76.4	1.2	74.6 – 78.2	70.0 – 82.9
Sample B	94.6	94.1	94.1	1.2	92.2 – 95.9	87.6 – 100.5
Sample C	93.1	96.9	96.9	1.2	94.6 – 99.1	90.1 – 103.7

Note: CI = Confidence Interval. TI = Tolerance Interval. Tolerance Intervals represent 95% Confidence Intervals for 99% of population.

Dissolution (t_{50})

Tablets using crosslinked material from each of the three manufacturing conditions were compressed and dissolution data were generated. Additionally, for sample C, given the large Span (see further analysis of particle size in Chapter 6), tablets were prepared using different mesh cuts across the particle size distribution to represent small, medium, and large particles to better understand the potential impact of particle size on the rate of release. Particles for the "small" mesh cut were measured as less than 212 μm; for the "medium" mesh cut, 212 – 425 μm; and for the "large" mesh cut, greater than 425 μm. Model equations that describe release mechanisms were fit to the dissolution data using SigmaPlot®.

Higuchi parameters for each set of dissolution data are found in Table 5.7 as well as the calculated t_{50}. As the Higuchi equation describes release kinetics as a function of the square root of time (Siepmann & Peppas, 2011), this correlation is provided in Figure 5.1 for each of the samples from the three different manufacturing conditions. Figure 5.2 displays the same correlation for tablets made from different particle sizes of sample C.

Table 5.7. Higuchi equation parameters for dissolution data for tablets made with particles from optimized manufacturing conditions

Sample	**Time* (min) / (% release)**	**k / (s.e.) / p-value**	**c / (s.e.) / p-value**	**R^2**	**Model p-value**	**Calculated t_{50}**
A	240 / (69)	4.4741 / (0.0876) / < 0.0001	0	0.9834	< 0.0001	125
B	600 / (75)	3.4301 / (0.1193) / < 0.0001	-5.7401 / (1.6949) / 0.0080	0.9892	< 0.0001	264
C	480 / (53)	2.8033 / (0.0983) / < 0.0001	-4.9222 / (1.2507) / 0.0043	0.9903	< 0.0001	384
C – Small	720 (65)	2.8346 / (0.0894) / < 0.0001	-6.7025 / (1.3995) / 0.0007	0.9901	< 0.0001	400
C – Medium	600 (56)	2.6230 / (0.1183) / < 0.0001	-4.5494 / (1.6804) / 0.0241	0.9820	< 0.0001	432
C – Large	720 (71)	2.8194 / (0.0640) / < 0.0001	0	0.9746	< 0.0001	315

*Time refers to the last dissolution sampling time point used for the Higuchi equation fitting.
k = Higuchi constant; s.e. = standard error; c = constant accounting for burst release (positive value) or lag time (negative value)

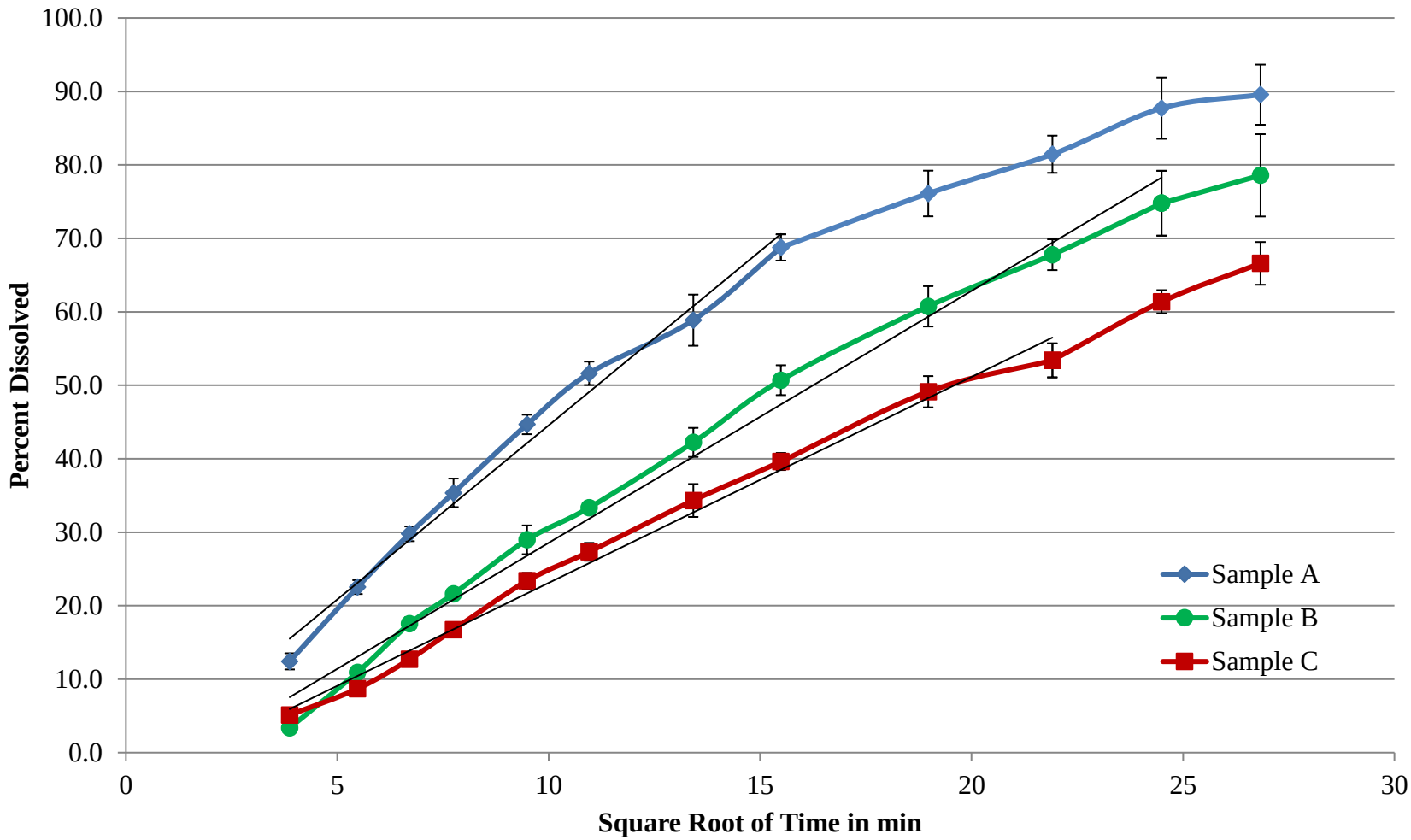

Figure 5.1. Drug release as a function of the square root of time for tablets compressed from material from each of the three optimized samples. A trendline is overlaid on the portion of the profile used to establish the Higuchi parameters.

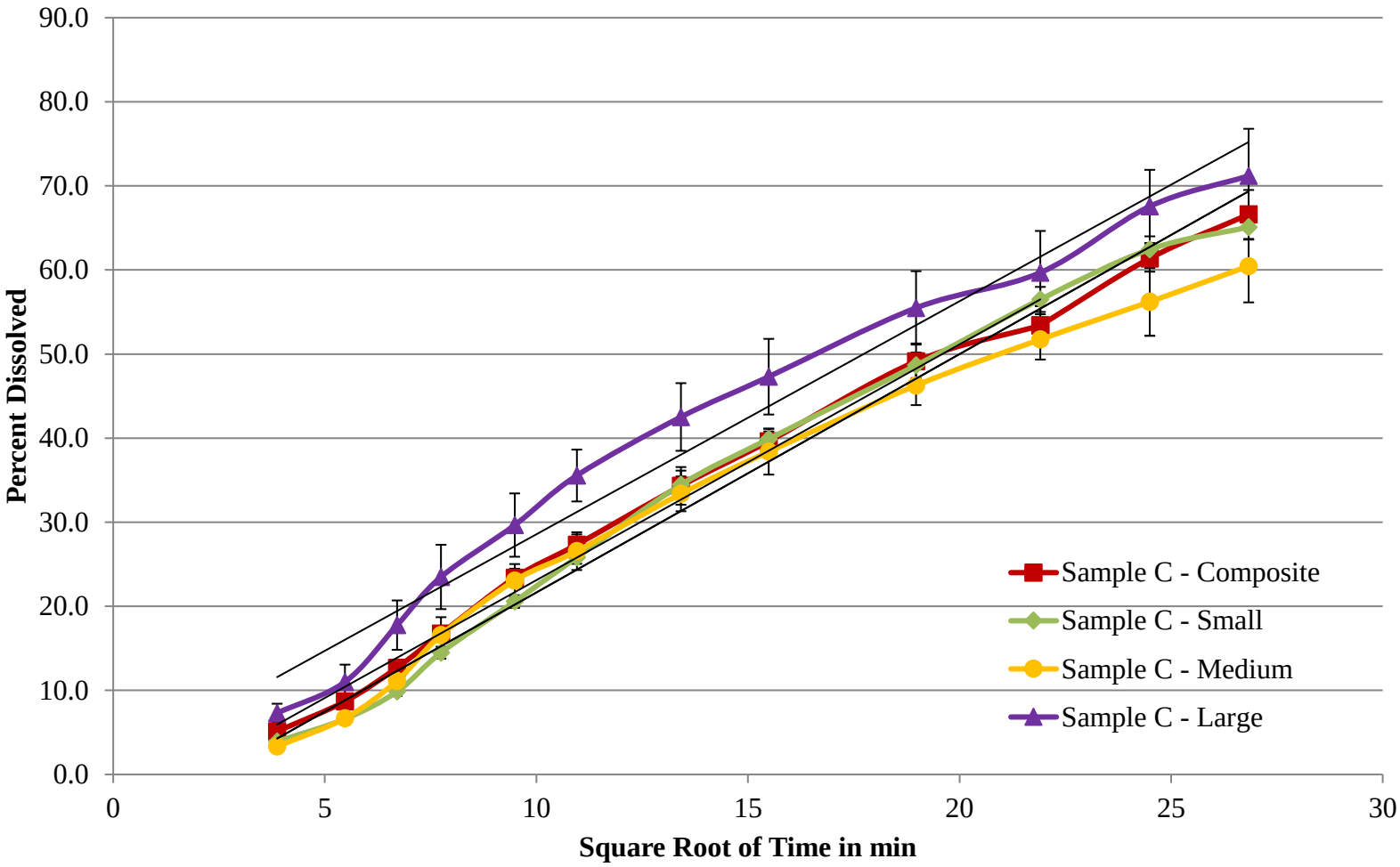

Figure 5.2. Drug release as a function of square root of time for tablets made from composite sample C as well as different particle size mesh cuts from sample C. A trendline is overlaid on the portion of the profile used to establish the Higuchi parameters.

The calculated Higuchi equations in Table 5.7 reveal that both sample B and sample C displayed greater sustained release capabilities than did sample A. The presence of a negative constant (c) for both sample B and sample C indicate a lag time in initial drug release, whereas no constant for sample A indicates no burst drug release nor a lag time. For the different particle size mesh cuts from sample C, tablets made with small and medium sized particles showed far greater sustained release properties than those made using large particles. The results for the composite C suggest that the large particles are interfering with the sustained release properties exhibited by the small and medium sized particles of the overall composite sample. The average of the t_{50} values derived for each of the different mesh cuts (382 minutes) is almost identical to the t_{50} calculated for the composite sample C (384 minutes). This is not unexpected based on the fact that the three mesh cuts represent equal mass fractions of the composite sample, showing that the different particle sizes are contributing equally to the overall sustained release profile.

For the tablets made from the large particles from sample C, it is likely the drug is not as evenly distributed within the chitosan-tripolyphosphate particles, such that larger concentrations of drug exist in particular areas of the tablets and are prone to small bursts of drug release when exposed to dissolution media. Excipients of a particle size similar to that of the active ingredient are key to drug uniformity when making dry blended solid dosage forms. The increased standard deviations at each of the sampling points and the lower R^2 value for the large particle sample C as compared to the small and medium particle samples for C, support these hypotheses. For tablets made from the small and medium particle mesh cuts of sample C, drug was able to be more uniformly dispersed,

allowing a more consistent and sustained release. The slightly longer release for the medium particle size as compared to the small particle size would suggest that the medium particles were composed of greater and more complex crosslinked structures with enhanced tortuosity that further inhibited drug release.

Table 5.8 presents the t_{50} for drug release from tablets produced with chitosan-tripolyphosphate crosslinked mixtures (optimized samples A, B, and C) along with the statistical predictions generated using Design Expert® point prediction node. The results were in agreement with the predicted mean values substantiating the adequacy of the models established from the initial design of experiments. While the confidence and tolerance intervals are extremely wide, the agreement between predicated and measured values confirms that chitosan-tripolyphosphate particles can be designed to obtain specific drug release profiles.

Table 5.8. t_{50} for drug release from tablets produced using chitosan-tripolyphosphate crosslinked mixtures and prediction statistics. As t_{50} values were calculated using the Higuchi equations derived using SigmaPlot® software, calculation of standard deviation is not applicable. All results represent percent (%) of drug released.

Optimized Sample	Calculated Results	Predicted Mean	Predicted Median	Predicted Std. Dev.	95% CI for Mean	99% TI for Individuals
Sample A	125	118	113	28	93 – 155	48 – 511
Sample B	264	248	228	83	186 – 349	76 – 3086
Sample C	384	358	319	140	218 – 701	86 – 64808

Note: CI = Confidence Interval. TI = Tolerance Interval. Tolerance Intervals represent values for 99% of population.

Environmental Scanning Electron Microscopy (eSEM)

Images of each of the chitosan-tripolyphosphate optimized samples were obtained at various magnifications using an eSEM to better understand the surface morphology of the particles. The images at the various magnifications are presented in Figure 5.3 (150x), Figure 5.4 (600x), Figure 5.5 (1000x), and Figure 5.6 (2500x). Images were also obtained for pure chitosan powder for comparison.

At lower magnification, where multiple particles are captured, the images show a much more uniform particle size distribution for sample A, sample B, and the pure chitosan powder than for sample C. For sample C, however, there is clearly a wider range of particle sizes suggesting a higher extent of aggregation, confirming the higher measured values for Span. The surface morphology of samples A, B, and C is clearly more complex than that of the pure chitosan, which appears as a material with a much smoother surface. The more irregular surface indicates the presence of the crosslinking. A denser structure than found with the pure chitosan powder form is evident with each of the three samples. Across the magnifications of 600, 1000, and 1500x, the surface of sample C appears denser with less void space evident. The difference between sample A and sample B is only evident at the 2500x magnification, where sample B appears more dense than sample A. Thus, these images confirm the increasing density results reported in Table 5.4 with sample C > sample B > sample A, which also suggest a correlation to greater crosslinking density.

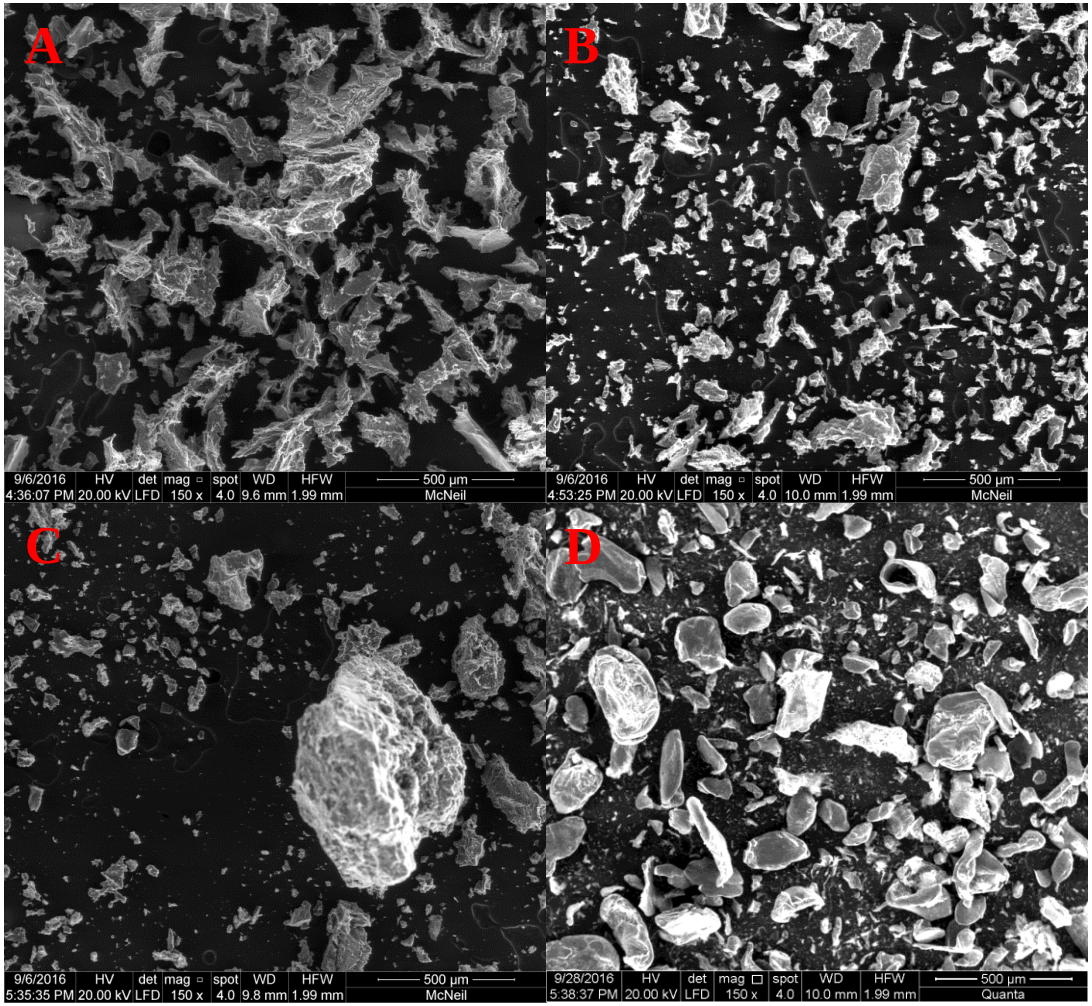

Figure 5.3. ESEM Images of optimized sample and chitosan powder at 150x magnification. Samples A, B, and C are labeled accordingly, while the pure chitosan powder is labeled sample D.

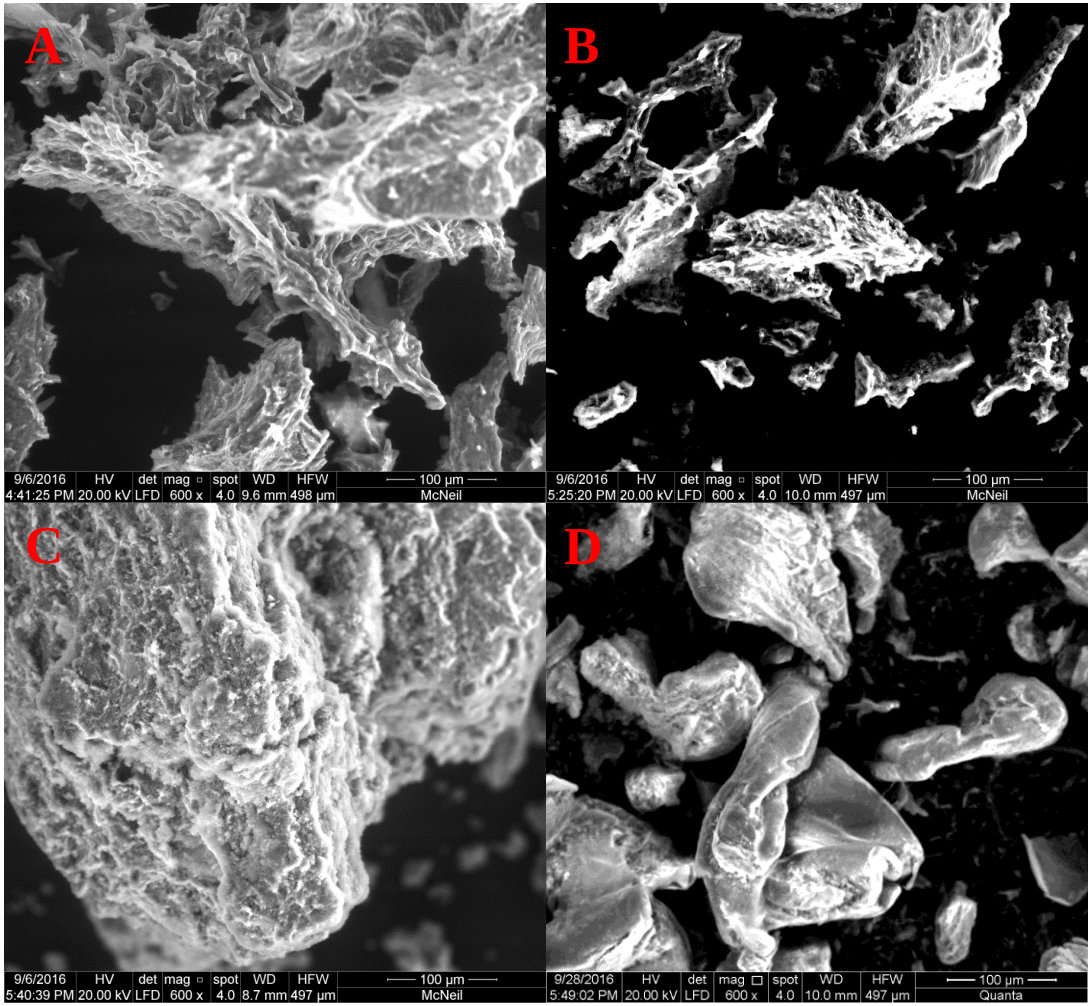

Figure 5.4. ESEM Images of optimized sample and chitosan powder at 600x magnification. Samples A, B, and C are labeled accordingly, while the pure chitosan powder is labeled sample D.

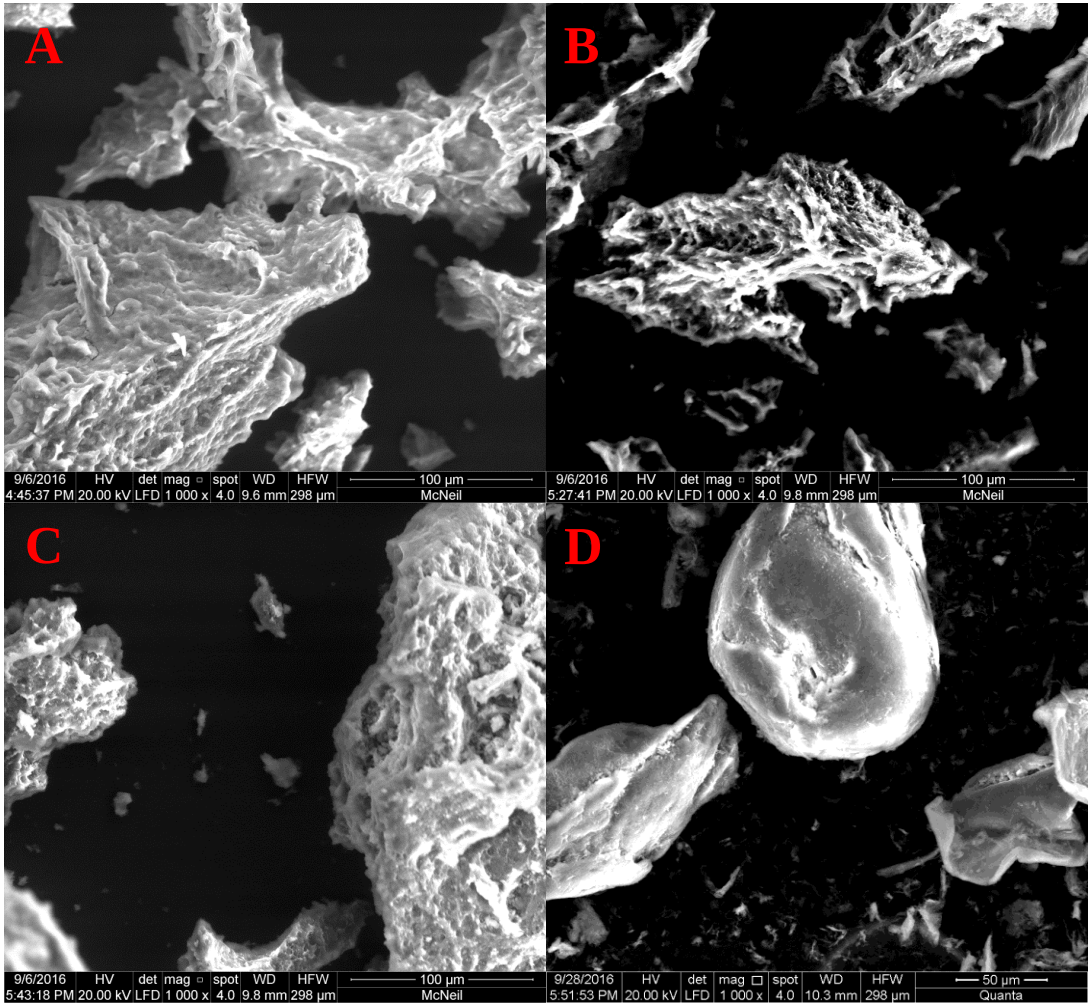

Figure 5.5. ESEM Images of optimized sample and chitosan powder at 1000x magnification. Samples A, B, and C are labeled accordingly, while the pure chitosan powder is labeled sample D.

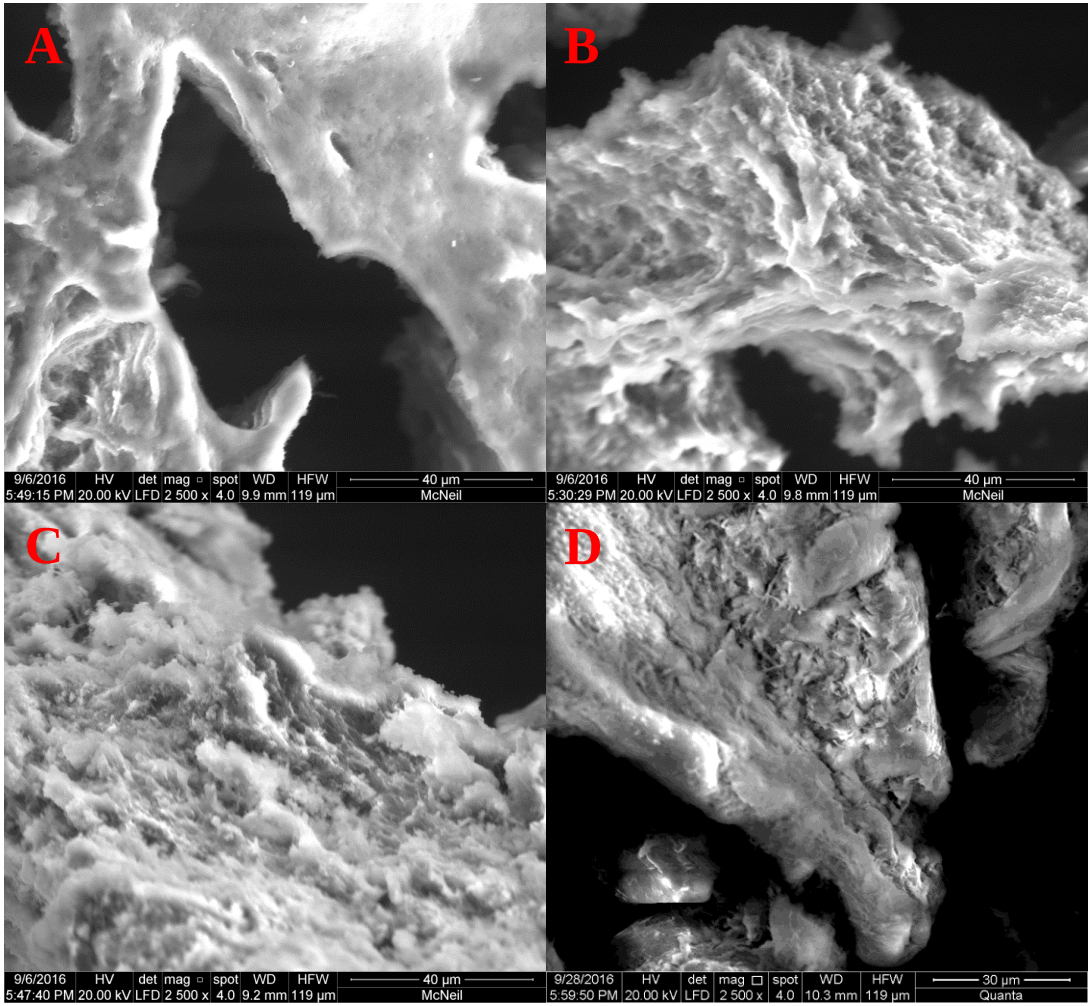

Figure 5.6. ESEM Images of optimized sample and chitosan powder at 2500x magnification. Samples A, B, and C are labeled accordingly, while the pure chitosan powder is labeled sample D.

Dynamic Vapor Sorption (DVS) Analysis

The sorption and desorption isotherms generated for each sample are depicted in Figure 5.7 (sample A), Figure 5.8 (sample B), Figure 5.9 (sample C), and Figure 5.10 (chitosan powder) where P/P_0 represents relative humidity as fraction. A summary of the isotherm data and hysteresis calculated for each of the optimized samples and pure chitosan are presented in Table 5.9. While sample B only achieved a maximum relative humidity value of approximately 85% (theoretical target, 90%), it was confirmed that equilibrium was achieved at this condition.

The isotherms are all of similar shape with subtle differences amongst them. Most notably, sample A lacks the "knee-shaped" bend that is observed in the sorption isotherms for sample B and sample C at ~10% RH and at ~20% RH for the powdered chitosan sample. This shape signifies the completion of the first monolayer of water sorbed to the surface of the sample, while the absence of this shape (Figure 5.7) would suggest that monolayers and multiple layers are being formed in parallel across the surface of the material rather than as a stepwise process (Saripella, 2012). Sample A exhibited the least extent of hysteresis, whereas the extent was greater with samples B and C with similar patterns, while the powdered chitosan sample showed the greatest extent of hysteresis. Hysteresis at high humidity (at least 80% for the samples here) is typically attributed to pore effects, sometimes referred to as "ink bottle" pores, where the energy required to remove moisture from such pores with small exposure diameters occurs at lower humidity conditions than expected (Ravikovitch, Domhnaill, Neimark, Schueth, & Unger, 1995).

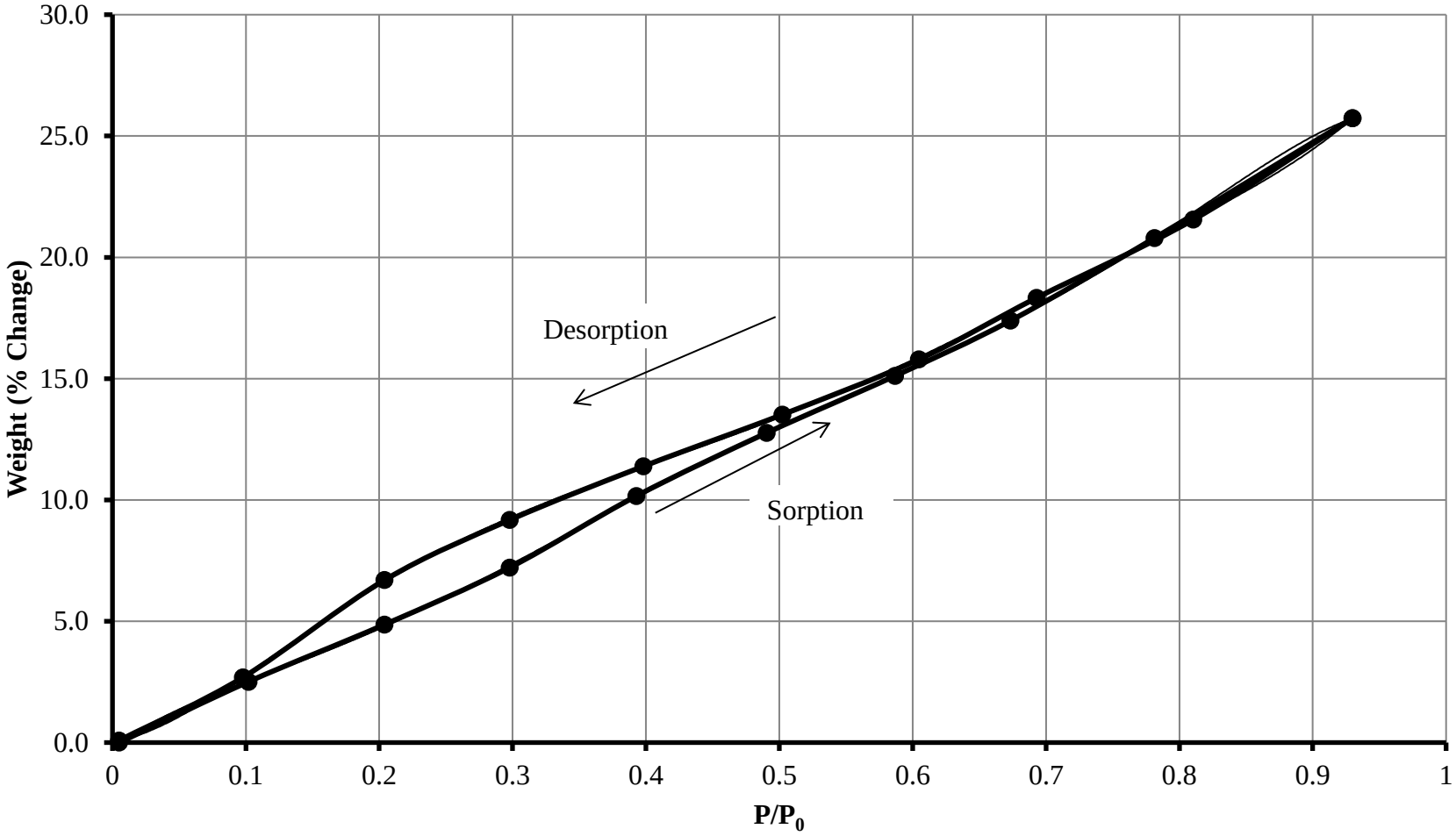

Figure 5.7. Sorption and Desorption Isotherms for Optimized Sample A

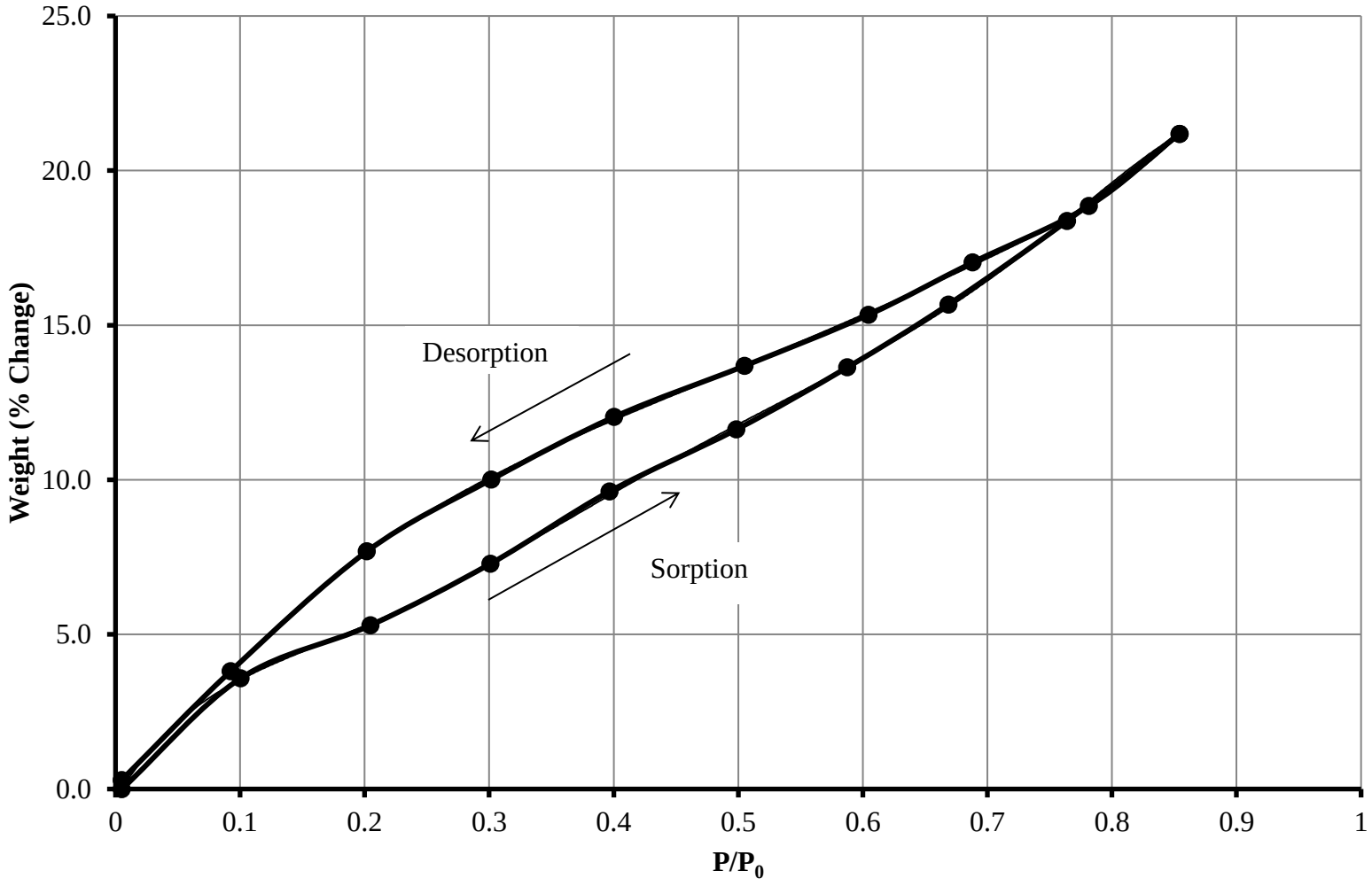

Figure 5.8. Sorption and Desorption Isotherms for Optimized Sample B

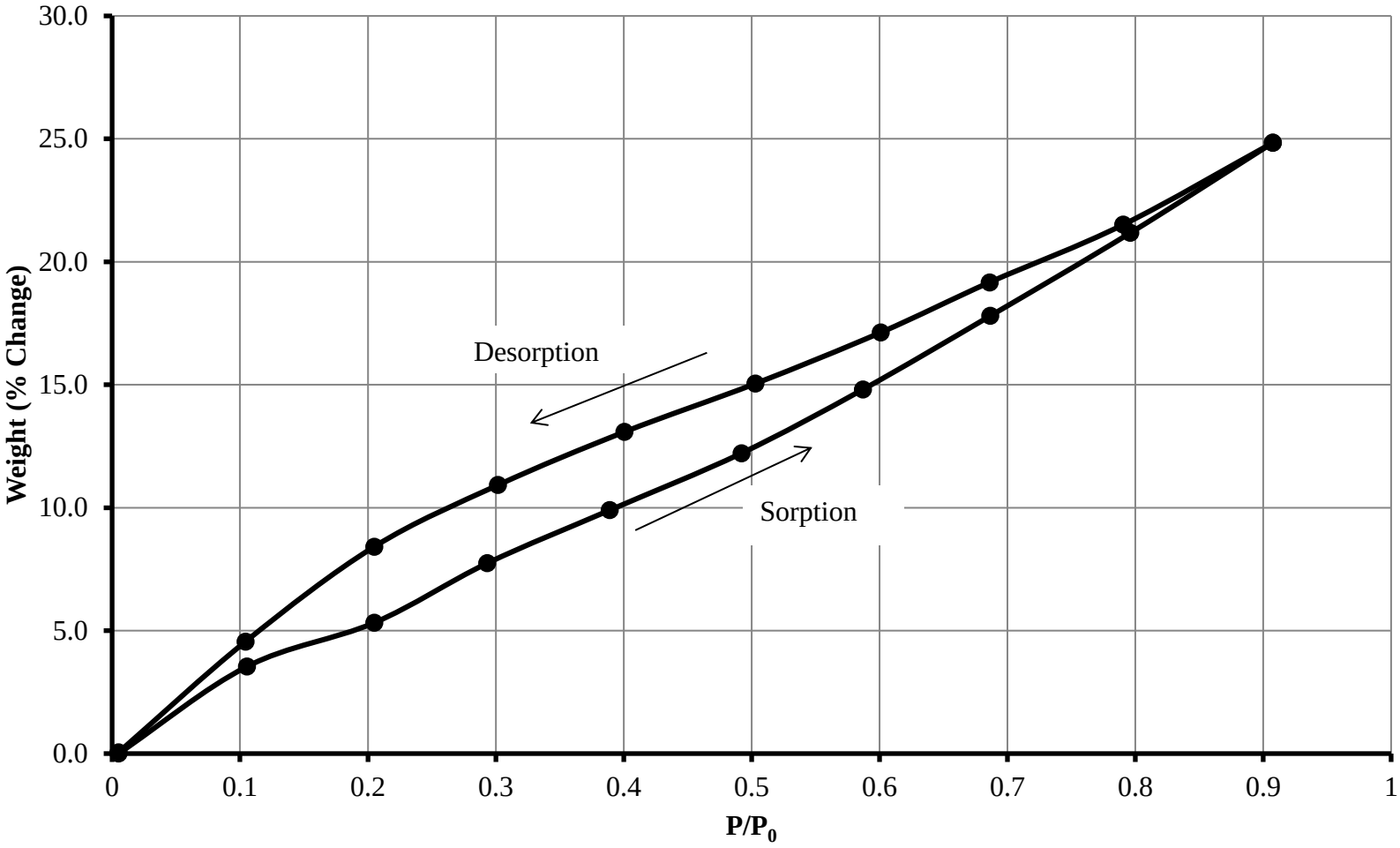

Figure 5.9. Sorption and Desorption Isotherms for Optimized Sample C

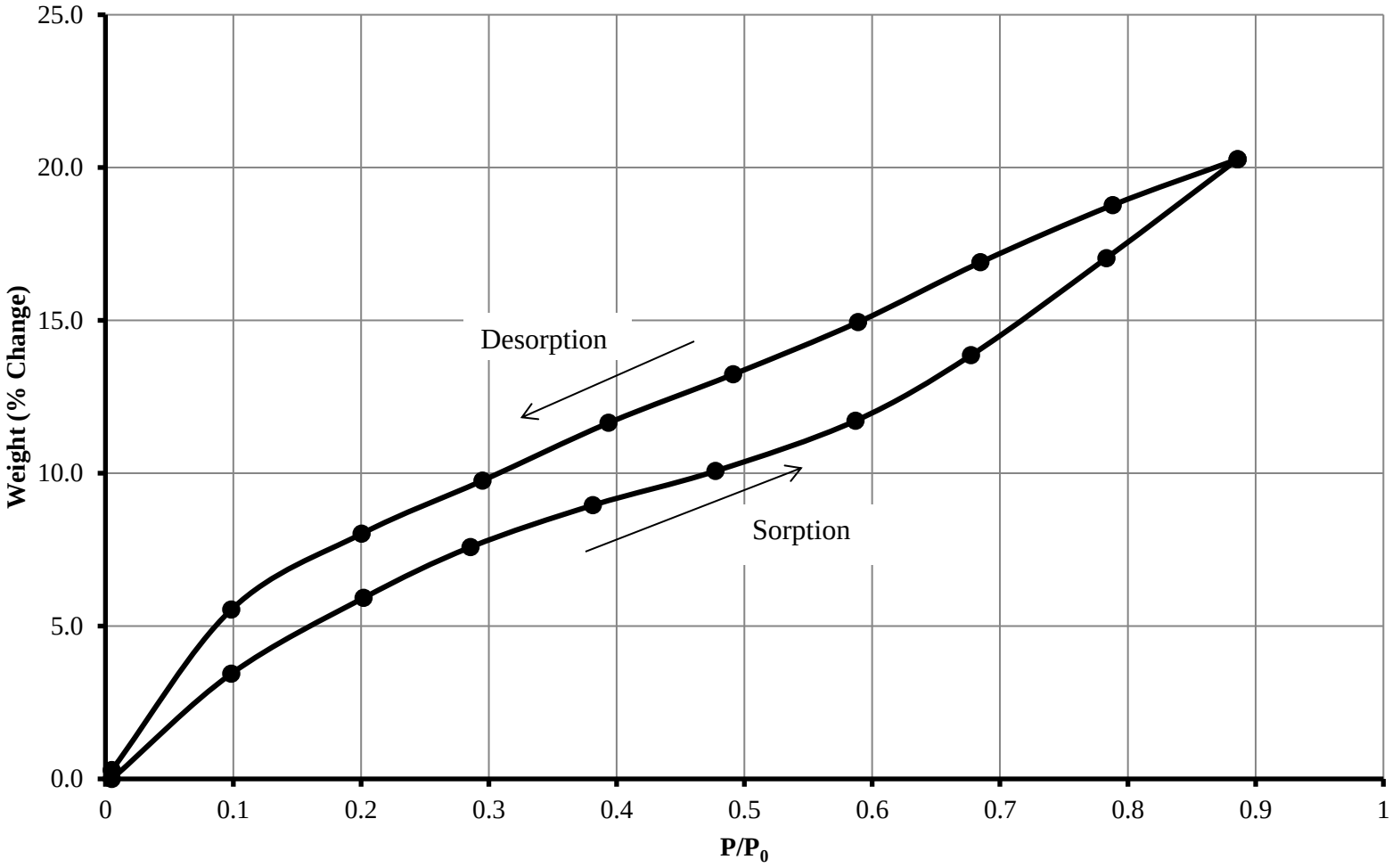

Figure 5.10. Sorption and Desorption Isotherms for Powdered Chitosan

Table 5.9. Moisture sorption, desorption, and hysteresis measured for each sample

Theoretical P/P_0	Chitosan Powder			Optimized Sample A			Optimized Sample B			Optimized Sample C		
	$\%M_s$	$\%M_d$	Hysteresis	$\%M_s$	$\%M_d$	Hysteresis	$\%M_s$	$\%M_d$	Hysteresis	$\%M_s$	$\%M_d$	Hysteresis
0.0	0.00	0.29	0.29	0.00	0.09	0.09	0.00	0.29	0.29	0.00	0.05	0.05
0.1	3.44	5.54	2.10	2.51	2.68	0.18	3.58	3.81	0.23	3.54	4.56	1.02
0.2	5.92	8.02	2.10	4.86	6.70	1.83	5.29	7.68	2.39	5.32	8.41	3.09
0.3	7.58	9.76	2.18	7.21	9.17	1.96	7.29	10.01	2.72	7.74	10.92	3.18
0.4	8.95	11.65	2.69	10.16	11.39	1.22	9.62	12.03	2.41	9.90	13.08	3.18
0.5	10.07	13.24	3.16	12.77	13.52	0.75	11.63	13.69	2.06	12.21	15.05	2.83
0.6	11.72	14.94	3.22	15.11	15.79	0.68	13.64	15.34	1.70	14.81	17.13	2.32
0.7	13.86	16.90	3.04	17.39	18.33	0.94	15.67	17.03	1.36	17.80	19.16	1.36
0.8	17.04	18.77	1.73	20.80	21.55	0.76	18.37	18.86	0.49	21.18	21.51	0.34
0.9	20.27	20.27	0.00	25.73	25.73	0.00	21.19	21.19	0.00	24.84	24.84	0.00

An alternative explanation for the hysteresis observed at lower relative humidity is primarily related to conformational changes in the polymer. As chitosan takes up moisture, the polymer chains are sometimes forced to contort to make room for the water molecules, which can result in exposure of more binding sites for the uptake of additional moisture (Shah & Augsburger, 2001). During the desorption process, the original or further contortion of the polymer chains could potentially trap this moisture as polymer swelling goes down, making it more difficult to remove the entrapped moisture and requiring lower relative humidity conditions than observed during the sorption process (Gregory, 1995). Similarly, since water acts as a plasticizer for most polymers, the uptake of water induces relaxation and subsequent swelling of the polymer chains. Upon removal of the plasticizer, polymers become more rigid, providing a less pliable exit pathway for the water, and some of the swelling observed could collapse, trapping water that again requires a lower relative humidity for removal (Levine, Slade, & Franks, 1988; Watt, 1980). The greatest hysteresis was observed with chitosan powder. This is not surprising given that this material is pure polymer, while the optimized samples also contain a certain amount of sodium tripolyphosphate depending on the initial ratio used during preparation. Tripolyphosphate is responsible for crosslinking in the samples and thus enhances the rigidity at certain sites along the polymer chains, whereas pure chitosan powder does not experience this. Even acknowledging that the ability of tripolyphosphates to take up moisture is well studied, most notably in the food industry (B. J. Lee, Hendricks, & Cornforth, 1998), it is an inorganic salt, and thus the process is expected to be reversible, with no contribution to the hysteresis. Due to these

compositional differences, a comparison of the hysteresis of the crosslinked compared to the powdered chitosan sample cannot be adequately rationalized.

Amongst the crosslinked samples, the greatest amount of hysteresis was observed in sample C, followed by sample B, and then sample A. This is also the order of sustained release capabilities, which suggests that the greater crosslinking density and chain entanglements increases the tortuosity for water to diffuse into, or dissolved drug to diffuse out of, the polymer, thereby slowing the diffusion rate (Prodduturi, Manek, Kolling, Stodghill, & Repka, 2004). Despite differences in sustained release capabilities, all samples expressed similar total water uptake at equilibrium at the highest P/P_0. This is similar to the observation by Prodduturi et al. in their analysis of films prepared with hydroxypropyl cellulose of different molecular weight where the total moisture content at equilibrium was similar despite various sustained release capabilities. The time to reach the equilibrium moisture content was shown to be an indicator of sustained release capabilities where slower uptake correlated to enhanced sustained release.

GAB Analysis

The moisture sorption data for each of the optimized samples as well as powdered chitosan were analyzed using SigmaPlot® v. 12.5 for Windows (Systat Software Inc., San Jose, CA) to fit the GAB equation to the sorption data by non-linear regression analysis. Results from the analysis are presented in Table 5.10 and show that the GAB equation for sorption isotherms proved to be an excellent fit ($R^2 \geq 0.998$) for each of the materials studied. Figure 5.11 shows the sorption isotherm for each sample with an overlay of the trendline based on the respective GAB equation derived.

Not surprisingly, parameter estimates for all of the optimization samples were quite similar, owing to similar sorption behavior across these samples. The grams of water in the form of a monolayer (W_m) were similar for the three optimization samples; almost double that of the powdered chitosan sample. Zografi et al. suggested that this parameter be corrected to account for the fact that only amorphous regions of a polymer can take up water. They accomplished this by dividing the W_m value by the fraction of the polymer that was amorphous. Although X-ray diffraction analysis can reveal a percent crystallinity in a solid sample, one would need access to each optimized sample with purely crystalline chitosan for comparison of the diffractograms to calculate the percent crystallinity in the optimized samples. Simply adding a correction factor would not be appropriate given that the crosslinked samples represent a mixture of multiple components and additional processing, rather than pure polymer in its original form.

While the slightly higher value for monolayer water observed with sample A, as compared to that of samples B and C, suggests an ability for sample A to take up more moisture in this form, the slight difference in values makes it difficult to assume it to be a distinguishing feature of sample A. These results may simply be related to subtle structural differences rather than any correlation between water uptake and subsequent sustained release capabilities. Further analysis of specific types of water is warranted. Interestingly, each of the optimized samples had more monolayer water, W_m on a g/g of sample basis, than did powdered chitosan, despite sample B and sample C having far greater sustained release capabilities. These results confirm that the presence of tripolyphosphate and/or the ionic crosslinking it engages in could be contributing to the higher level of monolayer water sorbed to the surface of the material.

Results for the powdered chitosan sample agree well with those obtained by Agrawal et al. (Agrawal et al., 2004) where similar evaluation was performed to compare chitosan and microcrystalline cellulose results. Subtle differences in these values can be attributed to differences in the chitosans used, in particular notable differences in molecular weight and degree of deacetylation.

Table 5.10. GAB Equation Parameters for Moisture Sorption Isotherms of Powdered Chitosan and Optimized Samples

Sample	C_G	K	W_m **(g/g of polymer)**	R^2
Optimized Sample A	2.807 (0.430)	0.500 (0.054)	0.196 (0.037)	0.999
Optimized Sample B	4.791 (0.595)	0.627 (0.035)	0.117 (0.011)	0.999
Optimized Sample C	3.422 (0.418)	0.546 (0.041)	0.164 (0.021)	0.999
Chitosan Powder	9.824 (1.401)	0.703 (0.020)	0.081 (0.004)	0.998

Values in parenthesis present standard error of the parameter estimate

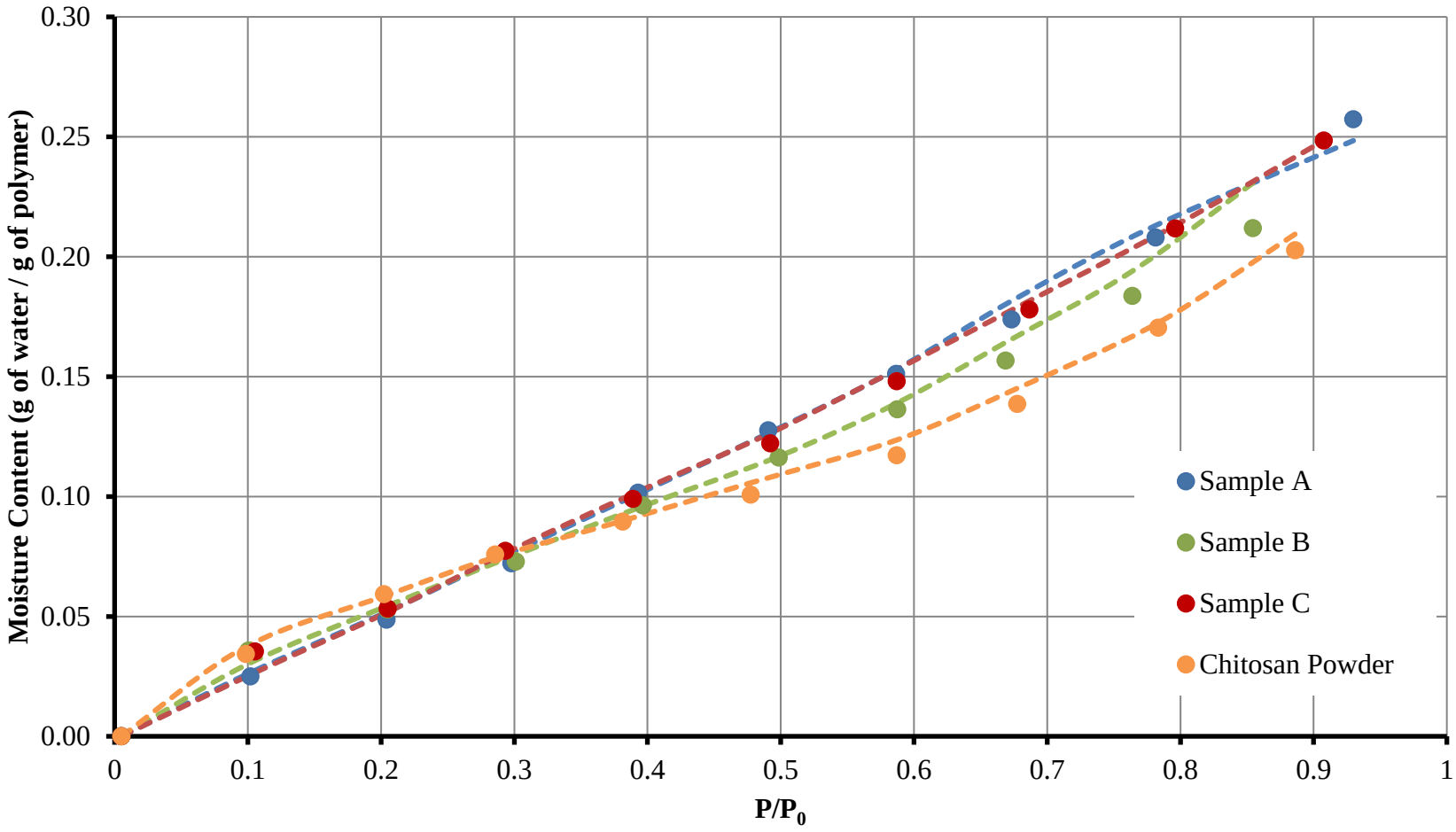

Figure 5.11. GAB Equation Fit for Sorption Isotherms. Experimental Data is shown as individual points while the GAB equation fit is represented as a dashed line.

Young and Nelson Analysis

Analysis of the moisture sorption and desorption data for each of the optimized samples as well as powdered chitosan was performed by fitting the Young and Nelson equations to the data in the manner previously described. SigmaPlot® v. 12.5 for Windows (Systat Software Inc., San Jose, CA) was used to fit the equations to the data by non-linear regression analysis. The calculated Young and Nelson relevant constants (*E*, *A*, and *B*) are presented in Table 5.11. Furthermore, the moisture distribution as a function of the type of water at theoretical relative humidity values of 50 and 90% during sorption and desorption for each of the samples is presented in Tables 5.12 and 5.13.

The corresponding sorption isotherms as a function of the type of water are presented in Figure 5.12 (sample A), Figure 5.13 (sample B), Figure 5.14 (sample C), and Figure 5.15 (powdered chitosan). Young and Nelson desorption isotherms are provided in the appendix as Figure 7.1 (sample A), Figure 7.2 (sample B), Figure 7.3 (sample C), and Figure 7.4 (powdered chitosan). Lastly, Figures 5.16 – 5.19 show the sorption and desorption isotherms along with the corresponding Young & Nelson fit.

Table 5.11. Computed Values of Parameters in Young and Nelson Equations Obtained by Analysis of Moisture Sorption and Desorption Isotherms of Samples

Optimized Sample	**E**	**A**	**B**	**R^2**
Sample A	0.524	0.0244 (0.003)	0.170 (0.012)	0.995
Sample B	0.140	0.0523 (0.004)	0.0706 (0.009)	0.994
Sample C	0.147	0.051 (0.005)	0.0883 (0.012)	0.988
Chitosan Powder	0.099	0.0462 (0.004)	0.0728 (0.010)	0.994

Values in parentheses indicate the standard error

Table 5.12. Moisture Distribution at 50% and 90% Relative Humidity Based on Fitting Young and Nelson Equations to Sorption Data

Relative Humidity (%)	Moisture Content (g/g)	$A\theta$[a] (g/g)	$A(\theta+\beta)$[b] (g/g)	$B\psi$[c] (g/g)
Optimized Sample A				
50	0.117	0.023 (19.56%)[d]	0.039 (33.07%)	0.079 (66.93%)
90	0.249	0.024 (9.76%)	0.091 (36.69%)	0.158 (63.31%)
Optimized Sample B				
50	0.114	0.048 (41.86%)	0.082 (71.83%)	0.032 (28.17%)
90	0.215	0.051 (23.92%)	0.156 (72.42%)	0.059 (27.58%)
Optimized Sample C				
50	0.121	0.048 (39.25%)	0.081 (66.57%)	0.041 (33.43%)
90	0.256	0.051 (19.79%)	0.176 (68.90%)	0.080 (31.10%)
Chitosan Powder				
50	0.106	0.044 (41.41%)	0.073 (68.84%)	0.033 (31.16%)
90	0.213	0.046 (21.59%)	0.149 (69.85%)	0.064 (30.15%)

[a]Monolayer adsorbed moisture

[b]The contribution of monolayer and multilayer adsorption

[c]Internally absorbed moisture

[d]Figures in parentheses represent the amount of moisture associated with each particular location as a percentage of the total moisture content at that particular relative humidity. In each case, the percent values for $A(\theta + \beta)$ and $B\psi$ should sum to 100%.

Table 5.13. Moisture Distribution at 50% and 90% Relative Humidity Based on Fitting Young and Nelson Equations to Desorption Data

Relative Humidity (%)	Moisture Content (g/g)	$A\theta$[a] (g/g)	$A(\theta+\beta)$[b] (g/g)	$B\psi$[c] (g/g)
Optimized Sample A				
50	0.090	0.016 (17.82%)[d]	0.034 (37.57%)	0.056 (62.43%)
90	0.258	0.023 (9.11%)	0.106 (40.94%)	0.152 (59.06%)
Optimized Sample B				
50	0.115	0.040 (34.53%)	0.068 (59.25%)	0.047 (40.75%)
90	0.216	0.043 (19.80%)	0.130 (59.95%)	0.087 (40.05%)
Optimized Sample C				
50	0.116	0.045 (38.32%)	0.077 (66.63%)	0.039 (33.37%)
90	0.259	0.050 (19.41%)	0.180 (69.50%)	0.079 (30.50%)
Chitosan Powder				
50	0.104	0.042 (40.39%)	0.071 (68.73%)	0.032 (31.27%)
90	0.214	0.046 (21.32%)	0.150 (70.24%)	0.064 (29.76%)

[a]Monolayer adsorbed moisture

[b]The contribution of monolayer and multilayer adsorption

[c]Internally absorbed moisture

[d]Figures in parentheses represent the amount of moisture associated with each particular location as a percentage of the total moisture content at that particular relative humidity. In each case, the percent values for $A(\theta + \beta)$ and $B\psi$ should sum to 100%.

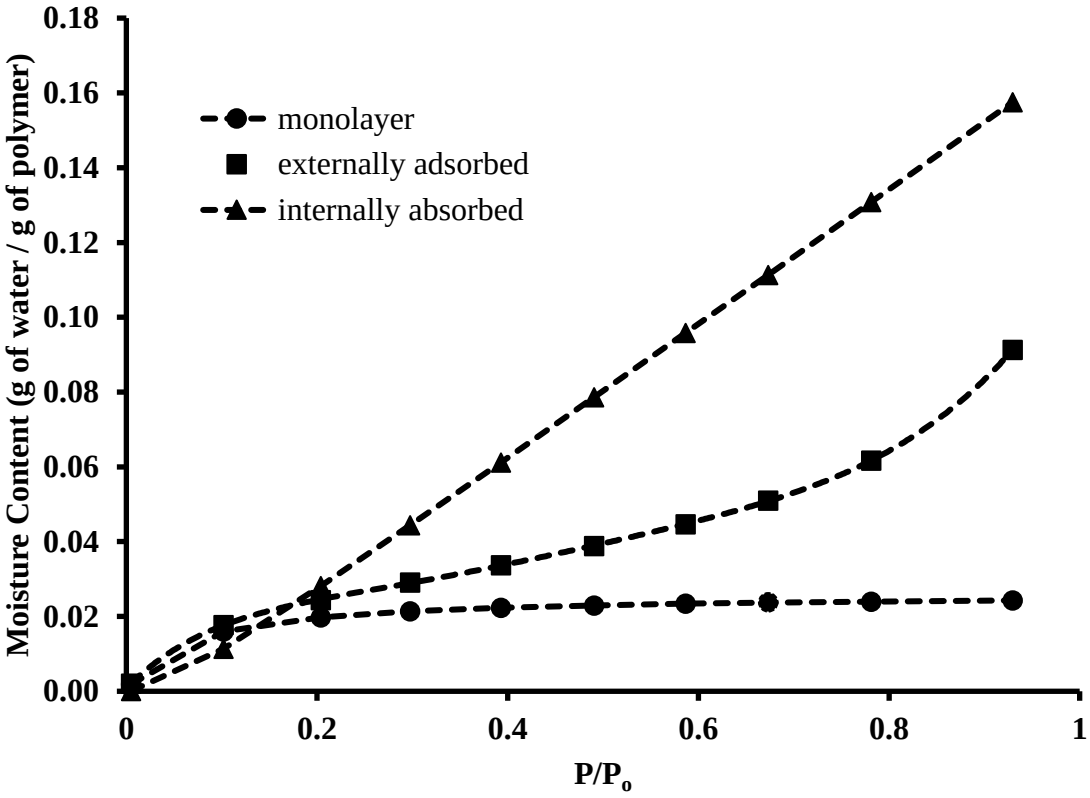

Figure 5.12. Moisture distribution patterns during sorption for optimized sample A according to the Young and Nelson equations

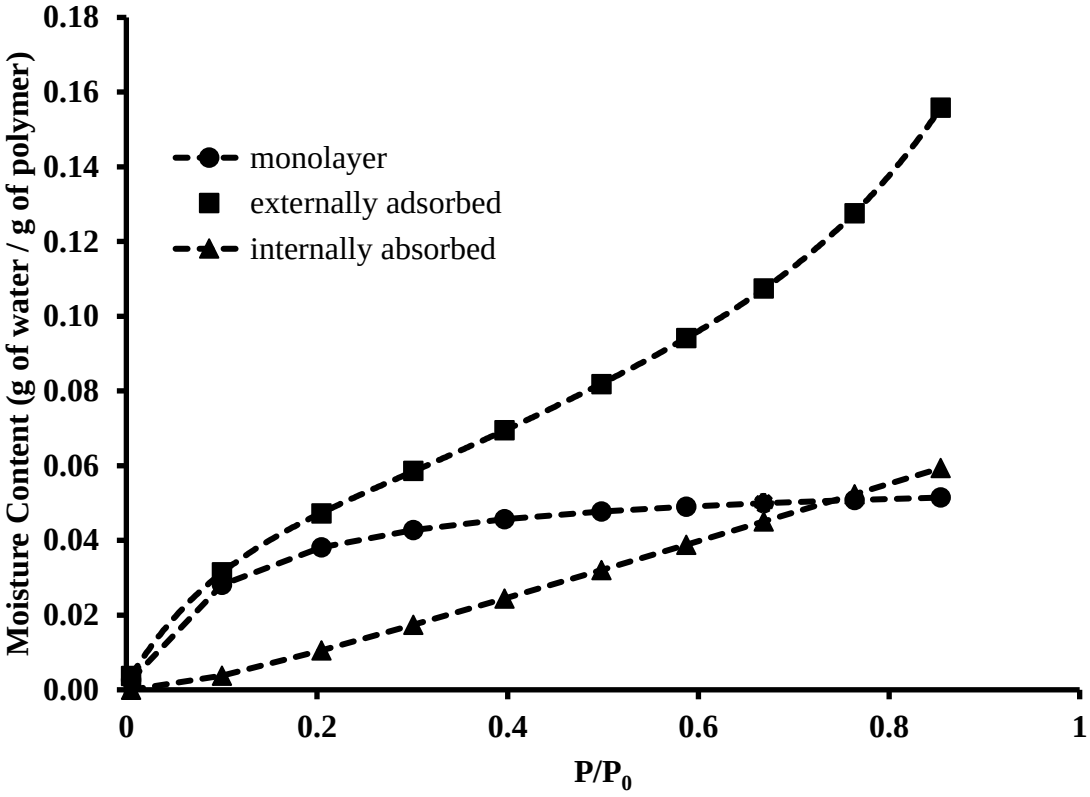

Figure 5.13. Moisture distribution patterns during sorption for optimized sample B according to the Young and Nelson equations

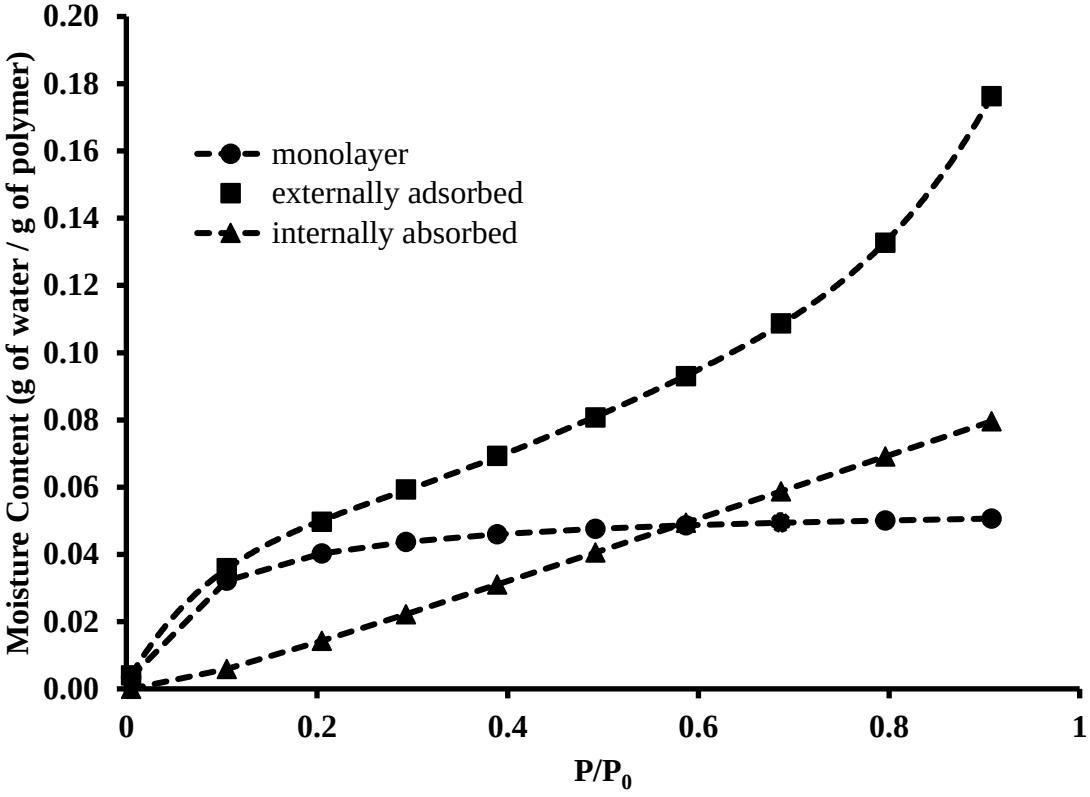

Figure 5.14. Moisture distribution patterns during sorption for optimization sample C according to the Young and Nelson equations

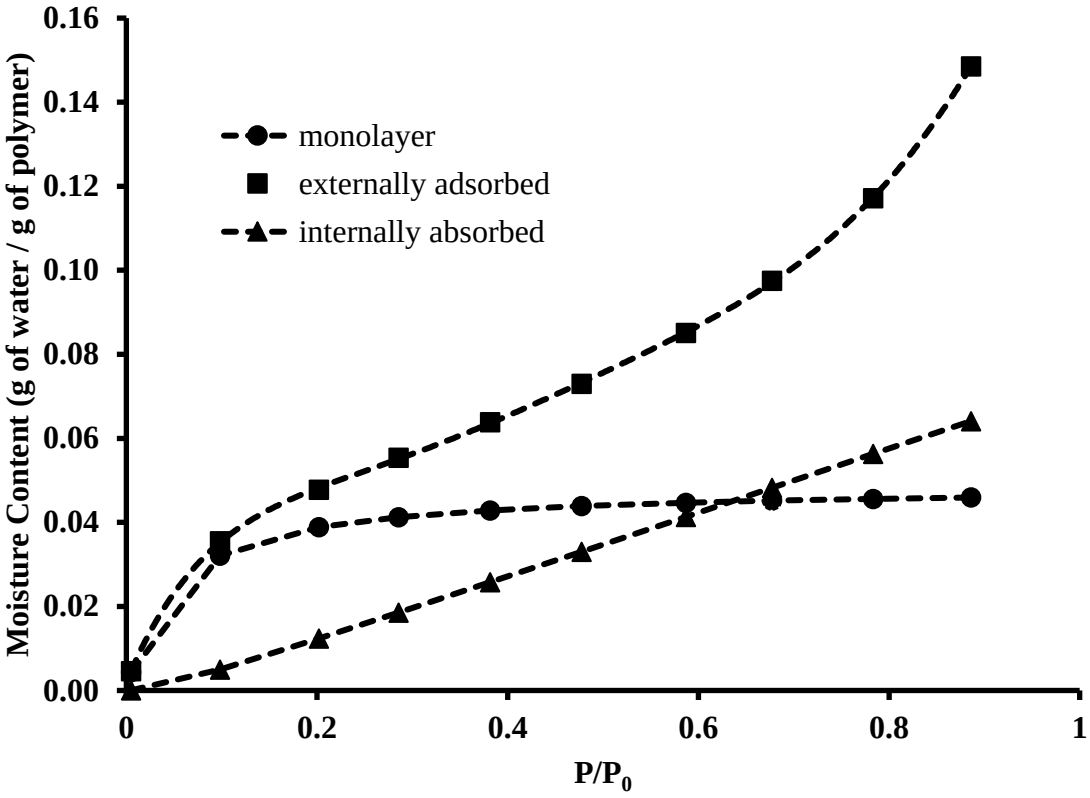

Figure 5.15. Moisture distribution patterns during sorption for powdered chitosan according to the Young and Nelson equations

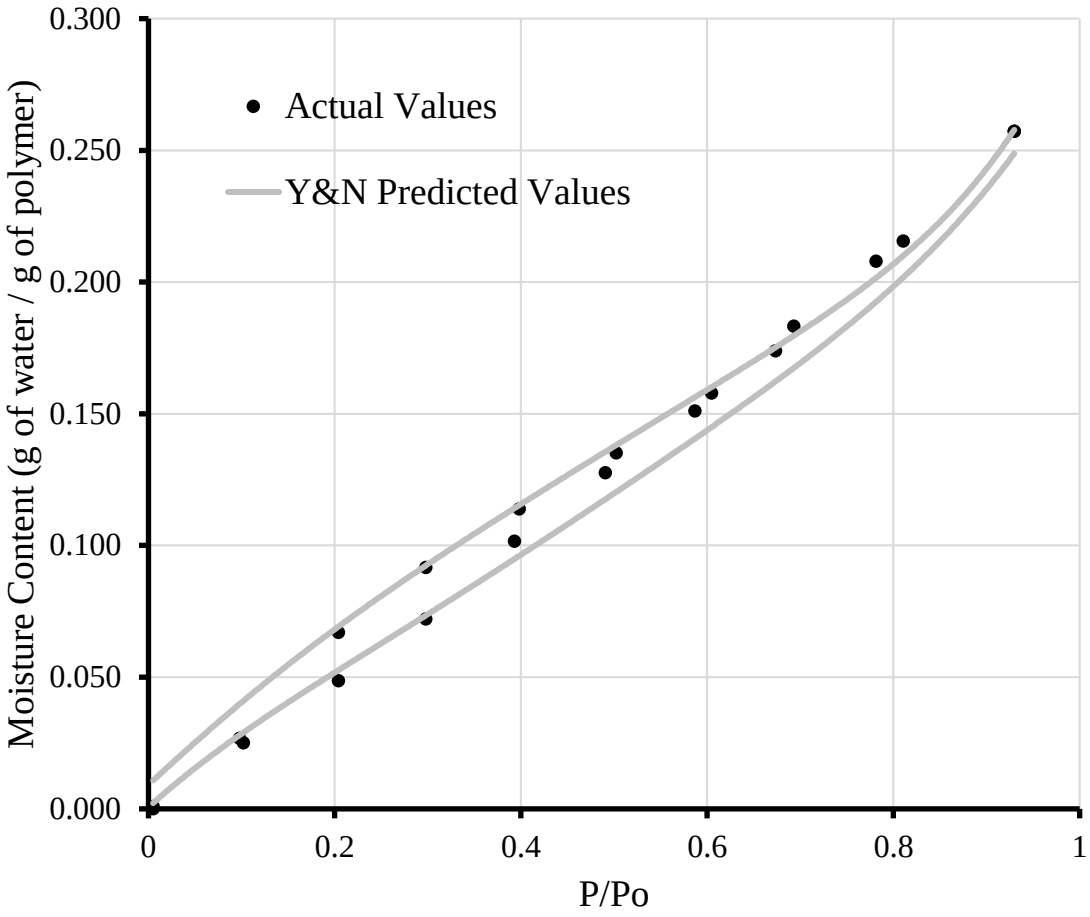

Figure 5.16. Young & Nelson equation fit for optimized sample A sorption and desorption isotherms

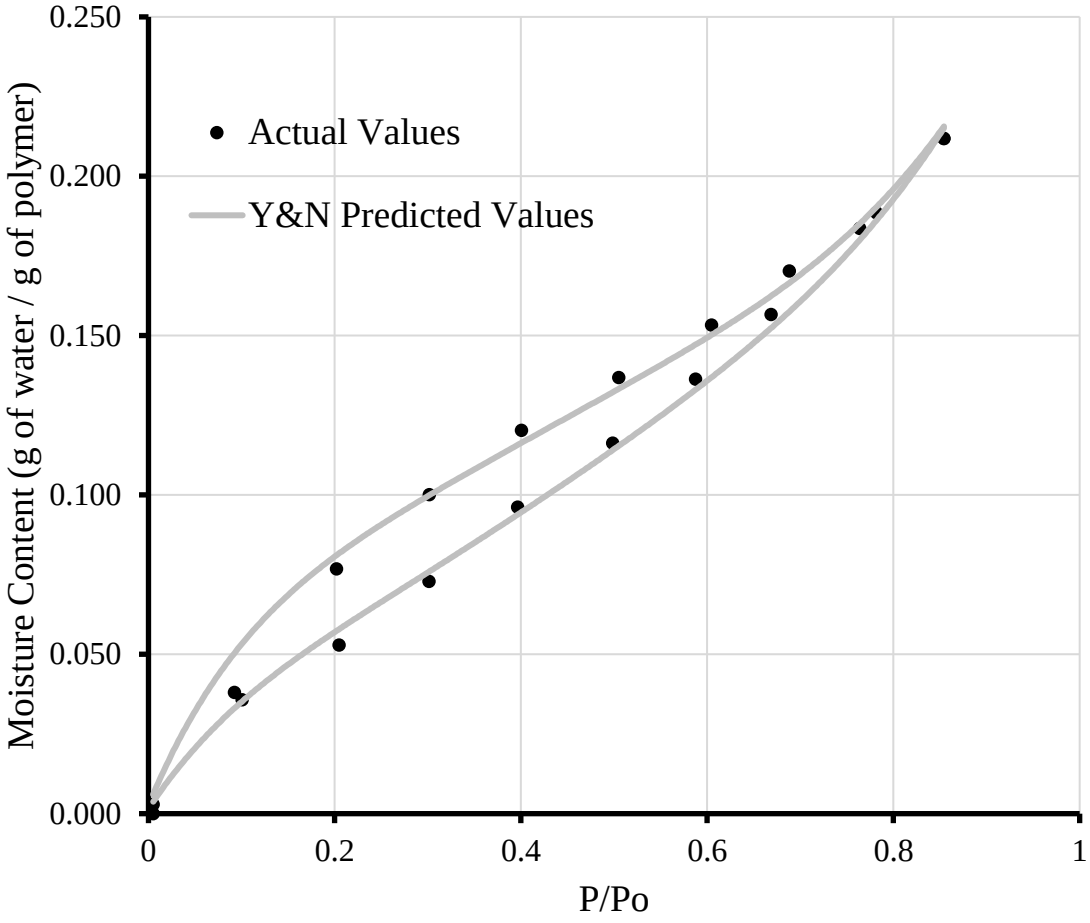

Figure 5.17. Young & Nelson equation fit for optimized sample B sorption and desorption isotherms

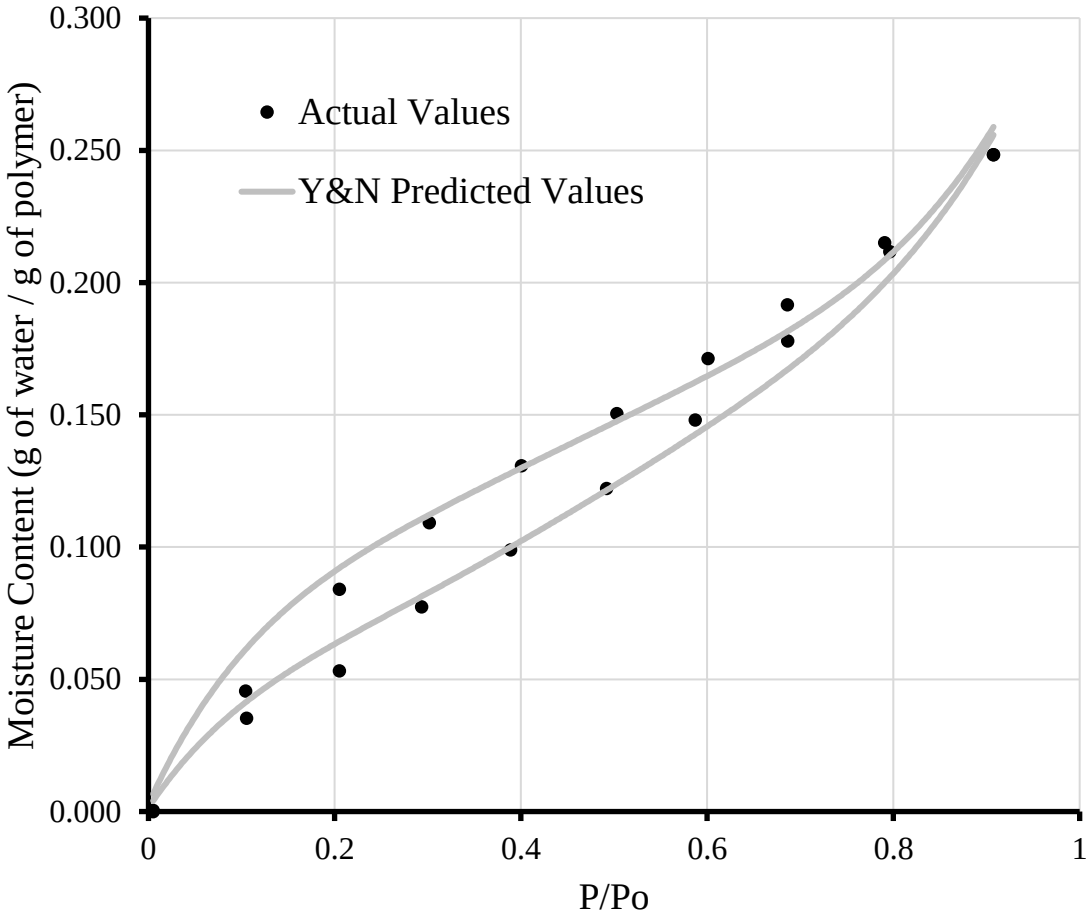

Figure 5.18. Young & Nelson equation fit for optimized sample C sorption and desorption isotherms

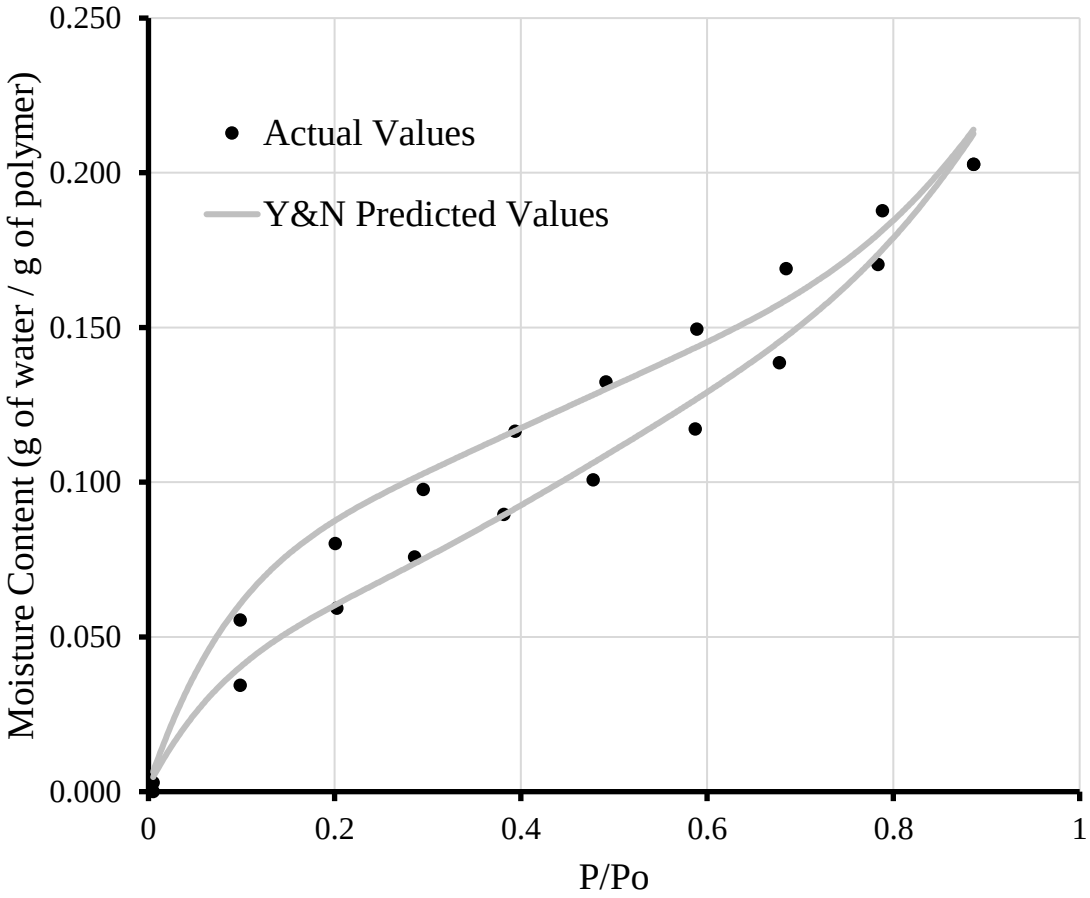

Figure 5.19. Young & Nelson equation fit for chitosan powder sorption and desorption isotherms

The calculation of Young and Nelson parameters exhibited good fit for all samples as represented by R^2 values in Table 5.11 as well as curve fit to plotted data in Figures 5.16 – 5.19.

Young and Nelson sorption isotherms for sample B (Figure 5.13) and sample C (Figure 5.14) exhibited similar patterns of the different types of moisture, which was also similar to the patterns observed by Agrawal et al. Here, the monolayer of water plateaued at approximately 0.04 g/g at roughly 40% RH; the internally absorbed moisture increases linearly until maximum P/P_0 is reached, with a moisture content endpoint similar to that of monolayer water; and lastly, the externally adsorbed water exhibits a sigmoidal increase and is the dominant species of water present. This pattern suggests a slow buildup of externally adsorbed moisture, which is required to create a concentration gradient sufficient to diffuse water into the crosslinked substance.

For sample A (Figure 5.12), the majority of the water content during sorption appears as absorbed water and represents a drastic increase as compared to sample B and sample C. These data suggest that as water adsorbs to the surface of the material, it more easily diffuses into the sample, which will result in dissolution of drug and drug diffusion out of the material. The initial attraction may be due to the high surface charge of the material as measured by Zeta Potential (Table 5.5) compared to the other substances, which creates a high affinity for water molecules. It should also be noted that the "knee-shaped" curve that was lacking in the sorption isotherm from sample A in Figure 5.7 is evident in the adsorbed monolayer of water for sample A in Figure 5.12. This curve is masked when all water types are combined due to the impact of the magnitude of the absorbed moisture. The relative ease of water absorption as compared to sample B and

sample C suggests a lower extent of crosslinking and a greater relative ability of the material to readily contort and allow for the uptake of moisture.

There is not a significant difference in the amount of internally absorbed water between sample B and sample C during sorption (Table 5.12) as measured by actual water quantity (g/g of sample) or as a function of total water content (%); however, this may be slightly impacted by the fact that sample B only achieved a maximum relative humidity of approximately 85% as opposed to 90% for sample C. Conversely, in the desorption isotherm summary (Table 5.13), the difference is slightly more apparent as a function of total water content (%) in which the internally absorbed water is approximately 7% and 10% greater for sample B than for sample C at 50% and 90% RH, respectively. This is also consistent with sustained release capabilities (sample C > sample B) suggesting that sample B has a greater capacity to internalize moisture, which subsequently would lead to greater drug dissolution and release.

While the estimate for the monolayer of water as determined by the Young and Nelson equations ($A\theta$) at maximum humidity is less than the value derived from the GAB analysis (W_m), the values are within an order of magnitude of one another suggesting that the Young and Nelson model can adequately describe the physical state of sorbed moisture. Not surprisingly, the biggest discrepancy in these values was for optimized sample A, which exhibited the greatest extent of absorbed water. Since the total water content between the GAB analysis and Young and Nelson remains unchanged, and the GAB analysis does not account for absorbed water, it is expected that when a higher extent of absorption is observed, a reduction in the other forms of moisture will occur.

Conclusions

The manufacture of optimized samples using the model equations generated from Chapter 4 showed that the established models were adequate in predicting the desired attribute (response) values. Thus, for the particular grade of chitosan used, one can successfully create a chitosan-tripolyphosphate crosslinked material with preferred characteristics.

The use of environmental scanning electron microscopy (eSEM) confirmed the general particle size characteristics but also revealed more irregular surfaces in samples where it was supposed that a greater extent of crosslinking was observed, which ultimately led to a greater extent of sustained drug release.

Lastly, dynamic vapor sorption analysis suggested a correlation between the quantity of water internally absorbed during sorption and desorption and its impact on sustained release capabilities. The presence of hysteresis in the plots of sorption and desorption data for each of the samples indicated some level of moisture absorption, which required lower levels of percent relative humidity to induce desorption.

CHAPTER 6

Micromeretics and Compression Analysis of Chitosan-Tripolyphosphate

Introduction

Direct compression remains the simplest and most convenient means of manufacturing tablets primarily due to lower costs associated with fewer manufacturing steps (Gohel, 2005). Additionally, the absence of heat and moisture present in granulation techniques leads to less risk for API degradation. Excipient manufacturers have long strived to improve their products by controlling and optimizing certain attributes, such as particle size, size distribution, density, and porosity, to create a robust material that can be used for direct compression. Ideally, if an excipient possesses acceptable flow characteristics and is compressible, there may be little need to include other excipients in a tablet.

Material compression or deformation is generally classified as occurring via one of three mechanisms as described by Ilić et al (2013):

> (a) elastic deformation as spontaneously reversible deformation of the compact in which, upon removal of the load, the powder mass reverts back to its original form, a process known as elastic relaxation; (b) plastic deformation as irreversible deformation that occurs after exceeding the yield point, where particles undergo viscous flow and stay deformed upon removal of the load; (c) fragmentation as an irreversible process of breakage of larger particles into smaller ones.

Several models and equations have been studied over the past century to understand the compression mechanisms of powders. Among the most popular include those attributed to Heckel (Heckel, 1961), Walker (Walker, 1923), Kawakita (Kawakita, Hattori, & Kishigami, 1974; Kawakita & Lüdde, 1971), Adams (Adams, Mullier, & Seville, 1994),

and Shapiro (Shapiro, 1944). While none of these models can predict the compressibility of all materials under all conditions, they are all based on the ability of a material to deform under pressure (Patel, Kaushal, & Bansal, 2007). Based on its popularity and proven applicability, the Heckel model is used in these studies. It is based on the assumptions that, under pressure, particles undergo plastic deformation and the volume reduction of the material follows first-order kinetics (Sun & Grant, 2001).

On the other hand, compactibility is a measure of the strength of the inter-particulate bonding that occurs when a material is held under pressure and is generally assessed by measuring tablet hardness or crushing strength (David & Augsburger, 1977). A greater extent of plastic deformation and/or fragmentation tends to lead to greater compactibility as particles are brought closer together and particle interfacial area is increased, leading to greater contact area for subsequent binding (Osamura et al., 2016).

The influence of particle size and density on the compressibility and compactibility has been evaluated extensively with varying conclusions (Alderborn & Nystrom, 1982; Johansson, Nicklasson, & Alderborn, 1998; McKenna & McCafferty, 1982; Patel et al., 2007; Santl, Ilic, Vrecer, & Baumgartner, 2012). For a general quantitative assessment of compressibility of a substance based on density, the Hausner Ratio and Carr's Index are both generally accepted measures of a material's flow and compressibility and have even been accepted by the United States Pharmacopeia due to the ease with which these values can be obtained (Carr, 1965; Hausner, 1967; United States Pharmacopeia National Formulary, 2016a). These values are limited in their understanding of a material and do not reveal any information on the mechanism of compression or the compaction of a substance. Generally speaking, the effect of particle

size distribution on compressibility depends on the mechanism of compression (Alderborn & Nystrom, 1982).

In the present study, the powder particle size distribution and density as well as the compressibility and compactibility of the Ch-TPP complexes were investigated and compared to other commonly used direct compression excipients.

Materials

Ch-TPP crosslinked material from optimized conditions in Chapter 5 were used for compressibility analysis. The same powdered chitosan used in crosslinking studies from DCV BioNutritionals (Wilmington, DE) with a 92% degree of deacetylation and an average molecular weight of 470 kD (Omwancha et al., 2011) was used as a control for comparison purposes. Other excipients for comparison included microcrystalline cellulose (Avicel® PH102 from FMC Biopolymer, Newark, DE), dicalcium phosphate anhydrous (A-Tab® from Innophos, Chicago Heights, IL), and pregelatinized starch (Starch® 1500 from Colorcon, West Point, PA).

Methods

Particle Size Analysis

A Sonic Sifter model L3P (Advantech Manufacturing Inc., New Berlin, WI) was used for particle size analysis. A sample size of 10 grams was used with a sieving time of 5 minutes, sift pulse setting turned "ON", and an amplitude setting of "4". A series of analyses was performed to understand the particle size distribution of each powder across the following United States Standard Sieves designated here by sieve number (aperture): 20 (850 μm), 25 (710 μm), 30 (600 μm), 35 (500 μm), 40 (425 μm), 45 (355 μm), 50 (300

μm), 60 (250 μm), 70 (212 μm), 80 (180 μm), 100 (150 μm), 120 (125 μm), 140 (106 μm), 170 (90 μm), 200 (75 μm), 230 (63 μm), 270 (53 μm), and 325 (45 μm).

Density Analysis

Bulk and tapped density were measured using a density tester model PT-TD200 (Pharma Test, Germany). Testing was performed as per USP <616> Bulk and Tapped Density of Powders (United States Pharmacopeia National Formulary, 2016a) using a 100 ml graduated cylinder and a sample weight of 15 grams and tapped density analysis after 10, 500, and 1250 taps.

Compressibility, Compactibility, and Heckel Plots

Compression was performed using an automated Korsch XP-1 (Berlin, Germany) single station press equipped with 3/8" diameter round standard concave B type compression tooling (Elizabeth Carbide, McKeesport, PA). Five tablets with a target mass of 250 mg were manufactured at each compression condition and the mass, thickness, and crushing strength (i.e. hardness) were measured for each tablet using an XS 105 analytical balance (Mettler Toledo, Columbus, OH), Pharmatron 8M tablet hardness tester (Dr. Schleuniger, Thun, Switzerland), and a model PK-0505CPX digital thickness gauge (Mitutoyo, Kawasaki, Japan). Tablet volume calculations were performed using TabletCAD® software (Natoli, St. Charles, MO).

Initial compression conditions were established by decreasing the distance between the upper and lower compression tooling punch tips until a tablet was produced that was capable of being handled and evaluated without integrity concerns. Subsequent conditions were the result of decreasing the punch tip distance by known intervals of approximately 0.1 mm from the initial setting.

For compressibility analysis, forces for each tablet compression as displayed on the Korsch XP-1, in units of kiloNewtons (kN), were converted to pressures in megaPascals (MPa) using both the tablet cross-sectional area as well as the calculated tablet surface area using the following formulas:

$$F_{MPa} = \frac{F_{kN}}{SA_{CS}} \cdot 0.001$$

$$F_{MPa} = \frac{F_{kN}}{SA_{Tablet}} \cdot 0.001$$

where F_{MPa} is the compression force in units of megaPascals, F_{kN} is the compression forces in units of kiloNewtons as calculated by the Korsch XP-1 software, SA_{CS} is the cross-sectional surface area for the compression tooling used in units of m^2 (calculated as 7.13×10^{-5} m^2 for 3/8" standard concave tooling), and SA_{Tablet} is actual surface area for each individual tablet in units of m^2 as calculated using the Natoli TabletCAD® software. The constant 0.001 is a factor for metric unit conversion from kilo to mega.

Radial tensile strength was calculated using the following equation (Fell & Newton, 1970):

$$\sigma_t = \frac{2 \cdot H}{\pi \cdot d \cdot h}$$

where H is the tablet crushing force in units of Newtons; d is the tablet diameter in units of meters and is fixed by compression tooling dimensions; and h is tablet height in units of meters. Compactibility was assessed by plotting the radial tensile strength (σ_t) against the compression forced used (Santl et al., 2012). The slope of the linear portion of this plot provides a measure of the overall compactibility of the material evaluated.

Heckel Plots (Heckel, 1961) were generated using the out-of-die method (Ilić et al., 2013) using the following equation:

$$-\ln \varepsilon = \ln\left(\frac{1}{1-D}\right) = K \cdot P + A$$

where *D* is the relative density of the tablet; *P* is the applied compression pressure in units of megaPascals; ε is the porosity of the material. The slope of this relationship, *K*, defined as the Heckel coefficient, and the *y*-intercept, *A*, are found by linear regression analysis of the linear portion of the curve. The porosity and relative density are determined via the following relationship and equations where:

$$\varepsilon = 1 - relative\ density$$

and:

$$relative\ density = \frac{apparent\ density}{true\ density}$$

where:

$$apparent\ density = \frac{mass}{envelope\ volume}$$

where the mass represents the mass of the tablet and the envelope volume represents the volume of the tablet. The true density is measured experimentally using a helium pycnometer (Hancock, 2003).

Results and Discussion

The results from particle size analysis are presented in Table 6.1, Figure 6.1, and Figure 6.2. Density results are presented in Table 6.2, which also includes data from literature for the other excipients used for comparison in these studies. Particle size results indicate an overall finer particle for the powdered chitosan as well as Sample A, also evidenced by the d10, d50, and d90 results. The 140 μm d50 for powdered chitosan

is similar to the mean particle size of 125 μm observed by Vaezifar et al. (2013). Generally speaking, each Ch:TPP sample is coarser than the powdered chitosan and the commonly used direct compression excipients, such as Avicel® PH102, Starch® 1500, and dibasic calcium phosphate anhydrous with measured d50 values of 106, 36, and 15 μm, respectively (Sarrate et al., 2015). This is not unexpected given that the Ch-TPP crosslinked material is the result of an ionic gelation process with subsequent aggregation versus a pure raw material. These results would suggest that perhaps assessment of particle size alone is generally not a good indicator of the compressibility/compactibility of an excipient (Jivraj, Martini, & Thomson, 2000).

The distribution and Span results suggest a more normal particle size distribution for chitosan, sample A, and sample B, whereas results for sample C reveal a coarser and more balanced distribution across the sieves used. The presence of ionic species in the sample C production media provided by the NaCl leads to a weaker ionic attraction between chitosan and tripolyphosphate (Huang & Lapitsky, 2011). The greater particle size observed in Sample C is a result of greater aggregation during particle formation, which is expected based on its zeta potential (18.2 mV, results presented in Chapter 5) that proved to be much lower than that of Sample A or Sample B. A lower zeta potential allows greater aggregation due to ionic repulsive forces that are weaker than those that can keep ionized particles apart (Fàbregas, 2013). Compared to other commonly used direct compression excipients, the particle size distribution of the chitosan samples is narrow, with Avicel®102, (DCPA), and pre-gelatinized starch (Starch® 1500), and dibasic calcium phosphate anhydrous with Span values of 1.86, 3.77, and 2.08, respectively (Sarrate et al., 2015).

Density results in Table 6.2 would suggest that powdered chitosan, sample A, and sample B each display "very poor" or "very, very poor" flow characteristics based on General Chapter <1174> Powder Flow definitions for the Hausner Ratio (HR) and Carr's Index (CI) (United States Pharmacopeia National Formulary, 2016c). Sample C shows "passable" results, better than results for Avicel® PH102 (Koo, 2001), comparable to results for Starch® 1500 (Colorcon, 2012), but not as favorable as results for dibasic calcium phosphate anhydrous (DCPA) (Kachrimanis, Petrides, & Malamataris, 2005), defined as "good" per USP <1174>. The qualitative assignment of flow characteristics per USP definition is an indicator that chitosan and Ch-TPP complexes might benefit from inclusion of a flow aid such as colloidal silicon dioxide during compression on a larger scale.

Table 6.1. Particle size results for chitosan and chitosan-tripolyphosphate powders analyzed

US Mesh Size	Chitosan		Ch-TPP Sample A		Ch-TPP Sample B		Ch-TPP Sample C	
	% Retained	Cumulative % Retained	% Retained	Cumulative % Retained	% Retained	Cumulative % Retained	% Retained	Cumulative % Retained
20	1.19	100.00	0.40	100.00	0.50	100.00	2.59	100.00
25	0.17	98.81	0.85	99.60	1.14	99.50	7.80	97.41
30	0.27	98.64	0.96	98.75	1.57	98.37	7.32	89.60
35	0.17	98.37	1.39	97.79	2.36	96.80	7.41	82.29
40	0.22	98.21	5.27	96.40	7.94	94.44	11.64	74.88
45	0.52	97.99	5.05	91.13	5.23	86.50	6.30	63.23
50	0.30	97.48	10.55	86.08	9.97	81.27	9.40	56.93
60	0.56	97.18	15.59	75.53	11.52	71.30	8.65	47.53
70	12.41	96.62	14.44	59.94	10.47	59.78	4.32	38.88
80	15.93	84.20	12.61	45.50	10.79	49.31	6.88	34.56
100	15.69	68.28	10.11	32.89	7.75	38.53	3.93	27.68
120	14.87	52.58	7.80	22.78	7.54	30.78	5.01	23.75
140	7.55	37.71	2.50	14.99	3.02	23.24	1.01	18.74
170	6.88	30.16	3.44	12.48	3.51	20.21	5.47	17.74
200	3.29	23.29	3.75	9.05	4.39	16.70	1.40	12.27
230	6.02	20.00	1.68	5.29	2.62	12.31	1.95	10.87
270	2.77	13.98	1.32	3.62	2.89	9.69	2.18	8.92
325	1.55	11.21	0.79	2.29	1.44	6.81	1.26	6.74
Pan	9.65	9.65	1.50	1.50	5.36	5.36	5.48	5.48
~d10 (μm)	49		99		70		70	
~d50 (μm)	140		234		233		330	
~d90 (μm)	232		391		464		783	
~Span	1.3		1.2		1.7		2.2	

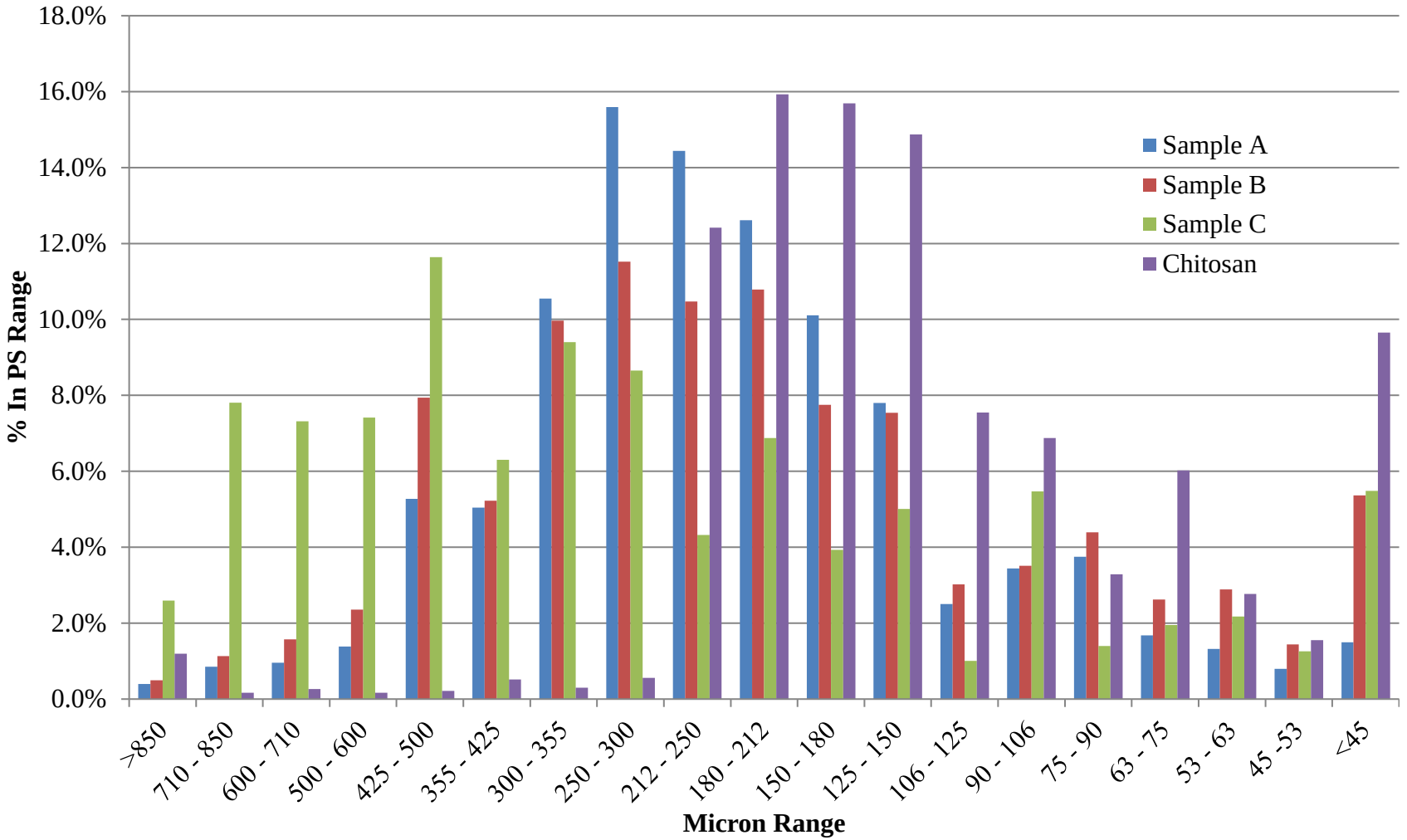

Figure 6.1. Particle size distribution bar graph by sieve cut

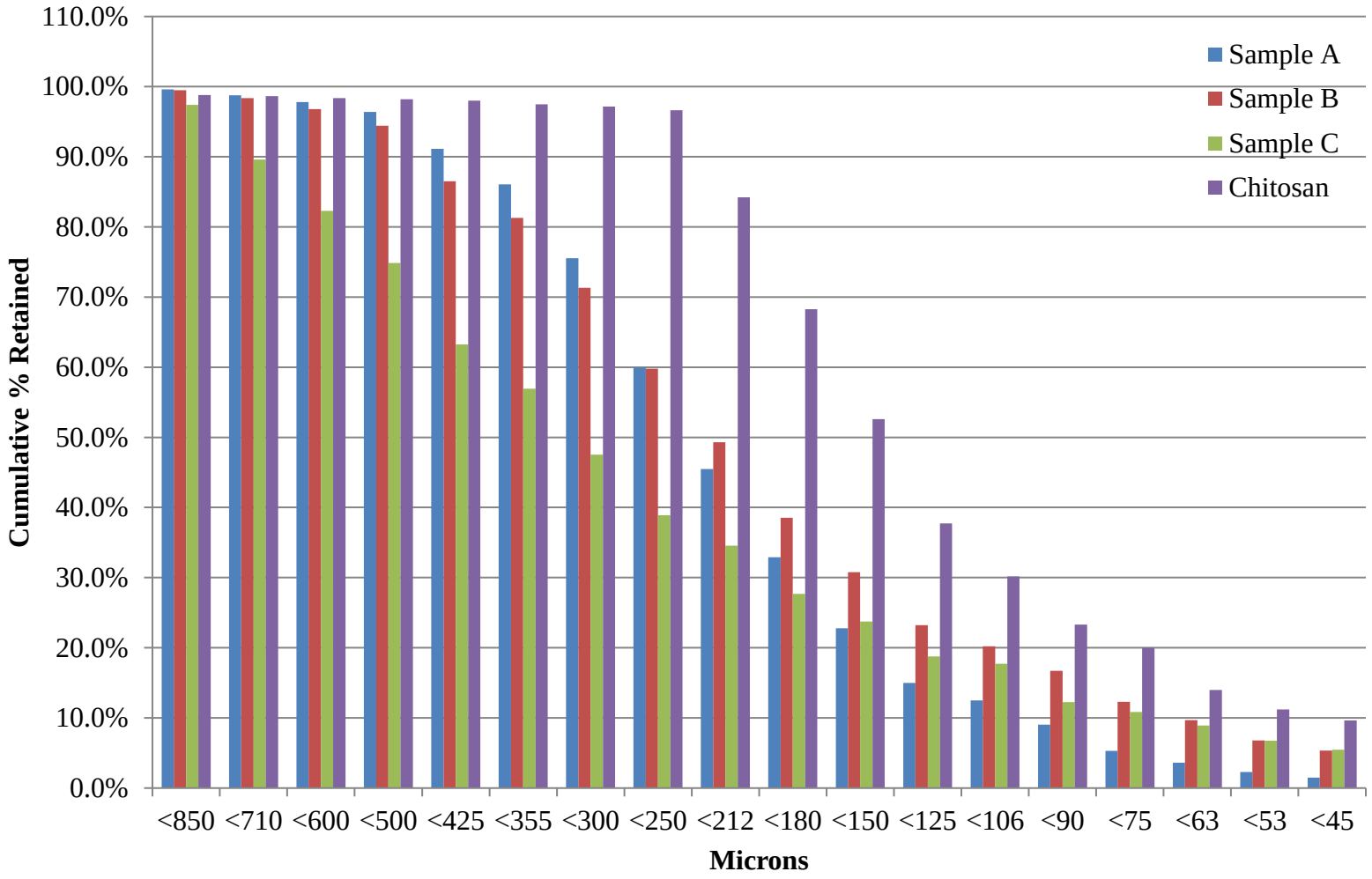

Figure 6.2. Cumulative particle size distribution

Table 6.2. Density results for chitosan, Ch-TPP powders, and some direct compression excipients

	Chitosan	Sample A	Sample B	Sample C	Avicel® PH102[a]	DCPA[b]	Starch®1500[c]
Bulk Density (g/ml)	0.232	0.203	0.238	0.294	0.309	0.800	0.610
Tapped Density (g/ml)	0.471	0.300	0.366	0.395	0.421	0.925	0.820
True Density (g/ml)	1.474[d]	1.616[d]	1.698[d]	1.705[d]	1.460	2.390	1.500
Carr's Index	50.77	32.43	34.92	25.49	26.60	13.51	25.61
Hausner Ratio	2.03	1.48	1.54	1.34	1.36	1.15	1.34
USP Definition For Carr's Index	Very, very poor	Very Poor	Very Poor	Passable	Poor	Good	Poor
USP Definition for Hausner Ratio	Very, very poor	Very Poor	Very Poor	Passable	Poor	Good	Passable

[a] Koo (2001) [b] Kachrimanis et al. (2005) [c] Colorcon (2012) [d] As previously presented in Chapter 5

Compression of pure chitosan and Ch-TPP sample A was not possible using the Korsch XP-1 equipment. While several authors have claimed to compress pure chitosan in the past, this was done using bench top hand presses with excessive dwell times of 5 – 30 seconds (Rege, 1999; Sabnis et al., 1997; Sawayanagi, Nambu, & Nagai, 1982), which do not compare to the typical fractions of a second observed in a production environment. Using such a method, the pure chitosan used in the these studies, as well as the Ch-TPP Sample A, were also compressible when using a Natoli bench top press as exemplified in chapter 5 for dissolution analysis. The use of a Korsch XP-1 was intended to better mimic the production environment with realistic compression forces and dwell times.

Furthermore, compressibility analysis of DCPA was not possible due to excessive sticking to punches, which led to an inability to reproducibly generate tablets for analysis. This observation has been documented in other studies where it was shown that compression of calcium phosphates without lubrication was not possible due to sticking (Schmidt & Herzog, 1993), smooth rollers were needed during roller compaction due to sticking observed with serrated rollers (Souihi et al., 2013), or capping was observed at commonly used compression pressures (Mir, 2008).

A summary of in-process testing results for the compression of Ch-TPP samples B and C is found in Table 6.3. A force/hardness curve is presented in Figure 6.3 with the results of the linear curve fitting presented in Table 6.4. A compactibility plot is shown in Figure 6.4 with the fitting parameters presented in Table 6.5. Transformation from tablet hardness to tensile strength eliminates tablet dimension as a factor and is a more accurate comparison of the strength of various compacts (Newton, Rowley, Fell, Peacock, & Ridgway, 1971).

Table 6.3. In-process testing results for compressibility analysis

	Conditions	Weight (mg)	Thickness (mm)	Hardness (kp)	Force (kN)
Ch-TPP Sample B	1	244 (5)	5.36 (0.06)	4.4 (0.1)	2.9 (0.1)
	2	248 (1)	5.36 (0.04)	5.1 (0.5)	3.2 (0.1)
	3	255 (4)	5.19 (0.04)	7.5 (0.6)	4.3 (0.4)
	4	255 (3)	4.99 (0.02)	10.9 (0.7)	5.4 (0.2)
	5	256 (2)	4.85 (0.04)	13.6 (1.1)	6.2 (0.2)
Ch-TPP Sample C	1	255 (2)	5.29 (0.03)	5.2 (0.4)	4.6 (0.2)
	2	252 (1)	4.91 (0.00)	8.6 (0.5)	6.4 (0.1)
	3	255 (2)	4.83 (0.01)	11.1 (0.8)	7.1 (0.1)
	4	254 (4)	4.60 (0.01)	15.7 (0.8)	8.6 (0.3)
	5	251 (3)	4.44 (0.01)	17.7 (0.7)	9.9 (0.4)
Avicel® PH102	1	249 (1)	5.75 (0.01)	4.6 (0.3)	1.8 (0.0)
	2	250 (1)	5.37 (0.00)	6.6 (0.2)	2.3 (0.0)
	3	252 (1)	4.89 (0.01)	11.2 (0.3)	3.4 (0.0)
	4	252 (1)	4.50 (0.00)	16.9 (0.8)	5.3 (0.1)
	5	251 (1)	4.15 (0.01)	27.8 (1.0)	9.1 (0.1)
Starch® 1500	1	251 (1)	4.85 (0.01)	0.5 (0.0)	3.4 (0.0)
	2	249 (1)	4.56 (0.01)	1.4 (0.1)	5.9 (0.0)
	3	248 (1)	4.27 (0.01)	3.5 (0.0)	11.3 (0.1)
	4	252 (1)	4.11 (0.01)	5.8 (0.1)	19.2 (0.2)
	5	252 (1)	4.05 (0.01)	7.3 (0.1)	30.3 (0.4)

Values in parenthesis are the standard deviation

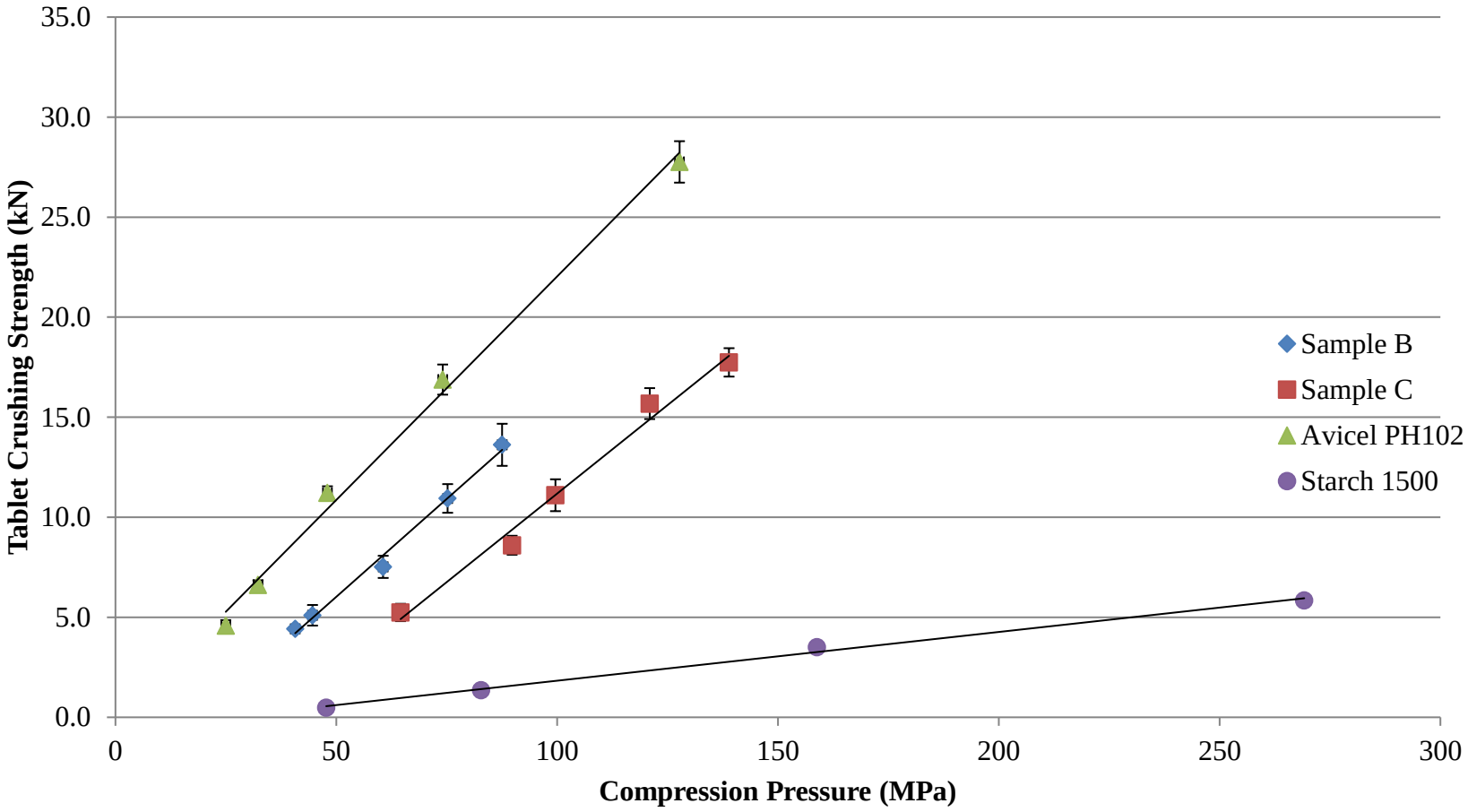

Figure 6.3. Effect of compression pressure on the tablet crushing strength
(n=5 tablets per data point)

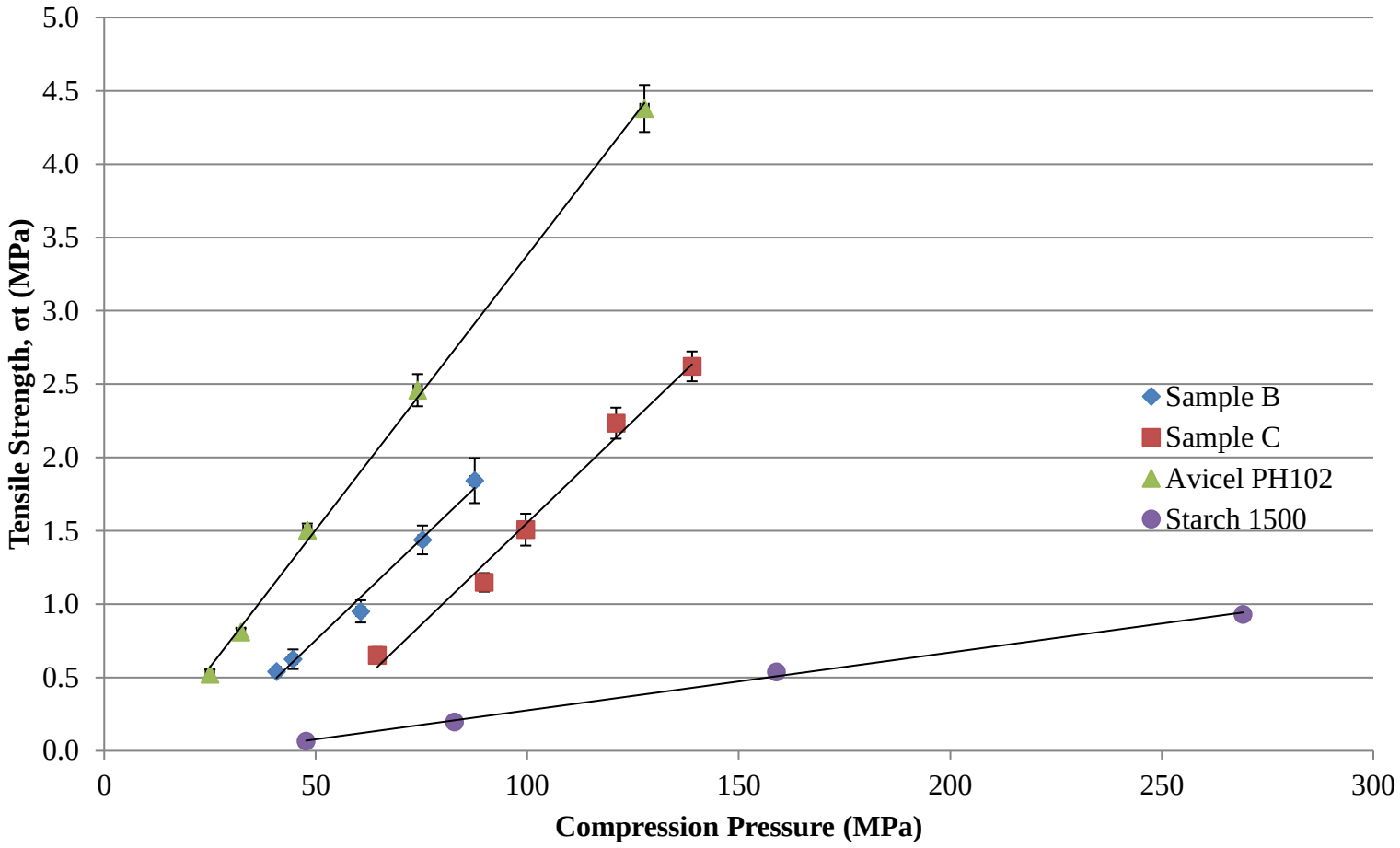

Figure 6.4. Effect of compression pressure on the tensile strength
(n=5 tablets per data point)

Table 6.4. Linear regression analysis of the dependence of crushing strength (kp) on the compression pressure (MPa)

Material	Linear regression equation	R^2
Ch-TPP Sample B	$y = 0.1957x - 3.7617$	0.9924
Ch-TPP Sample C	$y = 0.1769x - 6.5122$	0.9861
Avicel® PH102	$y = 0.2234x - 0.3082$	0.9947
Starch® 1500	$y = 0.0244x - 0.6069$	0.9956

Table 6.5. Compactibility (MPa) as calculated from the slope of the linear regression fit in Figure 6.4

Material	Compactibility, $C_p \times 10^2$ (MPa)	R^2
Ch-TPP Sample B	2.76	0.9883
Ch-TPP Sample C	2.77	0.9872
Avicel® PH102	3.74	0.9987
Starch® 1500	0.39	0.9973

The results in Figure 6.4 and Table 6.5 indicate the ranking of compactibility as measured by the slope of the linear regression equation to be Avicel® PH102 > Ch-TPP Sample B = Ch-TPP Sample C >> Starch® 1500. This ranking is similar to that observed by Mir et. al. (2008) when comparing the compaction of chitin and chitosan samples to other commonly used tableting excipients; however, it should be noted that the compactibility of Ch-TPP samples is closer to that of Avicel® PH102 than to that of chitin and chitosan pure powders reported by Mir et al. (2008). This observation, along with the inability to compress the pure chitosan sample, indicates a marked improvement in compression properties of Ch-TPP as compared to the pure form of chitosan used in the study.

Furthermore, the general pattern of compactibility in Figure 6.3 as it relates to Avicel® PH102 and the Ch-TPP complexes resembles that presented by Picker-Freyer and Brink (2006), who compared the compactibility of Avicel® PH200 and various molecular weight grades of chitosan, each of which were significantly lower than the molecular weight of chitosan used in this study. The bulk and tapped density of the pure chitosan samples used in their studies more closely match those measured for Ch-TPP samples B and C, confirming that the density of a material in addition to the relationship between bulk and tapped density (i.e. Hausner Ratio and Carr's Index) are important factors when assessing a material's ability to form a compact. Additionally, results from Rege et al. (1999) showed that compression analysis of different molecular weight grades of chitosan (low, medium, and high) revealed that compactibility of chitosan increased with decreasing molecular weight. These studies, where tablets were made using

exaggerated dwell times further corroborate the inability to compress the pure higher molecular weight chitosan used in the present study.

The lack of significant difference in compactibility between Ch-TPP sample B and sample C would suggest that Span and d50 may have conflicting contributions to compactibility. Studies by Šantl et al. (2012) showed that different mesh cuts of the same material showed differences in compactibility as a result of the extent of fragmentation. Larger particles have greater propensity to fragment during compression, leading to more exposed surface area capable of inter-particle bonding (McKenna & McCafferty, 1982; Patel et al., 2007). This may explain why Ch-TPP sample A was incapable of forming compacts as it was the Ch-TPP crosslinked structure with the smallest particles and thus the lowest potential for fragmentation. Based on this, one would also expect Ch-TPP Sample C to show greater compaction; however, Šantl et al. also suggested that a broader particle size distribution could lead to denser packing of the particles prior to compression, which could subsequently decrease the potential for fragmentation.

The out-of-die Heckel plot is presented in Figure 6.5 and the results from the linear curve fitting are presented in Table 6.6. The Heckel coefficient (K), equal to the slope of the linear fit, and its reciprocal value, referred to as yield pressure (P_y), both represent measures of compressibility of the different materials. Higher values for the Heckel coefficient and lower values for the yield pressure indicate higher compressibility (Ilić et al., 2013).

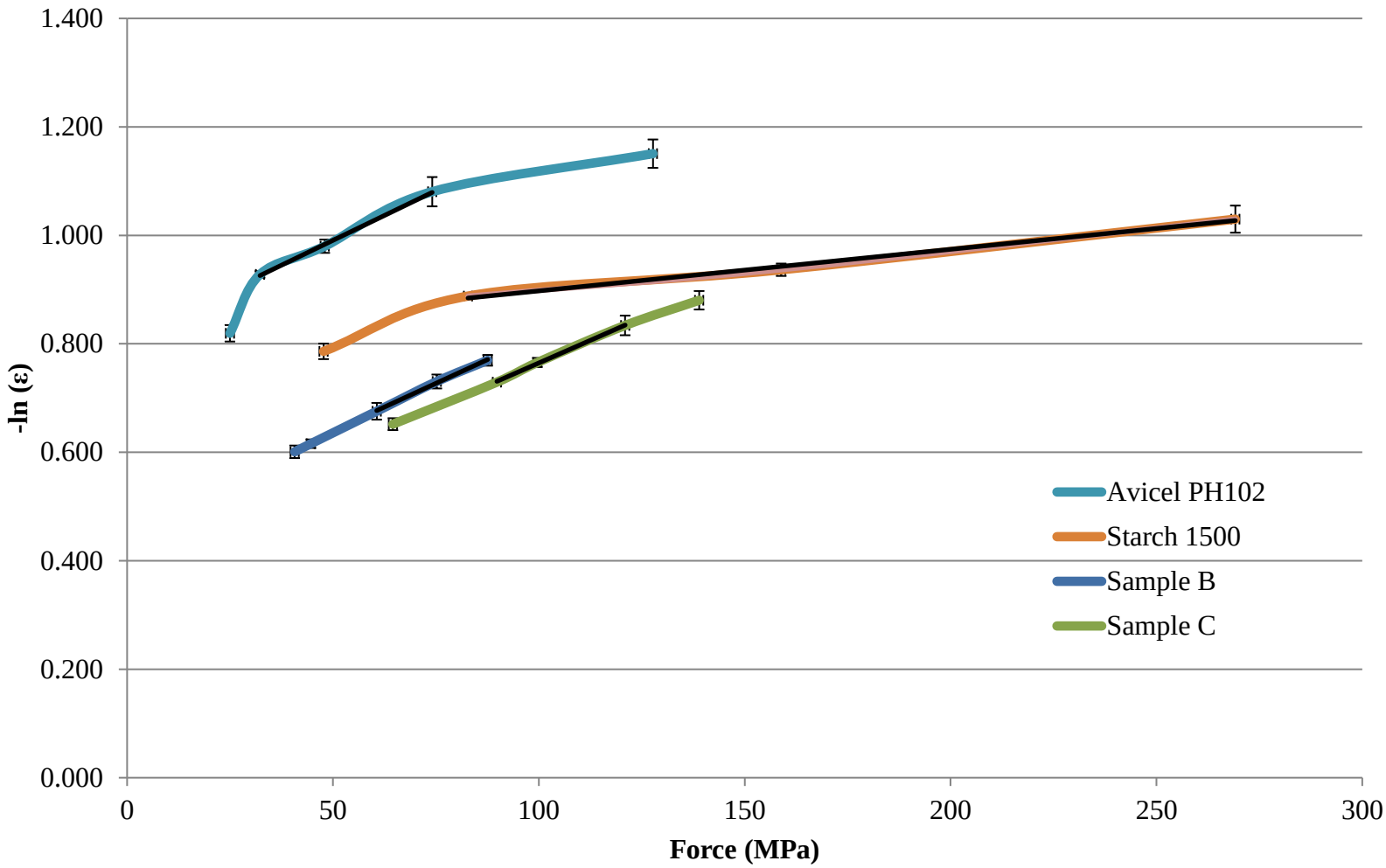

Figure 6.5. Out-of-die Heckel Plot for Ch-TPP and other common direct compression excipients (n=5 tablets per data point). The linear portion of each curve is overlaid in black.

Table 6.6. Results of out-of-die Heckel Plot linear regression curve fitting

Material	Heckel Coefficient, K (MPa^{-1})	P_y (MPa)	R^2
Ch-TPP Sample B	0.0035	285.7	0.9976
Ch-TPP Sample C	0.0033	303.0	0.9988
Avicel® PH102	0.0037	270.3	0.9985
Starch®1500	0.0008	1250.0	0.9945

The data from the out-die Heckel plot analysis yielded linear regression equations that described the data well (R^2 values > 0.99). These results show that the Ch-TPP complexes possess favorable compressibility, similar to that observed for Avicel® PH102 and markedly better, by a factor of ~5x, than the compressibility of Starch® 1500. Thus, Ch-TPP exemplifies an ability to undergo plastic deformation to a similar extent of Avicel® PH101 under compression, a base assumption when using the Heckel model (Ilić et al., 2013). Using the out-die method, there is no differentiation between elastic and inelastic plastic deformation, which can be identified using an in-die method; however, measurements by the out-of-die method is more representative of the final state of a tablet as administered to a patient (Ilić et al., 2013). In a similar out-of-die analysis of commonly used excipients, Avicel® grades PH101 and PH200 were also shown to have superior compressibility to lactose and corn starch (Ilić et al., 2013), suggesting that the Ch-TPP complexes also show improved compressibility compared to these excipients.

Conclusions

Powder analysis and direct compression analysis of Ch-TPP complexes (sample B and sample C) revealed a marked improvement in compressibility compared to pure chitosan, which could not be compressed under the experimental conditions. Ch-TPP sample B and sample C exhibited similar compressibility/compactibility characteristics despite displaying differences in particle size and overall shape of the particle size distribution curve. These samples did, however, have similar bulk density values, each of which was higher than that of sample A. Ch-TPP sample A was the only one of the three

samples that could not be compressed into a tablet under the compression conditions, suggesting that a higher density is conducive to tablet formation.

While tablets prepared with the Ch-TPP complexes using commonly employed compression pressures were not as hard as those prepared using Avicel® PH102, tablet hardness for Ch-TPP tablets indicates that the tablets can withstand downstream manufacturing and handling. The compressibility of the Ch-TPP samples as examined via a Heckel Plot showed comparable results to the Avicel® PH102 and marked improvement when compared to Starch®1500. These results indicate Ch-TPP complexes generated with specific physical properties, particularly density (i.e. bulk, tapped, and true), can serve as a direct compression excipient with little need for additional excipients to enhance the compressibility of the formulation.

CHAPTER 7

Appendix

Table 7.1. Analysis of Variance: d50 and Span
(Inverse Transformation for both d50 and Span)

	d50	Span
Source	p-value	
Model	0.0024	0.0036
A	0.0003	0.0049
B	0.6779	0.0688
D	0.9526	0.0951
E	0.9671	0.8330
AE	0.0300	0.0220
BD	0.0080	0.0057
Lack of Fit	0.0382	0.0181
Curvature	0.0951	0.6617
R^2	0.7741	0.7568
Adj R^2	0.6611	0.6351

Table 7.2. Analysis of Variance: True Density (No Transformation)

Source	**p-value**
Model	0.0021
A	0.4486
B	0.4192
C	0.0054
D	0.5179
E	0.0634
AB	0.0407
AD	0.0186
AE	0.0002
DE	0.0275
Lack of Fit	0.0948
Curvature	0.1012
R^2	0.8923
Adj R^2	0.7845

Table 7.3. Analysis of Variance: Zeta Potential (No Transformation)

Source	**p-value**
Model	< 0.0001
A	0.1206
B	< 0.0001
D	< 0.0001
E	0.0217
AB	0.0016
BD	< 0.0001
Lack of Fit	0.2980
Curvature	0.5571
R^2	0.9842
Adj R^2	0.9763

Table 7.4. Analysis of Variance: Yield (No Transformation)

Source	**p-value**
Model	0.7927
A	0.3578
B	0.3478
C	0.6007
D	0.1558
E	0.6408
AB	0.6302
AC	0.8760
AD	0.6702
AE	0.5630
BC	0.6527
BD	0.5416
BE	0.7171
CD	0.8185
CE	0.7901
DE	0.6789
Lack of Fit	0.0002
Curvature	0.0002
R^2	0.7449
Adj R^2	-0.5304

Table 7.5. Analysis of Variance: t_{50} (No Transformation)

Source	**p-value**
Model	0.0183
A	0.3969
B	0.7368
C	0.0386
AB	0.0153
Lack of Fit	0.8806
Curvature	0.0448
R^2	0.4949
Adj R^2	0.3506

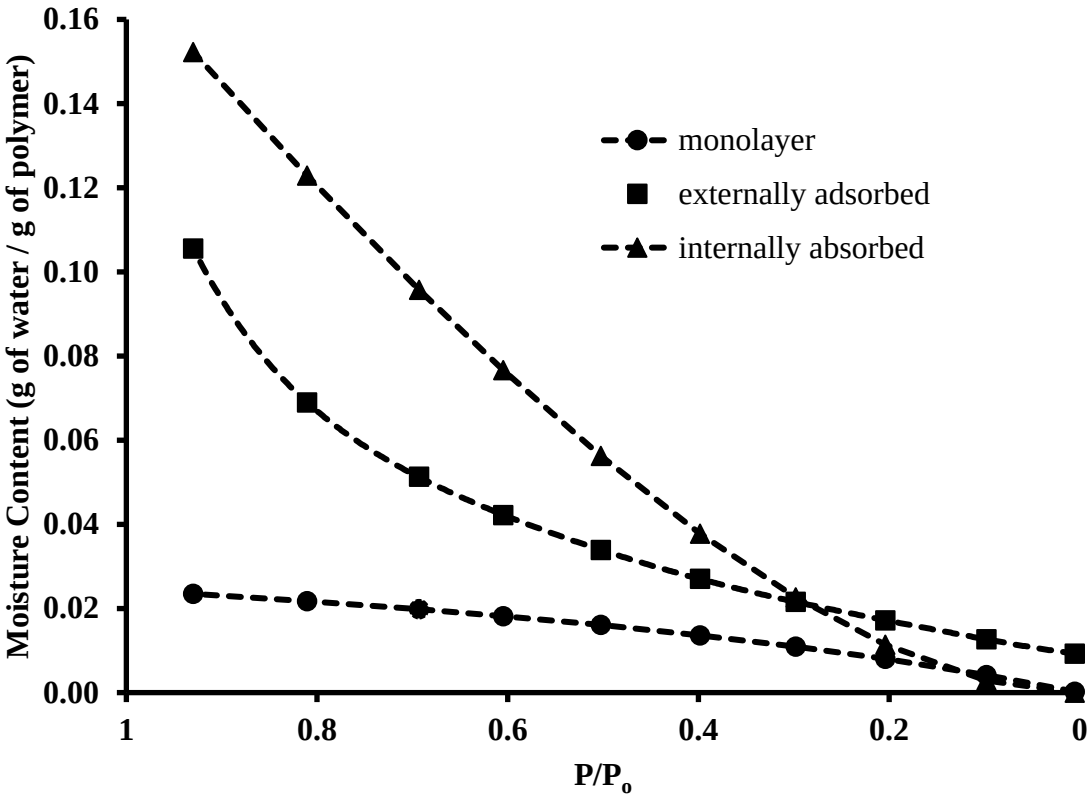

Figure 7.1. Moisture distribution patterns during desorption for optimized sample A according to the Young and Nelson equations

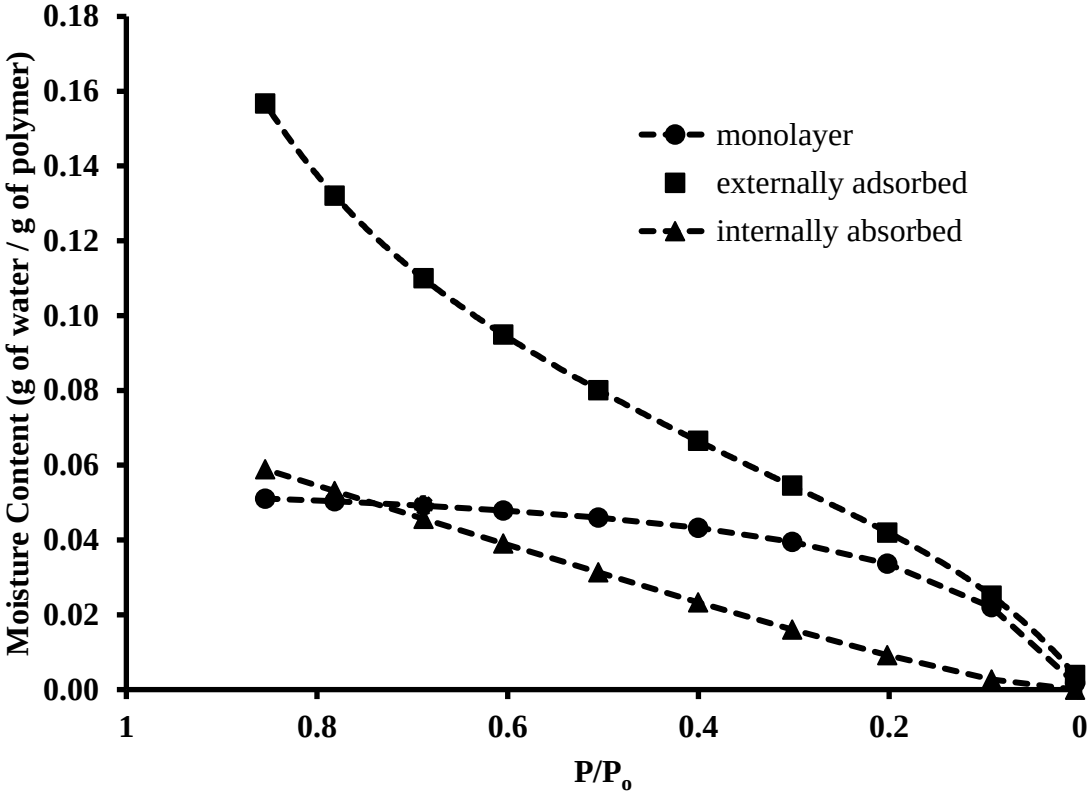

Figure 7.2. Moisture distribution patterns during desorption for optimized sample B according to the Young and Nelson equations

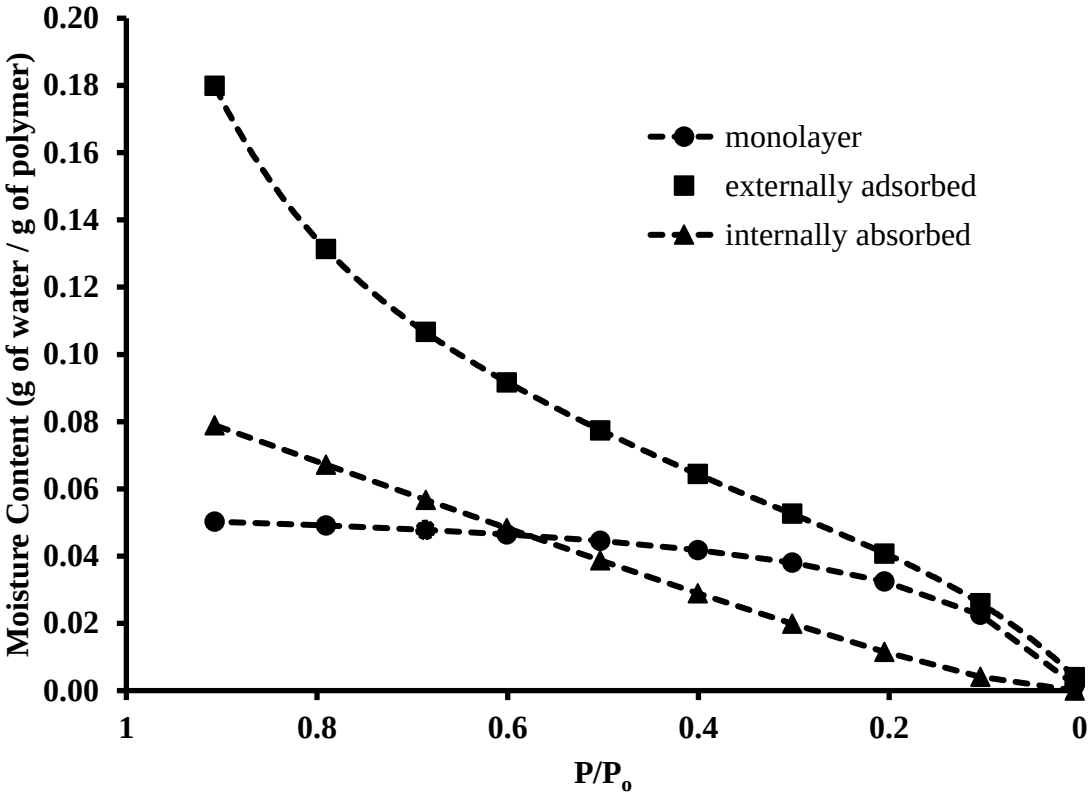

Figure 7.3. Moisture distribution patterns during desorption for optimized sample C according to the Young and Nelson equations

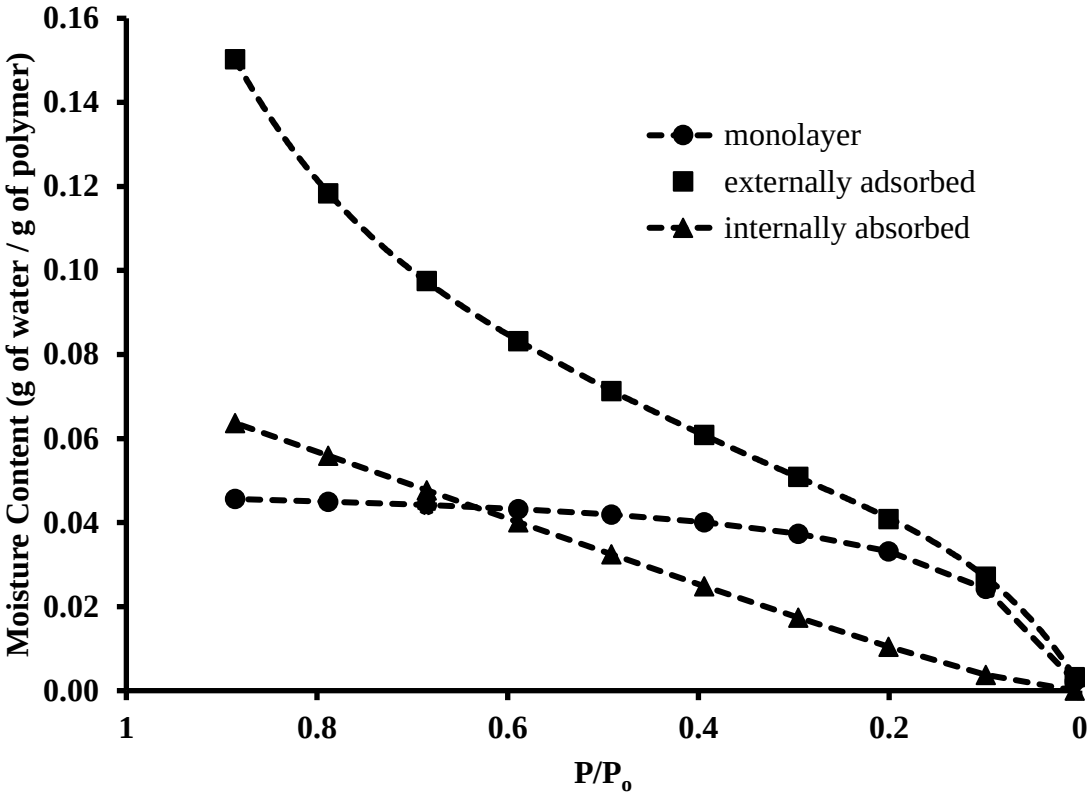

Figure 7.4. Moisture distribution patterns during desorption for chitosan powder according to the Young and Nelson equations

References

Adams, M. J., Mullier, M. A., & Seville, J. P. K. (1994). Agglomerate strength measurement using a uniaxial confined compression test. *Powder Technology, 78*(1), 5-13. doi:http://dx.doi.org/10.1016/0032-5910(93)02777-8

Agency Response Letter GRAS Notice No. GRN 000397. (2011). Retrieved from https://www.fda.gov/Food/IngredientsPackagingLabeling/GRAS/NoticeInventory/ucm287638.htm.

Agnihotri, S. A., Mallikarjuna, N. N., & Aminabhavi, T. M. (2004). Recent advances on chitosan-based micro- and nanoparticles in drug delivery. *Journal of Controlled Release, 100*(1), 5-28. doi:http://dx.doi.org/10.1016/j.jconrel.2004.08.010

Agrawal, A. M., Manek, R. V., Kolling, W. M., & Neau, S. H. (2004). Water Distribution Studies Within Microcrystalline Cellulose and Chitosan using Differential Scanning Calorimetry and Dynamic Vapor Sorption Analysis. *Journal of Pharmaceutical Sciences, 93*(7), 1766-1779. doi:10.1002/jps.20085

Aguirre-Loredo, R. Y., Rodriguez-Hernandez, A. I., & Velazquez, G. (2017). Modelling the effect of temperature on the water sorption isotherms of chitosan films. *Food Science and Technology (Campinas), 37*, 112-118.

Ahlneck, C., & Zografi, G. (1990). The molecular basis of moisture effects on the physical and chemical stability of drugs in the solid state. *International journal of pharmaceutics, 62*(2-3), 87-95. doi:10.1016/0378-5173(90)90221-o

Alderborn, G., & Nystrom, C. (1982). Studies on direct compression of tablets. IV. The effect of particle size on the mechanical strength of tablets. *Acta Pharm Suec, 19*(5), 381-390.

Allen, L., & Ansel, H. C. (2013). *Ansel's pharmaceutical dosage forms and drug delivery systems*: Lippincott Williams & Wilkins.

Anderson, R. B. (1946). Modifications of the Brunauer, Emmett and Teller Equation. *Journal of the American Chemical Society, 68*(4), 686-691. doi:10.1021/ja01208a049

Anderson, R. B., & Hall, W. K. (1948). Modifications of the Brunauer, Emmett and Teller Equation II. *Journal of the American Chemical Society, 70*(5), 1727-1734. doi:10.1021/ja01185a017

Armstrong, N. A. (2006). *Pharmaceutical Experimental Design and Interpretation* (Vol. Second Edition). Boca Raton, FL: CRC Press, Taylor & Francis Group.

Artursson, P., Lindmark, T., Davis, S. S., & Illum, L. (1994). Effect of chitosan on the permeability of monolayers of intestinal epithelial cells (Caco-2). *Pharm Res, 11*(9), 1358-1361.

Aulton, M. E., & Taylor, K. M. (2013). *Aulton's pharmaceutics: the design and manufacture of medicines*: Elsevier Health Sciences.

Baker, R. W. L., H.K. (1974). Controlled Release: Mechanism and rates. In T. C. L. Tanquary, R.E. (Ed.), *Controlled Release of Biologically Active Agents* (pp. 15-71). New York: Plenum Press.

Baldrick, P. (2010). The safety of chitosan as a pharmaceutical excipient. *Regulatory Toxicology and Pharmacology, 56*(3), 290-299. doi:http://dx.doi.org/10.1016/j.yrtph.2009.09.015

Basu, S., Shivhare, U. S., & Mujumdar, A. S. (2006). Models for Sorption Isotherms for Foods: A Review. *Drying Technology, 24*(8), 917-930. doi:10.1080/07373930600775979

Beattie, R. M., & Walker-Smith, J. A. (1994). Use of enteric coated prednisolone in Crohn's disease. *Archives of Disease in Childhood, 71*(3), 282.

Bell, L. N., & Labuza, T. P. (2000). *Moisture sorption : practical aspects of isotherm measurement and use* (2nd ed. ed.). Cambridge: American Association of Cereal Chemists.

Bharate, S. S., Bharate, S. B., & Bajaj, A. N. (2010). Interactions and incompatibilities of pharmaceutical excipients with active pharmaceutical ingredients: a comprehensive review. *Journal of Excipients and Food Chemicals*.

Biagini, G., Bertani, A., Muzzarelli, R., Damadei, A., DiBenedetto, G., Belligolli, A., . . . Rizzoli, C. (1991). Wound management with N-carboxybutyl chitosan. *Biomaterials, 12*(3), 281-286.

Boquet, R., Chirife, J., & Iglesias, H. A. (1978). Equations for fitting water sorption isotherms of foods. *International Journal of Food Science & Technology, 13*(4), 319-327.

Bowman, K., & Leong, K. W. (2006). Chitosan nanoparticles for oral drug and gene delivery. *International Journal of Nanomedicine, 1*(2), 117-128.

Brittain, H. G. (1995). Overview of physical characterization methodology. In H. G. Brittain (Ed.), *Physical characterization of pharmaceutical solids* (pp. 1-35). New York: Dekker.

Brunauer, S., Deming, L. S., Deming, W. E., & Teller, E. (1940). On a theory of the van der Waals adsorption of gases. *Journal of the American Chemical society, 62*(7), 1723-1732.

Brunauer, S., Emmett, P. H., & Teller, E. (1938). Adsorption of Gases in Multimolecular Layers. *Journal of the American Chemical Society, 60*(2), 309-319. doi:10.1021/ja01269a023

Calvo, P., Remuñán-López, C., Vila-Jato, J. L. and Alonso, M. J. (1997). Novel hydrophilic chitosan-polyethylene oxide nanoparticles as protein carriers. *J. Appl. Polym. Sci., 63*, 125-132. doi:10.1002/(SICI)1097-4628(19970103)63:1<125::AID-APP13>3.0.CO;2-4

Carr, R. L. (1965). Evaluating flow properties of solids. *Chem. Eng., 72*(69-72).

Chávez de Paz, L. E. R., Anton; Howard, Kenneth A.; Sutherland, Duncan S.; Wejse, Peter L. (2011). Antimicrobial Effect of Chitosan Nanoparticles on Streptococcus mutans Biofilms. *Applied and Environmental Microbiology, 77*(11), 3892-3895. doi:10.1128/aem.02941-10

Chen, R. H. T., M. L. (1998). Effect of temperature on the intrinsic viscosity and conformation of chitosans in dilute HCl solution. *Int J Biol Macromol, 23*(2), 135-141.

Chen, X., Wen, H., & Park, K. (2010). Challenges and new technologies of oral controlled release. *Oral controlled release formulation design and drug delivery: Theory to Practice, 16*, 257-277.

Chien, Y. W., & Swarbrick, J. (1992). Novel drug delivery systems.

Chitin and Chitosan Final Registration Review Decision. (Document ID: EPA-HQ-OPP-2007-0566-0019). (2008).

Clark, G. L., & Smith, A. F. (1936). X-ray Diffraction Studies of Chitin, Chitosan, and Derivatives. *The Journal of Physical Chemistry*, *40*(7), 863-879.

Colombo, P., Bettini, R., Santi, P., & Peppas, N. A. (2000). Swellable matrices for controlled drug delivery: gel-layer behaviour, mechanisms and optimal performance. *Pharmaceutical Science & Technology Today*, *3*(6), 198-204.

Colorcon. (2012). Technical Bulletin: Starch 1500 - Partially Pregelatinized Maize Starch. Retrieved from https://www.colorcon.com/literature/marketing/ex/Starch%201500/Tech%20Bulletin_Starch1500_properties.pdf

Costa, P., & Sousa Lobo, J. M. (2001). Modeling and comparison of dissolution profiles. *European Journal of Pharmaceutical Sciences*, *13*(2), 123-133. doi:http://doi.org/10.1016/S0928-0987(01)00095-1

Curotto, E., & Aros, F. (1993). Quantitative Determination of Chitosan and the Percentage of Free Amino Groups. *Analytical Biochemistry*, *211*(2), 240-241. doi:http://dx.doi.org/10.1006/abio.1993.1263

David, S. T., & Augsburger, L. L. (1977). Plastic Flow during Compression of Directly Compressible Fillers and Its Effect on Tablet Strength. *Journal of Pharmaceutical Sciences*, *66*(2), 155-159. doi:http://dx.doi.org/10.1002/jps.2600660205

De Boer, J. (1953). The Dynamic Character of Adsorption. Clarendon: Oxford.

de Boer, J. H. (1968). (2nd ed.). Oxford: Claredon Press.

De Campos, A. M., Sánchez, A., & Alonso, M. a. J. (2001). Chitosan nanoparticles: a new vehicle for the improvement of the delivery of drugs to the ocular surface. Application to cyclosporin A. *Int J Pharm, 224*(1–2), 159-168. doi:http://dx.doi.org/10.1016/S0378-5173(01)00760-8

Deacon, M. P., McGurk, S., Roberts, C. J., Williams, P. M., Tendler, S. J., Davies, M. C., . . . Harding, S. E. (2000). Atomic force microscopy of gastric mucin and chitosan mucoadhesive systems. *Biochem J, 348 Pt 3*, 557-563.

Desai, K. G. H., & Park, H. J. (2005). Preparation and characterization of drug-loaded chitosan–tripolyphosphate microspheres by spray drying. *Drug Development Research, 64*(2), 114-128. doi:10.1002/ddr.10416

Deuchi, K., Kanauchi, O., Imasato, Y., & Kobayashi, E. (1995). Effect of the Viscosity or Deacetylation Degree of Chitosan on Fecal Fat Excreted from Rats Fed on a High-fat Diet. *Biosci Biotechnol Biochem, 59*(5), 781-785. doi:10.1271/bbb.59.781

DiMatteo, M. R., & DiNicola, D. D. (1982). Achieving patient compliance: The psychology of the medical practitioner's role.

Dodane, V., Amin Khan, M., & Merwin, J. R. (1999). Effect of chitosan on epithelial permeability and structure. *Int J Pharm, 182*(1), 21-32.

Dong, Y. N., Wai Kiong; Shen, Shoucang; Kim, Sanggu; Tan, Reginald B.H. (2013). Scalable ionic gelation synthesis of chitosan nanoparticles for drug delivery in static mixers. *Carbohydrate Polymers, 94*(2), 940-945. doi:http://dx.doi.org/10.1016/j.carbpol.2013.02.013

Drebushchak, V. A., Shakhtshneider, T. P., Apenina, S. A., Medvedeva, A. S., Safronova, L. P., & Boldyrev, V. V. (2006). Thermoanalytical investigation of drug–excipient interaction. Phase II. Activated mixtures of piroxicam with cellulose and chitosan. *Journal of Thermal Analysis and Calorimetry, 86*(2), 303-309. doi:10.1007/s10973-005-7440-y

Dudhani, A. R., & Kosaraju, S. L. (2010). Bioadhesive chitosan nanoparticles: Preparation and characterization. *Carbohydrate Polymers, 81*(2), 243-251. doi:http://dx.doi.org/10.1016/j.carbpol.2010.02.026

El Hadrami, A., Adam, L. R., El Hadrami, I., & Daayf, F. (2010). Chitosan in Plant Protection. *Marine Drugs, 8*(4), 968-987. doi:10.3390/md8040968

Fàbregas, A. M., M.; García-Montoya, E.; Pérez-Lozano, P.; Carrillo, C.; Sarrate, R.; Sánchez, N.; Ticó, J. R.; Suñé-Negre, J. M. (2013). Impact of physical parameters on particle size and reaction yield when using the ionic gelation method to obtain cationic polymeric chitosan–tripolyphosphate nanoparticles. *Int J Pharm, 446*(1–2), 199-204. doi:http://dx.doi.org/10.1016/j.ijpharm.2013.02.015

Fan, W. Y., Wei; Xu, Zushun; Ni, Hong. (2012). Formation mechanism of monodisperse, low molecular weight chitosan nanoparticles by ionic gelation technique. *Colloids and Surfaces B: Biointerfaces, 90*, 21-27. doi:http://dx.doi.org/10.1016/j.colsurfb.2011.09.042

Fang, N., Chan, V., Mao, H. Q., & Leong, K. W. (2001). Interactions of phospholipid bilayer with chitosan: effect of molecular weight and pH. *Biomacromolecules, 2*(4), 1161-1168.

Fell, J. T., & Newton, J. M. (1970). Determination of tablet strength by the diametral-compression test. *Journal of Pharmaceutical Sciences, 59*(5), 688-691. doi:10.1002/jps.2600590523

Felt, O., Buri, P., & Gurny, R. (1998). Chitosan: A Unique Polysaccharide for Drug Delivery. *Drug Development and Industrial Pharmacy, 24*(11), 979-993. doi:10.3109/03639049809089942

Fisher, R. A. (1926). *The Design of Experiments* (Edinburgh Ed.). London: Oliver & Boyd Ltd.

Fyhr, P., & Downie, K. (2003). Extended release drug delivery technology. *Innovations in Pharmaceutical Technology*(September), 80-86.

Gan, Q., & Wang, T. (2007). Chitosan nanoparticle as protein delivery carrier—Systematic examination of fabrication conditions for efficient loading and release. *Colloids and Surfaces B: Biointerfaces, 59*(1), 24-34. doi:http://dx.doi.org/10.1016/j.colsurfb.2007.04.009

Gan, Q., Wang, T., Cochrane, C., & McCarron, P. (2005). Modulation of surface charge, particle size and morphological properties of chitosan–TPP nanoparticles intended for gene delivery. *Colloids and Surfaces B: Biointerfaces, 44*(2–3), 65-73. doi:http://dx.doi.org/10.1016/j.colsurfb.2005.06.001

Gohel, M. C. J., P.D. (2005). A review of co-processed directly compressible excipients. *J Pharm Pharm Sci, 8*(1), 76-93.

Goy, R. C., Britto, D. d., & Assis, O. B. (2009). A review of the antimicrobial activity of chitosan. *Polímeros, 19*(3), 241-247.

Gregory, R. B. (1995). Protein Hydration and Glass Transition Behavior In R. B. Gregory (Ed.), *Protein-solvent interactions* (pp. xix,570p.). New York, N.Y.: Dekker.

Guan, J., Cheng, P., Huang, S. J., Wu, J. M., Li, Z. H., You, X. D., . . . Zhang, H. (2011). Optimized Preparation of Levofloxacin-loaded Chitosan Nanoparticles by Ionotropic Gelation. *Physics Procedia, 22*, 163-169. doi:http://dx.doi.org/10.1016/j.phpro.2011.11.026

Guggenheim, E. A. (1966). *Applications of statistical mechanics*. Oxford: Clarendon Press.

Guthy, E. (1996). Enteric-coated fish oil in Crohn's disease. *N Engl J Med, 335*(18), 1397-1398.

Hamaura, T., & Newton, J. M. (1999). Interaction between water and poly(vinylpyrrolidone) containing polyethylene glycol. *Journal of pharmaceutical sciences, 88*(11), 1228-1233. doi:10.1021/js980354c

Hancock, B. C. C., Joshua T; Mullarney, Matthew P; Zinchuk, Andrey V. . (2003). The relative densities of pharmaceutical powders, blends, dry granulations, and immediate-release tablets. *Pharmaceutical Technology, April*, 64-80.

Harish Prashanth, K. V., Kittur, F. S., & Tharanathan, R. N. (2002). Solid state structure of chitosan prepared under different N-deacetylating conditions. *Carbohydrate Polymers, 50*(1), 27-33. doi:http://doi.org/10.1016/S0144-8617(01)00371-X

Hassan, M. A., Li, T. P., & Noor, Z. Z. (2009). Coagulation and flocculation treatment of wastewater in textile industry using chitosan. *Journal of Chemical and Natural Resources Engineering, 4*(1), 43-53.

Hausner, H. H. (1967). Friction conditions in a mass of metal powder. *Int. J. Powder Metall., 3*(7-13).

He, P. D., S. S.; Illum, L. (1999). Chitosan microspheres prepared by spray drying. *Int J Pharm, 187*(1), 53-65.

Heckel, R. W. (1961). Density-pressure relationships in powder compression. *Transactions of the Metallurgical Society of AIME, 221*, 671-675.

HemCon Bandage PRO Hemorrhage Control Bandages. (2015). Retrieved from https://www.boundtree.com/hemcon-bandage-pro-hemorrhage-control-bandages-group-3858-150.aspx?search=1211-209

Heng, P. W., Chan, L., & Ong, K. (2003). Influence of storage conditions and type of plasticizers on ethylcellulose and acrylate films formed from aqueous dispersions. *J Pharm Pharm Sci, 6*, 334-344.

Higuchi, T. (1963). Mechanism of Sustained-Action Medication. Theoretical Analysis of Rate of Release of Solid Drugs Dispersed in Solid Matrices. *J Pharm Sci, 52*, 1145-1149.

Hoare, T. R., & Kohane, D. S. (2008). Hydrogels in drug delivery: progress and challenges. *Polymer, 49*(8), 1993-2007.

Hollenbeck, R. G., Peck, G. E., & Kildsig, D. O. (1978). Application of immersional calorimetry to investigation of solid-liquid interactions: Microcrystalline cellulose-water system. *Journal of Pharmaceutical Sciences, 67*(11), 1599-1606.

Howard, M. A., Neau, S. H., & Sack, M. J. (2006). PEO and MPEG in high drug load extruded and spheronized beads that are devoid of MCC. *International Journal of Pharmaceutics, 307*(1), 66-76.

Hu, B., Pan, C., Sun, Y., Hou, Z., Ye, H., & Zeng, X. (2008). Optimization of fabrication parameters to produce chitosan-tripolyphosphate nanoparticles for delivery of tea catechins. *J Agric Food Chem, 56*(16), 7451-7458. doi:10.1021/jf801111c

Huang, Y., & Lapitsky, Y. (2011). Monovalent Salt Enhances Colloidal Stability during the Formation of Chitosan/Tripolyphosphate Microgels. *Langmuir, 27*(17), 10392-10399. doi:10.1021/la201194a

Huynh, C. T., & Lee, D. S. (2014). Controlled Release. In S. Kobayashi & K. Müllen (Eds.), *Encyclopedia of Polymeric Nanomaterials* (pp. 1-12). Berlin, Heidelberg: Springer Berlin Heidelberg.

Ilić, I., Govedarica, B., Šibanc, R., Dreu, R., & Srčič, S. (2013). Deformation properties of pharmaceutical excipients determined using an in-die and out-die method. *Int J Pharm, 446*(1–2), 6-15. doi:http://dx.doi.org/10.1016/j.ijpharm.2013.02.001

Illum, L. (1998). Chitosan and Its Use as a Pharmaceutical Excipient. *Pharmaceutical Research, 15*(9), 1326-1331. doi:10.1023/A:1011929016601

Iyer, U., Hong, W.-H., Das, N., & Ghebre-Sellassie, I. (1990). Comparative evaluation of three organic solvent and dispersion-based ethylcellulose coating formulations. *Pharm. Technol, 14*(9), 68-86.

Jackson, K., Young, D., & Pant, S. (2000). Drug–excipient interactions and their affect on absorption. *Pharmaceutical Science & Technology Today, 3*(10), 336-345.

Jayanthi, B., Manna, P., Madhusudhan, S., Mohanta, G., & Manavalan, R. (2011). Per oral extended release products-An overview.

Jha, I., Iyengar, L., & Rao, A. P. (1988). Removal of cadmium using chitosan. *Journal of Environmental Engineering, 114*(4), 962-974.

Jivraj, M., Martini, L. G., & Thomson, C. M. (2000). An overview of the different excipients useful for the direct compression of tablets. *Pharmaceutical Science & Technology Today, 3*(2), 58-63. doi:http://dx.doi.org/10.1016/S1461-5347(99)00237-0

Johansson, B., Nicklasson, F., & Alderborn, G. (1998). Effect of pellet size on degree of deformation and densification during compression and on compactability of microcrystalline cellulose pellets. *Int J Pharm, 163*(1–2), 35-48. doi:http://dx.doi.org/10.1016/S0378-5173(97)00355-4

Jonassen, H., Kjøniksen, A.-L., & Hiorth, M. (2012). Stability of Chitosan Nanoparticles Cross-Linked with Tripolyphosphate. *Biomacromolecules, 13*(11), 3747-3756. doi:10.1021/bm301207a

Jonassen, H. K., Anna-Lena; Hiorth, Marianne. (2012). Effects of ionic strength on the size and compactness of chitosan nanoparticles. *Colloid and Polymer Science, 290*(10), 919-929. doi:10.1007/s00396-012-2604-3

Joshi, H. N., & Wilson, T. D. (1993). Calorimetric Studies of Dissolution of Hydroxypropyl Methylcellulose E5 (HPMC E5) in Water. *Journal of Pharmaceutical Sciences, 82*(10), 1033-1038. doi:http://dx.doi.org/10.1002/jps.2600821018

Kachrimanis, K., Noisternig, M. F., Griesser, U. J., & Malamataris, S. (2006). Dynamic moisture sorption and desorption of standard and silicified microcrystalline cellulose. *European Journal of Pharmaceutics and Biopharmaceutics, 64*(3), 307-315. doi:http://dx.doi.org/10.1016/j.ejpb.2006.05.019

Kachrimanis, K., Petrides, M., & Malamataris, S. (2005). Flow rate of some pharmaceutical diluents through die-orifices relevant to mini-tableting. *Int J Pharm, 303*(1–2), 72-80. doi:http://dx.doi.org/10.1016/j.ijpharm.2005.07.003

Kawakita, K., Hattori, I., & Kishigami, M. (1974). Characteristic Constants in Kawakita's Powder Compression Equation. *Journal of the Research Association of Powder Technology, Japan, 11*(8), 453-460. doi:10.4164/sptj1964.11.453

Kawakita, K., & Lüdde, K.-H. (1971). Some considerations on powder compression equations. *Powder Technology, 4*(2), 61-68. doi:http://dx.doi.org/10.1016/0032-5910(71)80001-3

Kean, T., & Thanou, M. (2010). Biodegradation, biodistribution and toxicity of chitosan. *Advanced Drug Delivery Reviews, 62*(1), 3-11. doi:http://dx.doi.org/10.1016/j.addr.2009.09.004

Kean, T., & Thanou, M. (2011). Chitin and chitosan: sources, production and medical applications *Renewable resources for functional polymers and biomaterials* (pp. 292-318).

Ko, J., Park, H., Hwang, S., Park, J., & Lee, J. (2002). Preparation and characterization of chitosan microparticles intended for controlled drug delivery. *Int J Pharm, 249*(1–2), 165-174. doi:http://dx.doi.org/10.1016/S0378-5173(02)00487-8

Ko, J. A., Park, H. J., Park, Y. S., Hwang, S. J., & Park, J. B. (2003). Chitosan microparticle preparation for controlled drug release by response surface methodology. *J Microencapsul, 20*(6), 791-797. doi:10.1080/0265204031000160051 4

Kojima, H., Yoshihara, K., Sawada, T., Kondo, H., & Sako, K. (2008). Extended release of a large amount of highly water-soluble diltiazem hydrochloride by utilizing counter polymer in polyethylene oxides (PEO)/polyethylene glycol (PEG) matrix tablets. *European Journal of Pharmaceutics and Biopharmaceutics, 70*(2), 556-562.

Konecsni, K., Low, N. H., & Nickerson, M. T. (2012). Chitosan–tripolyphosphate submicron particles as the carrier of entrapped rutin. *Food Chemistry, 134*(4), 1775-1779. doi:http://dx.doi.org/10.1016/j.foodchem.2012.03.070

Koo, O. M. Y. H., Paul W.S. . (2001). The Influence of Microcrystalline Cellulose Grade on Shape and Shape Distributions of Pellets Produced by Extrusion-Spheronization. *Chemical and Pharmaceutical Bulletin, 49*(11), 1383-1387. doi:10.1248/cpb.49.1383

Korsmeyer, R. W., Gurny, R., Doelker, E., Buri, P., & Peppas, N. A. (1983). Mechanisms of solute release from porous hydrophilic polymers. *Int J Pharm, 15*(1), 25-35. doi:http://dx.doi.org/10.1016/0378-5173(83)90064-9

Koukaras, E. N. P., Sofia A.; Bikiaris, Dimitrios N.; Froudakis, George E. (2012). Insight on the Formation of Chitosan Nanoparticles through Ionotropic Gelation with Tripolyphosphate. *Molecular Pharmaceutics, 9*(10), 2856-2862. doi:10.1021/mp300162j

Kurita, K., Kaji, Y., Mori, T., & Nishiyama, Y. (2000). Enzymatic degradation of β-chitin: susceptibility and the influence of deacetylation. *Carbohydrate Polymers, 42*(1), 19-21.

Lee, B. J., Hendricks, D. G., & Cornforth, D. P. (1998). Effect of sodium phytate, sodium pyrophosphate and sodium tripolyphosphate on physico-chemical characteristics of restructured beef. *Meat Science, 50*(3), 273-283.

Lee, S.-T., Mi, F.-L., Shen, Y.-J., & Shyu, S.-S. (2001). Equilibrium and kinetic studies of copper (II) ion uptake by chitosan-tripolyphosphate chelating resin. *Polymer, 42*(5), 1879-1892.

Levina, M., & Rajabi-Siahboomi, A. R. (2004). The influence of excipients on drug release from hydroxypropyl methylcellulose matrices. *Journal of Pharmaceutical Sciences, 93*(11), 2746-2754.

Levine, H., Slade, L., & Franks, F. (1988). *Water as a plasticizer: physico-chemical aspects of low-moisture polymeric systems*

Water Science Reviews 3: Cambridge University Press.

Lim, S. S., P.A. (1993). Preparation and Pasting Properties of Wheat and Corn Starch Phosphates. *Cereal Chemistry, 70(2),* 137-144.

List of Distributors Receiving Warning Letters for Weight Loss Products. (2015). Retrieved from http://www.fda.gov/Food/ComplianceEnforcement/WarningLetters/ucm188136.htm.

Liu, H., Yang, X.-G., Nie, S.-F., Wei, L.-L., Zhou, L.-L., Liu, H., . . . Pan, W.-S. (2007). Chitosan-based controlled porosity osmotic pump for colon-specific delivery system: Screening of formulation variables and in vitro investigation. *Int J Pharm, 332*(1), 115-124.

Maderuelo, C., Zarzuelo, A., & Lanao, J. M. (2011). Critical factors in the release of drugs from sustained release hydrophilic matrices. *Journal of Controlled Release, 154*(1), 2-19.

Mathur, M., & Mishra, R. (2016). A Review on Osmotic Pump Drug Delivery System. *International Journal of Pharmaceutical Sciences and Research, 7*(2), 453.

Mckay, G., Blair, H., & Gardner, J. (1982). Adsorption of dyes on chitin. I. Equilibrium studies. *Journal of Applied Polymer Science, 27*(8), 3043-3057.

McKenna, A., & McCafferty, D. F. (1982). Effect on particle size on the compaction mechanism and tensile strength of tablets. *J Pharm Pharmacol, 34*(6), 347-351.

Mhurchu, C. N., Dunshea-Mooij, C., Bennett, D., & Rodgers, A. (2005). Effect of chitosan on weight loss in overweight and obese individuals: a systematic review of randomized controlled trials. *Obesity Reviews, 6*(1), 35-42. doi:10.1111/j.1467-789X.2005.00158.x

Mir, V. G. H., J.; Antikainen, O.; Revoredo, O.B.; Colarte, A.I.; Nieto, O.M.; Yliruusi, J. (2008). Direct compression properties of chitin and chitosan. *Eur J Pharm Biopharm, 69*(3), 964-968. doi:10.1016/j.ejpb.2008.01.029

Mitra, S. G., U.; Ghosh, P.C.; Maitra, A.N. (2001). Tumour targeted delivery of encapsulated dextran-doxorubicin conjugate using chitosan nanoparticles as carrier. *J Control Release, 74*(1-3), 317-323.

Montgomery, D. C. (2008). *Design and analysis of experiments* (7 ed.). New York, NY: John Wiley & Sons, Inc.

Morris, G. A. C., Jonathan; Smith, Alan; Adams, Gary G.; Harding, Stephen E. (2011). The effect of prolonged storage at different temperatures on the particle size

distribution of tripolyphosphate (TPP) – chitosan nanoparticles. *Carbohydrate Polymers, 84*(4), 1430-1434. doi:http://dx.doi.org/10.1016/j.carbpol.2011.01.044

Moura, C. M. d., Moura, J. M. d., Soares, N. M., & Pinto, L. A. d. A. (2011). Evaluation of molar weight and deacetylation degree of chitosan during chitin deacetylation reaction: Used to produce biofilm. *Chemical Engineering and Processing: Process Intensification, 50*(4), 351-355. doi:https://doi.org/10.1016/j.cep.2011.03.003

Mucha, M., & Pawlak, A. (2002). Complex study on chitosan degradability. *POLIMERY-WARSAW-, 47*(7/8), 509-516.

Muzzarelli, R. A., Ilari, P., & Tomasetti, M. (1993). Preparation and characteristic properties of 5-methyl pyrrolidinone chitosan. *Carbohydrate Polymers, 20*(2), 99-105.

Muzzarelli, R. A. A., Boudrant, J., Meyer, D., Manno, N., DeMarchis, M., & Paoletti, M. G. (2012). Current views on fungal chitin/chitosan, human chitinases, food preservation, glucans, pectins and inulin: A tribute to Henri Braconnot, precursor of the carbohydrate polymers science, on the chitin bicentennial. *Carbohydrate Polymers, 87*(2), 995-1012. doi:http://doi.org/10.1016/j.carbpol.2011.09.063

Nakamura, K., Hatakeyama, T., & Hatakeyama, H. (1981). Studies on Bound Water of Cellulose by Differential Scanning Calorimetry. *Textile Research Journal, 51*(9), 607-613. doi:10.1177/004051758105100909

Nakamura, K., Hatakeyama, T., & Hatakeyama, H. (1983). Relationship between hydrogen bonding and bound water in polyhydroxystyrene derivatives. *Polymer, 24*(7), 871-876. doi:http://dx.doi.org/10.1016/0032-3861(83)90206-9

Newton, J. M., Rowley, G., Fell, J. T., Peacock, D. G., & Ridgway, K. (1971). Computer analysis of the relation between tablet strength and compaction pressure. *J Pharm Pharmacol, 23*, 195s-201s.

Ngah, W., & Isa, I. (1998). Comparison study of copper ion adsorption on chitosan, Dowex A-1, and Zerolit 225. *Journal of Applied Polymer Science, 67*(6), 1067-1070.

Nguyen, T. V. N., Thi Thu Ha; Wang, San-Lang; Vo, Thi Phuong Khanh; Nguyen, Anh Dzung. (2016). Preparation of chitosan nanoparticles by TPP ionic gelation combined with spray drying, and the antibacterial activity of chitosan nanoparticles and a chitosan nanoparticle–amoxicillin complex. *Research on Chemical Intermediates*, 1-11. doi:10.1007/s11164-016-2428-8

Nishimura, K. N., S.; Seo, H.; Nishi, N.; Tokura, S.; Azuma, I. (1986). Macrophage activation with multi-porous beads prepared from partially deacetylated chitin. *J Biomed Mater Res, 20*(9), 1359-1372. doi:10.1002/jbm.820200910

Noguchi, H. (1981). *Water Activity: Influences on Food Quality* (L. S. Rockland, GF Ed.). New York: Academic Press.

Nokhodchi, A., Ford, J. L., & Rubinstein, M. H. (1997). Studies on the interaction between water and (hydroxypropyl)methylcellulose. *Journal of pharmaceutical sciences, 86*(5), 608-615. doi:10.1021/js960279a

Nokhodchi, A., Raja, S., Patel, P., & Asare-Addo, K. (2012). The Role of Oral Controlled Release Matrix Tablets in Drug Delivery Systems. *BioImpacts : BI, 2*(4), 175-187. doi:10.5681/bi.2012.027

Norlander, B., Gotthard, R., & Strom, M. (1990). Pharmacokinetics of a 5-aminosalicylic acid enteric-coated tablet in patients with Crohn's disease or ulcerative colitis and in healthy volunteers. *Aliment Pharmacol Ther, 4*(5), 497-505.

Oehlert, G. W. (2010). *A First Course in Design and Analysis of Experiments*: University of Minnesota.

Ogawa, K., Hirano, S., Miyanishi, T., Yui, T., & Watanabe, T. (1984). A new polymorph of chitosan. *Macromolecules, 17*(4), 973-975.

Ogawa, K., Yui, T., & Miya, M. (1992). Dependence on the Preparation Procedure of the Polymorphism and Crystallinity of Chitosan Membranes. *Biosci Biotechnol Biochem, 56*(6), 858-862. doi:10.1271/bbb.56.858

Omari, A., Chauveteau, G., & Tabary, R. (2003). Gelation of polymer solutions under shear flow. *Colloids and Surfaces A: Physicochemical and Engineering Aspects, 225*(1–3), 37-48. doi:http://dx.doi.org/10.1016/S0927-7757(03)00319-4

Omwancha, W., Kouba, C., Yelamanchili, S., & Neau, S. H. (2011). Colon-specific drug delivery using ethylcellulose and chitosan in the coat of compression-coated tablets. *Drug Development and Industrial Pharmacy, 37*(8), 945-953. doi:10.3109/03639045.2010.551773

Osamura, T., Takeuchi, Y., Onodera, R., Kitamura, M., Takahashi, Y., Tahara, K., & Takeuchi, H. (2016). Characterization of tableting properties measured with a multi-functional compaction instrument for several pharmaceutical excipients and actual tablet formulations. *Int J Pharm, 510*(1), 195-202. doi:http://dx.doi.org/10.1016/j.ijpharm.2016.05.024

Parikh, N. H., Porter, S. C., & Rohera, B. D. (1993). Aqueous ethylcellulose dispersion of ethylcellulose. I. Evaluation of coating process variables. *Pharmaceutical Research, 10*(4), 525-534.

Patel, S., Kaushal, A. M., & Bansal, A. K. (2007). Effect of Particle Size and Compression Force on Compaction Behavior and Derived Mathematical Parameters of Compressibility. *Pharmaceutical Research, 24*(1), 111-124. doi:10.1007/s11095-006-9129-8

Pati, F. A., B.; Dhara, S. (2011). Development of chitosan–tripolyphosphate fibers through pH dependent ionotropic gelation. *Carbohydrate Research, 346*(16), 2582-2588. doi:http://dx.doi.org/10.1016/j.carres.2011.08.028

Patil, P. C., Daksha; Wagh, Milind. (2012). A Review on ionotropic gelation method: novel approach for controlled gastroretentive gelispheres. *International Journal of Pharmacy & Pharmaceutical Sciences, 4, Supplement 4*(October), 27-32.

Paul, S., Jayan, A., Sasikumar, C. S., & Cherian, S. M. (2014). Extraction and purification of chitosan from chitin isolated from sea prawn (Fenneropenaeus indicus). *Asian Journal of Pharmaceutical and Clinical Research, 7*(4).

Peniche-Covas, C., Alvarez, L., & Argüelles-Monal, W. (1992). The adsorption of mercuric ions by chitosan. *Journal of Applied Polymer Science, 46*(7), 1147-1150.

Perrie, Y., & Rades, T. (2012). Pharmaceutics: Drug Delivery and Targeting (Second Edition ed., pp. 8). London: Pharmaceutical Press.

Picker-Freyer, K. M., & Brink, D. (2006). Evaluation of powder and tableting properties of chitosan. *AAPS PharmSciTech, 7*(3), E152-E161. doi:10.1208/pt070375

Porter, S. C. (1989). Controlled-release film coatings based on ethylcellulose. *Drug Development and Industrial Pharmacy, 15*(10), 1495-1521.

Prajapati, G., & Patel, R. (2010). Design and in vitro evaluation of novel nicorandil sustained release matrix tablets based on combination of hydrophillic and hydrophobic matrix systems. *International Journal of Pharmaceutical Sciences review and research, 1*, 33-35.

Prodduturi, S., Manek, R. V., Kolling, W. M., Stodghill, S. P., & Repka, M. A. (2004). Water vapor sorption of hot-melt extruded hydroxypropyl cellulose films: effect on physico-mechanical properties, release characteristics, and stability. *J Pharm Sci, 93*(12), 3047-3056. doi:10.1002/jps.20222

Puvvada, Y. S., Vankayalapati, S., & Sukhavasi, S. (2012). Extraction of chitin from chitosan from exoskeleton of shrimp for application in the pharmaceutical industry. *International Current Pharmaceutical Journal, 1*(9), 258-263.

Rampino, A. B., Massimiliano; Blasi, Paolo; Bellich, Barbara; Cesàro, Attilio. (2013). Chitosan nanoparticles: Preparation, size evolution and stability. *Int J Pharm, 455*(1–2), 219-228. doi:http://dx.doi.org/10.1016/j.ijpharm.2013.07.034

Ravi Kumar, M. N. V. (2000). A review of chitin and chitosan applications. *Reactive and Functional Polymers, 46*(1), 1-27. doi:http://doi.org/10.1016/S1381-5148(00)00038-9

Ravikovitch, P. I., Domhnaill, S. C. O., Neimark, A. V., Schueth, F., & Unger, K. K. (1995). Capillary Hysteresis in Nanopores: Theoretical and Experimental Studies of Nitrogen Adsorption on MCM-41. *Langmuir, 11*(12), 4765-4772. doi:10.1021/la00012a030

Rege, P. R. S., D.J.; Block, L.H. (1999). Chitinosans as tableting excipients for modified release delivery systems. *Int J Pharm, 181*(1), 49-60. doi:http://dx.doi.org/10.1016/S0378-5173(98)00416-5

Remuñán-López, C. B., Roland. (1997). Mechanical, water uptake and permeability properties of crosslinked chitosan glutamate and alginate films. *Journal of Controlled Release, 44*(2–3), 215-225. doi:http://dx.doi.org/10.1016/S0168-3659(96)01525-8

Ren, D., Yi, H., Wang, W., & Ma, X. (2005). The enzymatic degradation and swelling properties of chitosan matrices with different degrees of N-acetylation. *Carbohydrate Research, 340*(15), 2403-2410.

Rinaudo, M. (2006). Chitin and chitosan: Properties and applications. *Progress in Polymer Science, 31*(7), 603-632. doi:http://dx.doi.org/10.1016/j.progpolymsci.2006.06.001

Sabnis, S., Rege, P., & Block, L. H. (1997). Use of Chitosan in Compressed Tablets of Diclofenac Sodium: Inhibition of Drug Release in an Acidic Environment. *Pharmaceutical Development and Technology*, *2*(3), 243-255. doi:10.3109/10837459709031444

Sakurai, K., Shibano, T., Kimura, K., & Takahashi, T. (1985). Crystal structure of chitosan. *Sen'i Gakkaishi, 41*(9), T361-T368.

Sakurai, K., Takagi, M., & Takahashi, T. (1984). CRYSTAL STRUCTURE OF CHITOSAN. *Sen'i Gakkaishi, 40*(7), T246-T253.

Samal, S. K. D., Mamoni; Van Vlierberghe, Sandra; Kaplan, David L.; Chiellini, Emo; van Blitterswijk, Clemens; Moroni, Lorenzo; Dubruel, Peter. (2012). Cationic

polymers and their therapeutic potential. *Chemical Society Reviews, 41*(21), 7147-7194. doi:10.1039/C2CS35094G

Sansom, L. N. (1999). Oral extended-release products. *Australian prescriber, 22*(4).

Santl, M., Ilic, I., Vrecer, F., & Baumgartner, S. (2012). A compressibility and compactibility study of real tableting mixtures: the effect of granule particle size. *Acta Pharm, 62*(3), 325-340. doi:10.2478/v10007-012-0028-8

Saripella, K. K. V. (2012). *Crospovidone in Water Uptake and Extrusion-Spheronization Studies: Particle Size Effects.* (Ph.D.), University of the Sciences, ProQuest Dissertations Publishing. (UMI Number: 3515950)

Sarrate, R., Ticó, J. R., Miñarro, M., Carrillo, C., Fàbregas, A., García-Montoya, E., . . . Suñé-Negre, J. M. (2015). Modification of the morphology and particle size of pharmaceutical excipients by spray drying technique. *Powder Technology, 270, Part A*, 244-255. doi:http://dx.doi.org/10.1016/j.powtec.2014.08.021

Sawayanagi, Y., Nambu, N., & Nagai, T. (1982). Directly Compressed Tablets containing Chitin or Chitosan in Addition to Lactose or Potato Starch. *CHEMICAL & PHARMACEUTICAL BULLETIN, 30*(8), 2935-2940. doi:10.1248/cpb.30.2935

Sayed, S., & Jardine, A. (2015). Chitosan derivatives as important biorefinery intermediates. Quaternary tetraalkylammonium chitosan derivatives utilized in anion exchange chromatography for perchlorate removal. *International journal of molecular sciences, 16*(5), 9064-9077.

Schipper, N. G., Varum, K. M., & Artursson, P. (1996). Chitosans as absorption enhancers for poorly absorbable drugs. 1: Influence of molecular weight and

degree of acetylation on drug transport across human intestinal epithelial (Caco-2) cells. *Pharm Res, 13*(11), 1686-1692.

Schmidt, P. C., & Herzog, R. (1993). Calcium phosphates in pharmaceutical tableting. *Pharmacy World and Science, 15*(3), 116-122. doi:10.1007/BF02113939

Sezer, A. D., & Akbuğa, J. (1995). Controlled release of piroxicam from chitosan beads. *Int J Pharm, 121*(1), 113-116. doi:http://dx.doi.org/10.1016/0378-5173(94)00413-Y

Shah, U., & Augsburger, L. (2001). Evaluation of the functional equivalence of crospovidone NF from different sources. I. Physical characterization. *Pharmaceutical development and technology, 6*(1), 39-51. doi:10.1081/PDT-100000012

Shapiro, I. (1944). *Ph.D. Thesis.* (Ph.D.), University of Minnesota.

Shirsat, A. C., Sohan. (2015). Application of quality by design approach to optimize process and formulation parameters of rizatriptan loaded chitosan nanoparticles. *Journal of Advanced Pharmaceutical Technology & Research, 6*(3), 88-96. doi:10.4103/2231-4040.157983

Shokri, J., & Adibkia, K. (2013). Application of Cellulose and Cellulose Derivatives in Pharmaceutical Industries. In T. v. d. Ven & L. Godbout (Eds.), *Cellulose - Medical, Pharmaceutical and Electronic Applications* (pp. Ch. 03). Rijeka: InTech.

Shu, X. Z. Z., K.J. (2002). The influence of multivalent phosphate structure on the properties of ionically cross-linked chitosan films for controlled drug release.

European Journal of Pharmaceutics and Biopharmaceutics, *54*(2), 235-243. doi:http://dx.doi.org/10.1016/S0939-6411(02)00052-8

Siegel, R. A., & Rathbone, M. J. (2012). Overview of controlled release mechanisms *Fundamentals and Applications of Controlled Release Drug Delivery* (pp. 19-43): Springer.

Siepmann, J., & Peppas, N. A. (2011). Higuchi equation: Derivation, applications, use and misuse. *Int J Pharm, 418*(1), 6-12. doi:http://dx.doi.org/10.1016/j.ijpharm.2011.03.051

Siew, A. (2013). Ethyl cellulose aqueous dispersion: a coating system for oral sustained-release dosage forms. *Pharmaceutical Technology*.

Smith, J., Wood, E., & Dornish, M. (2004). Effect of chitosan on epithelial cell tight junctions. *Pharmaceutical Research, 21*(1), 43-49.

Souihi, N., Dumarey, M., Wikström, H., Tajarobi, P., Fransson, M., Svensson, O., . . . Trygg, J. (2013). A quality by design approach to investigate the effect of mannitol and dicalcium phosphate qualities on roll compaction. *Int J Pharm, 447*(1–2), 47-61. doi:http://dx.doi.org/10.1016/j.ijpharm.2013.02.036

Sparkes, B. G., & Murray, D. G. (1986). Chitosan based wound dressing materials: Google Patents.

Srikanth, M., Sunil, S., Rao, N., Uhumwangho, M., & Murthy, K. R. (2010). Ion-exchange resins as controlled drug delivery carriers. *Journal of Scientific Research, 2*(3), 597.

Stevenson, C. L., Santini, J. T., & Langer, R. (2012). Reservoir-based drug delivery systems utilizing microtechnology. *Advanced Drug Delivery Reviews, 64*(14), 1590-1602.

Sun, C., & Grant, D. J. W. (2001). Influence of Elastic Deformation of Particles on Heckel Analysis. *Pharmaceutical Development and Technology, 6*(2), 193-200. doi:10.1081/PDT-100000738

Szymańska, E., & Winnicka, K. (2015). Stability of chitosan—a challenge for pharmaceutical and biomedical applications. *Marine Drugs, 13*(4), 1819-1846.

Thanou, M., Verhoef, J. C., & Junginger, H. E. (2001). Chitosan and its derivatives as intestinal absorption enhancers. *Adv Drug Deliv Rev, 50 Suppl 1*, S91-101.

Tiwari, S. B., & Rajabi-Siahboomi, A. R. (2008). Modulation of drug release from hydrophilic matrices. *Pharm Tech Eur, 1*.

Tokumitsu, H. I., H.; Fukumori, Y. (1999). Chitosan-gadopentetic acid complex nanoparticles for gadolinium neutron-capture therapy of cancer: preparation by novel emulsion-droplet coalescence technique and characterization. *Pharm Res, 16*(12), 1830-1835.

Tsai, M.-L., Chen, R.-H., Bai, S.-W., & Chen, W.-Y. (2011). The storage stability of chitosan/tripolyphosphate nanoparticles in a phosphate buffer. *Carbohydrate Polymers, 84*(2), 756-761. doi:http://dx.doi.org/10.1016/j.carbpol.2010.04.040

Ummadi, S., Shravani, B., Rao, N. R., Reddy, M. S., & Sanjeev, B. (2013). Overview on controlled release dosage form. *System, 7*(8).

Understanding and Interpreting Particle Size Distribution Calculations. (n.d.). Retrieved from http://www.horiba.com/scientific/products/particle-

characterization/education/general-information/data-interpretation/understanding-particle-size-distribution-calculations/

United States Pharmacopeia National Formulary, C. (2016a). General Chapters: <616> Bulk Density and Tapped Density of Powders (Vol. 38(2), pp. 456). USP-NF Online (USP 39-NF 34).

United States Pharmacopeia National Formulary, C. (2016b). General Chapters: <711> Dissolution (Vol. 40(6), pp. 540). USP-NF Online (USP 39-NF 34).

United States Pharmacopeia National Formulary, C. (2016c). General Chapters: <1174> Powder Flow (Vol. 28(2), pp. 618). USP-NF Online (USP 39-NF 34).

United States Pharmacopeia National Formulary, C. (2016d). NF Monographs: Chitosan (Vol. 35(1), pp. 7242-7247). USP-NF Online (USP 39-NF 34 S2).

Vaezifar, S. R., Shahnaz; Golozar, Mohammad Ali; Karbasi, Saied; Morshed, Mohammad; Kamali, Mahdi (2013). Effects of Some Parameters on Particle Size Distribution of Chitosan Nanoparticles Prepared by Ionic Gelation Method. *Journal of Cluster Science, 24*, 891-903. doi:10.1007/s10876-013-0583-2

Van den Berg, C. (1981). Wageningen: Agricultural University of Wageningen.

Varma, M. V., Kaushal, A. M., Garg, A., & Garg, S. (2004). Factors affecting mechanism and kinetics of drug release from matrix-based oral controlled drug delivery systems. *American Journal of drug delivery, 2*(1), 43-57.

Vårum, K., Ottøy, M., & Smidsrød, O. (2001). Acid hydrolysis of chitosans. *Carbohydrate Polymers, 46*(1), 89-98.

Vílchez, S., Manich, A. M., Miras, J., Molina, R., Erra, P., & Esquena, J. (2016). Dynamic vapour sorption and thermoporometry of polyamide fabrics coated with

chitosan hydrogels. *Thermochimica Acta*, *639*, 47-52. doi:http://dx.doi.org/10.1016/j.tca.2016.07.004

Viljoen, J. M., Steenekamp, J. H., Marais, A. F., & Kotzé, A. F. (2014). Effect of moisture content, temperature and exposure time on the physical stability of chitosan powder and tablets. *Drug Development and Industrial Pharmacy*, *40*(6), 730-742. doi:10.3109/03639045.2013.782501

Wakerly, Z., Fell, J., Attwood, D., & Parkins, D. (1997). Studies on drug release from pectin/ethylcellulose film-coated tablets: a potential colonic delivery system. *Int J Pharm*, *153*(2), 219-224.

Walker, E. E. (1923). The properties of powder. Part VI. The compressibility of powders. *Transactions of the Faraday Society*, *19*, 73-82.

Wang, W., & Xu, D. (1994). Viscosity and flow properties of concentrated solutions of chitosan with different degrees of deacetylation. *Int J Biol Macromol*, *16*(3), 149-152.

Wang, Y. L., Puwang; Truong-Dinh Tran, Thao; Zhang, Juan; Kong, Lingxue. (2016). Manufacturing Techniques and Surface Engineering of Polymer Based Nanoparticles for Targeted Drug Delivery to Cancer. *Nanomaterials*, *6*(2), 26.

Wanjun, T., Cunxin, W., & Donghua, C. (2005). Kinetic studies on the pyrolysis of chitin and chitosan. *Polymer Degradation and Stability*, *87*(3), 389-394.

Watt, I. C. (1980). Adsorption-Desorption Hysteresis in Polymers. *14*(2), 245 - 255.

Win, P. P., Shin-ya, Y., Hong, K.-J., & Kajiuchi, T. (2003). Formulation and characterization of pH sensitive drug carrier based on phosphorylated chitosan

(PCS). *Carbohydrate Polymers, 53*(3), 305-310. doi:http://dx.doi.org/10.1016/S0144-8617(03)00068-7

Wu, Y., Yang, W., Wang, C., Hu, J., & Fu, S. (2005). Chitosan nanoparticles as a novel delivery system for ammonium glycyrrhizinate. *Int J Pharm, 295*(1-2), 235-245. doi:10.1016/j.ijpharm.2005.01.042

Xu, J., McCarthy, S. P., Gross, R. A., & Kaplan, D. L. (1996). Chitosan film acylation and effects on biodegradability. *Macromolecules, 29*(10), 3436-3440.

Xu, Y., & Du, Y. (2003). Effect of molecular structure of chitosan on protein delivery properties of chitosan nanoparticles. *Int J Pharm, 250*(1), 215-226. doi:http://dx.doi.org/10.1016/S0378-5173(02)00548-3

Yang, Y., Hu, W., Wang, X., & Gu, X. (2007). The controlling biodegradation of chitosan fibers by N-acetylation in vitro and in vivo. *Journal of Materials Science: Materials in Medicine, 18*(11), 2117-2121.

Young, J. H., & Nelson, G. L. (1967a). Theory and hysteresis between sorption and desorption isotherms in biological materials. *Trans Am Soc Agric Eng, 10*, 260-263.

Young, J. H., & Nelson, G. L. (1967b). Research and hysteresis between sorption and desorption isotherms of wheat. *Trans Am Soc Agric Eng, 10*, 756-761.

Zacour, A. C., Silva, M. E., Cecon, P. R., Bambirra, E. A., & Vieira, E. C. (1992). Effect of dietary chitin on cholesterol absorption and metabolism in rats. *J Nutr Sci Vitaminol (Tokyo), 38*(6), 609-613.

Zeng, X., & Ruckenstein, E. (1998). Cross-linked macroporous chitosan anion-exchange membranes for protein separations. *Journal of Membrane Science, 148*(2), 195-205.

Zhang, H., & Neau, S. H. (2002). In vitro degradation of chitosan by bacterial enzymes from rat cecal and colonic contents. *Biomaterials, 23*(13), 2761-2766. doi:http://doi.org/10.1016/S0142-9612(02)00011-X

Zhang, L., & Kosaraju, S. L. (2007). Biopolymeric delivery system for controlled release of polyphenolic antioxidants. *European Polymer Journal, 43*(7), 2956-2966. doi:http://dx.doi.org/10.1016/j.eurpolymj.2007.04.033

Zografi, G., & Kontny, M. J. (1986). The interactions of water with cellulose-and starch-derived pharmaceutical excipients. *Pharmaceutical Research, 3*(4), 187-194.